GEOLOGICAL SURVEY OF CANADA
PAPER 90-17

SHEAR-SENSE INDICATORS: A REVIEW

Simon Hanmer and Cees Passchier

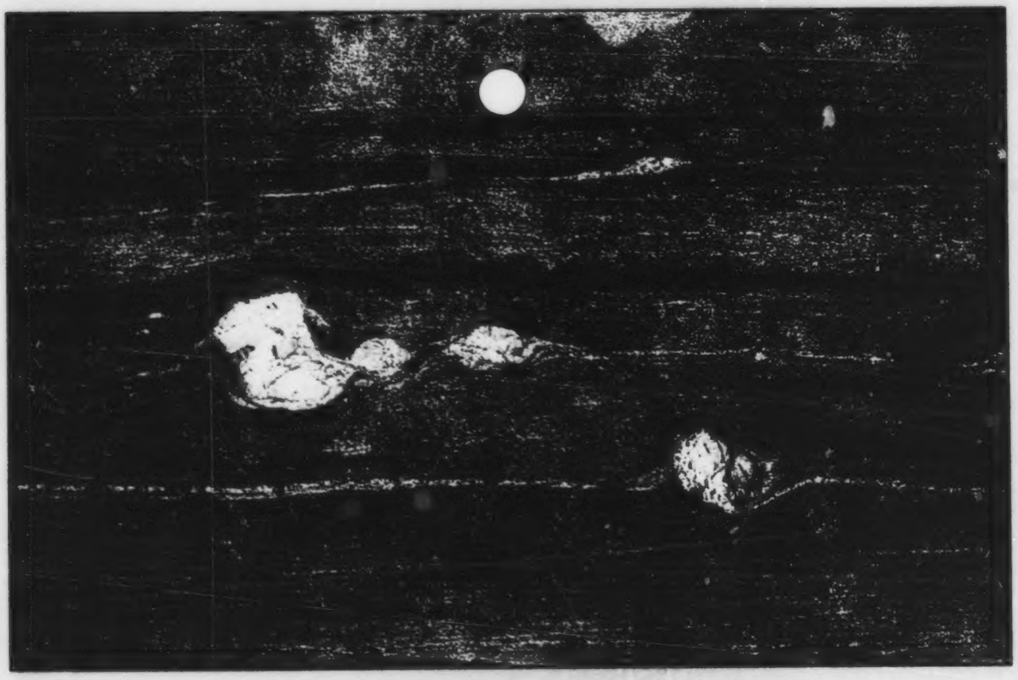

1991

Energy, Mines and Resources Canada
Énergie, Mines et Ressources Canada

Canada

THE ENERGY OF OUR RESOURCES
THE POWER OF OUR IDEAS

92-01301/

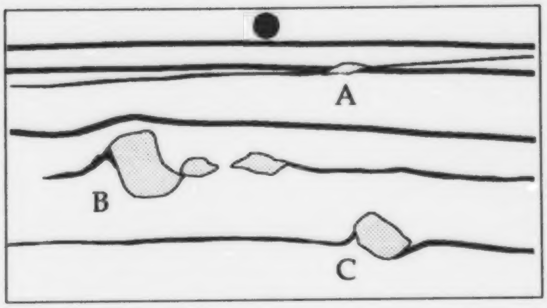

Cover description

Feldspar inclusions and polycrystalline feldspar wings, derived from pegmatite in an ultramylonite with a dextral sense of shear. The observation surface is the XZ plane of the finite strain ellipsoid and the mylonitic foliation and banding are parallel to the shear plane. The stubby feldspar of the immature "*stair-step*" structure (A) makes a slightly greater angle with the shear plane than do its highly attenuated wings. In the mature examples (B and C), the long axes of both the stubby inclusions make the same angle with respect to the shear plane and their attenuated wings no longer describe a stair-step geometry, but lie "*in-plane*". If we consider the inter-relationships between rotation rate, orientation and aspect ratio of inclusions in a flowing medium, the development of these structures is readily explained in terms of general noncoaxial flow, as opposed to simple shear. Central Metasedimentary Belt boundary zone, Grenville Province, Québec. See Figure 50. (GSC 204105-Q)

GEOLOGICAL SURVEY OF CANADA
PAPER 90-17

SHEAR-SENSE INDICATORS: A REVIEW

Simon Hanmer and Cees Passchier

1991

© Minister of Supply and Services Canada 1991

Available in Canada through

authorized bookstore agents and other bookstores

or by mail from

Canada Communication Group — Publishing
Ottawa, Canada K1A 0S9

and from

Geological Survey of Canada offices:

601 Booth Street
Ottawa, Canada K1A 0E8

3303-33rd Street N.W.,
Calgary, Alberta T2L 2A7

A deposit copy of this publication is also available for
reference in public libraries across Canada

Cat. No. M44-90/17E
ISBN 0-660-14050-O

Price subject to change without notice

Authors' addresses

Simon Hanmer
Continental Geoscience Division
Geological Survey of Canada
601 Booth Street
Ottawa, Ontario
K1A 0E8

Cees Passchier
Faculteit Aardwetenschappen
Rijksuniversiteit Utrecht
Budapestlaan 4, Utrecht
The Netherlands

Original manuscript received: 1990 - 06
Final version approved for publication: 1991 - 02

CONTENTS

1 Abstract/Résumé

3 Introduction
4 Acknowledgments

5 **Flow and rheology in progressive deformation**
5 Flow
5 Velocity fields, stretching rate and angular velocity
6 Coaxial and noncoaxial flow
8 Kinematical vorticity number (W_k)
11 Spin
13 Progressive deformation
14 Partitioning of the rotational component of the flow
14 Kinematic framework
14 Orienting the flow in the field
15 Shear plane and shear direction
16 Fault bends, terminations and flow type
16 Rotation
16 Why do finite strains rotate in noncoaxial flows?
16 Rotation : rate and direction
19 Partitioning and repartitioning
19 Isotropic media
20 Rotating anisotropy
22 Non-rotating anisotropy
23 Strain and flow refraction
24 Where to look

25 **Shape fabrics (foliations)**
25 Simple shape fabrics
25 Strain-sensitive fabrics
25 Strain-insensitive fabrics
27 Complex shape fabrics
28 C/S fabrics
30 Asymmetrical extensional shear bands
32 Comparison of fabrics
33 Deflection of foliations and layers
33 Shear zones
33 Inclusions

34 **Inclusions and appendages**
34 Porphyroblasts
36 Stiff inclusions
36 Theoretical prelude
37 'Naked' inclusions
37 Winged porphyroclasts
40 General winged inclusions
44 Back-rotated structures
44 Apparent back-rotation
45 Back-rotated foliation segments
47 Laboratory simulation and tentative models
49 Mica fish
52 Pressure shadows and fringes
52 Pressure fringes
52 Displacement-controlled fibres
53 Face-controlled fibres

55 Fibre stiffness
55 A paradox?
56 Fibre growth
56 Pressure shadows
57 Rotated pressure shadows
58 Quarter structures
59 Tiling and domino-structures

60 **Veins and folds**
60 Veins and vein arrays
60 Fibrous veins
61 Deformed veins
63 Rheological interfaces and induced noncoaxial flow
63 Incompetent veins
64 Competent veins
64 Fold asymmetry

67 References

Figures

5 1. Velocity fields
5 2. Deformation paths
6 3. Flow types in 2D
7 4. Progressive deformation
7 5. Material lines in flow
8 6. Kinematically indeterminate strain
8 7. A frame of reference
9 8. Averaged angular velocity
9 9. Fixed material lines
9 10. Shear-induced vorticity
10 11. Kinematical vorticity number (W_k)
11 12. Internal versus external rotation
12 13. The rotational component of flow
12 14. Noncoaxial non-spinning flow
12 15. Noncoaxial spinning flow
13 16. Progressive extension and shortening
14 17. Kinematic indicators
15 18. Kinematic framework in the field
15 19. Strain gradient and shear plane
16 20. Fault bends and terminations
17 21. Rheologically controlled flow
17 22. Zero stretching rate in the flow plane
18 23. Rotation of inclusions and markers
20 24. Rotating anisotropy and flow partitioning
21 25. Non-rotating anisotropy and flow partitioning
22 26. Refraction in multilayers
23 27. Refraction and folds
23 28. Refraction and shear zones
24 29. Where to look
25 30. Strain sensitive simple fabrics
26 31. Strain insensitive simple fabrics
27 32. Locally sigmoid strain-insensitive foliation
28 33. C/S fabrics versus asymmetrical extensional shear bands
29 34. Natural C/S fabrics
30 35. Asymmetrical extensional shear bands

31 36. Why are extensional shears bands asymmetrical?
31 37. Deflections and shear zones
32 38. Deflection and inclusions
34 39. Rotated garnet porphyroblast
35 40. To rotate, or not to rotate...
36 41. Rotated porphyroblast or fossilized crenulation?
37 42. 'Naked' inclusions
38 43. Winged inclusion geometry
39 44. Experimental 'winged' porphyroclasts I
39 45. Experimental 'winged' porphyroclasts II
41 46. Natural winged porphyroclasts
41 47. Natural winged inclusions I
42 48. Natural winged inclusions II
42 49. Natural winged inclusions III
43 50. Fast wings and slow inclusions
44 51. In-plane winged inclusions in simple shear
45 52. Kinematically equivocal rotated boudinage
46 53. Natural back-rotated layer segments
46 54. Natural back-rotated swells
47 55. Asymmetrical pull-aparts in experiment
48 56. Natural shear-modified blocky boudin
48 57. Back-rotation of foliation segments
49 58. Mica fish
50 59. Face-controlled deformable fibres
53 60. Displacement-controlled rigid fibres
54 61. Natural rigid fibres
54 62. Simple pressure shadows
55 63. Rotated pressure shadows
56 64. Material quarters and noncoaxial flow
57 65. Quarter structures
58 66. 'Tuilage' or tiling
60 67. Sigmoid tension gashes
60 68. Quartz veins with fibrous fill
61 69. Displacement-controlled fibres in dilational veins
61 70. Face-controlled fibres in dilational veins
61 71. Folded boudins
62 72. Oblique internal foliation in concordant veins
62 73. Oblique boudin trains
63 74. Local induced flow
64 75. In-plane separation of boudins
64 76. Fold asymmetry
65 77. Rotation of fold axial planes
65 78. Sheath folds
65 79. Fold axes parallel to the flow direction
66 80. Asymmetrical amplification of a single fold
66 81. Fold mechanisms and bulk flow

SHEAR-SENSE INDICATORS: A REVIEW

Abstract

The critical evaluation of the kinematic significance of natural geological deformation structures, with particular reference to the determination of shear-sense, requires a high degree of familiarity with the basic concepts of flow, and the influence of material properties (discontinuities, rheological layering, anisotropy) on the nature of flow at the local scale. This contribution begins with a chapter on flow, followed by three chapters which critically examine geological deformation structures which are commonly used as shear-sense indicators: foliations, stiff inclusions and their attendant wings and, finally, folds and veins.

Résumé

L'évaluation critique de la signification cinématique des structures de déformation naturelles, surtout en ce qui concerne la détermination du sens de cisaillement, exige que l'on possède des compétences de base dans le domaine de l'écoulement et de l'influence des propriétés matérielles rhéologiques (discontinuités, litage ou rubanement, anisotropie) sur l'écoulement à l'échelle locale. Le premier chapitre du présent ouvrage porte sur l'écoulement déformationel et est suivi de trois chapitres qui présentent un examen critique de la signification cinématique des foliations, des objets durs et de leurs appendices connexes et, enfin, des plis et des veines déformées.

INTRODUCTION

Rocks do not suffer deformation; they enjoy it. (Rob Knipe, 1982; quoted in Groshong 1988; Geological Society of America Bulletin, p. 1329).

A truly benevolent creator would have implanted a regular three-dimensional grid in rocks prior to their deformation ... He chose to set a problem by providing only parts of that grid .... (Hirsinger and Hobbs, 1983; Journal of Structural Geology, p. 307).

During the past decade, geologists have attempted, with varying degrees of success, to identify meso- to microscopic-scale deformation structures which can be utilized as reliable indicators of the sense of movement in shear zones. Earth scientists are increasingly recognizing the importance of shear zones, especially as they pertain to the contact zones between tectonic plates, or to the boundaries of allochthonous masses occurring at all scales within orogenic belts. It is obvious that, having identified the existence of a shear zone, the first question to resolve concerns its movement history. Thus, the ability to recognize and to correctly use structures from which one may reliably deduce shear-sense is becoming an essential part of the field geologist's repertoire. Only through understanding of the mechanisms, processes and progressive development of the structure can we critically evaluate the kinematic significance of an observed geometry.

It is often possible to propose more than one origin for a given shape. Since the kinematic significance of the observed geometry depends on the structural path which led to its development, the ability to critically discriminate between causal models is a prerequisite to the undertaking of kinematic analysis, whatever the level of involvement of the scientist. Geologists attempting to unravel the structural history of a specimen, an outcrop or a region should seek to cross-check and confirm their initial interpretations. The onus is on them to verify that a given structure is not a chance occurrence, but is part of a population of such structures whose geometry is systematically consistent with the kinematic model proposed for their formation. They must seek to identify an assemblage of kinematically independent structures, formed by different processes, all of whose progressive development histories indicate a consistent sense of shear.

To the non-specialist, the seemingly esoteric nature of much of the literature on shear-sense indicators may appear to represent a major hurdle. Leaping that hurdle involves two steps: (i) understanding the nature of flow and of the rotations of planes and lines that result from it and (ii) understanding the physical processes inherent in the development of the structure. While the former may appear potentially complex at first, it is the latter which is the most difficult. This is because the development of fabrics and structures by inhomogeneous flow in crystalline materials is incompletely understood. Nevertheless, there are at least two reasons why the scientist who would work with natural structures should strive to take both of these steps. (1) The accumulating evidence strongly suggests that natural deformations commonly represent significant deviations from the idealized simple models presented in many text books and (2) the nature of the flow at the scale at which geologists make their observations may strongly deviate from the type of flow at the bulk scale.

In Part I, *Flow and Rheology in Progressive Deformation*, we present an overview of the theoretical aspects of flow which are essential to deciphering shear-sense indicators, without which access to the rest of the paper would be severely limited. Initially we examine flow in an homogeneous, isotropic medium and then consider the influence of material properties, such as anisotropy and rheological layering, on the nature of the flow. Part II is divided into three chapters in which we critically examine an assemblage of naturally occurring tectonic structures which have been utilized in the literature as shear-sense indicators. Our philosophy in this paper will not only be to describe the geometry of a given structure, but also to examine its progressive development, from which its kinematic significance may be deduced. Furthermore, we will examine the influence of variation in the nature of the flow on the geometry of such structures. Classifying natural structures into groups is always a somewhat arbitrary exercise, one which no two geologists would necessarily agree upon. For better or worse, we have chosen following scheme. *Shape Fabrics (Foliations)* considers the kinematic significance of foliations, both with respect to their formation and their rotational behaviour. *Inclusions* deals with the rotation of stiff inclusions and anisotropic objects as well as, where relevant, their attendant appendages, be they 'wings', 'tails', shadows or fringes. *Veins and Folds* is self explanatory.

It would not be appropriate here for us to attempt to review the basic theory of deformation. For those readers seeking to improve their understanding of the elementary principles of deformation, we would recommend consulting one or several of the excellent, comprehensive texts presently available (e.g. Ramsay, 1967; Means, 1976; Hobbs et al., 1976; Ramsay and Huber, 1983). For those readers lacking adequate library facilities and funds, we suggest that the book by Park (1989) represents good value for money.

Our aim here is to examine types of flow, and the kinematically significant structures which form in them, from a perspective which should be accessible to all interested geologists, yet may also prove useful to the specialist. Regardless of what the

Inimitable Bard has to say about those who have similar ideas at the same moment, the stimulus for us to write this contribution jointly comes from our participation in the *Subcommission on the Rheology of Rocks*, part of the Commission on Tectonics (COMTEC) of the International Union of Geological Sciences (IUGS). Other members of these groups are also preparing reviews, textbooks and manuals on aspects of structural geology, placing particular emphasis on access, both conceptual and material. We would like to propose this paper as our contribution to this communal effort.

This is not the first attempt to review aspects of shear-sense analysis (Simpson and Schmid, 1983; Hanmer, 1984a; Simpson, 1986; White et al., 1986; Ramsay and Huber, 1987; Passchier, 1988), but up until now, reviews have either concentrated on simple shear, or have been conceptually difficult for the general readership. Our hope for the present contribution is that it will enable the reader to attain a degree of familiarity and feel comfortable with such conceptual tools as are necessary to competently undertake shear-sense analysis of naturally deformed materials. What follows is not a 'definitive' account of visible shear criteria. Rather, we would hope that our contribution will stimulate others to critically re-examine some of the structures and the interpretations which we present here and to reassess the kinematic significance which we and others have placed upon them. The great majority of shear-sense indicators are insufficiently understood. Although we review here the already published interpretations of these structures, as well as presenting some of our own views, it is not our intention to convey the erroneous impression that most of the problems have been solved. In some cases, the appropriate questions have perhaps not yet been asked!

ACKNOWLEDGMENTS

We are particularly indebted to Jean-Pierre Burg, Rick Law, Marc St-Onge, Carol Simpson, and Paul Williams for their detailed comments on all or parts of the manuscript as well as Tim Bell, John Henderson, Jack Henderson, Jacques Malavieille, Jacques Martignole and John Percival. We also thank Larry Lane and Jacques Malavieille for the use of their microphotos in Figures 58 and 61.

FLOW AND RHEOLOGY IN PROGRESSIVE DEFORMATION

FLOW

In the following paragraphs, we shall present a simple, nonmathematical summary of flow and progressive deformation. For a more rigorous, quantitative approach, we recommend that the interested reader consult some of the geologically oriented sources on the subject (Elliot, 1972; Ramberg, 1975; Ghosh and Ramberg, 1976; Means et al., 1980; Lister and Williams, 1983; Passchier, 1986).

Velocity fields, stretching rate and angular velocity

Deformation describes the change in shape and orientation, as well as the displacement, of volumes of material between initial and final states. Throughout this contribution, we will use the term *deformation* in this general sense. The term *strain* has a more restricted significance, referring only to the change in shape, or distortion, of the object. With change in shape, material lines may change in length and undergo rotation with respect to a reference frame. In homogeneous progressive deformation, material lines all tend to rotate towards a common plane: that plane is termed the *flow plane*.

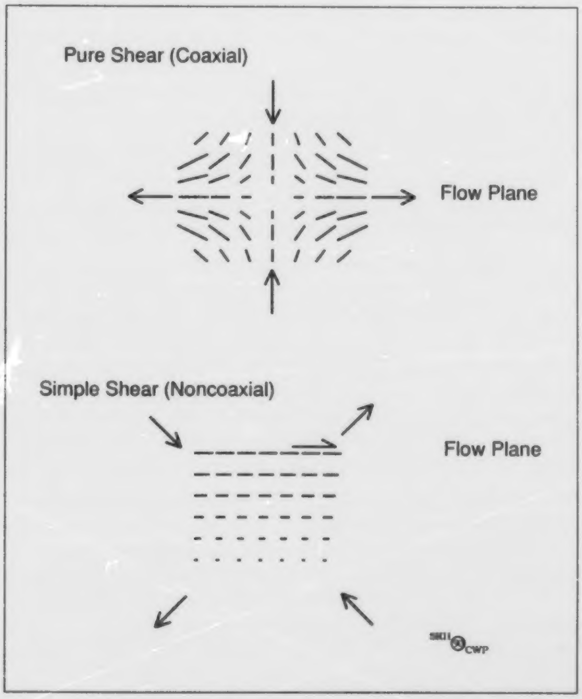

Figure 1. Velocity fields representing the 2D displacements of material particles for pure shear and simple shear flows. Lengths of the markers are proportional to velocities. Note that the markers represent *velocities* and not displacements. The instantaneous stretching axes are indicated (arrows). In simple shear the displacement vector is also shown.

Flow is the instantaneous displacement of material particles making up a deforming body. If the flow is homogeneous, the pattern of instantaneous particle velocities can be described by a simple *velocity field*, or flow pattern (Fig. 1). A velocity field is like a snapshot, describing the instantaneous motion of a population of material particles at a given instant in time. However, as geologists, we are more likely to be able to observe *displacements* rather than particle velocities. Displacements result when flow acts on a material for more than just an instant. If the time period is as small as possible, the correspondingly small displacement is an *infinitesimal increment* of deformation. A sequence of infinitesimal increments of deformation is like a movie, describing the accumulation of finite displacements of material particles with time. The difference in the distribution of particles between the initial state and the deformed state is known as *finite deformation*. The process of ongoing deformation from the initial state to the deformed state is known as *progressive deformation* (Fig. 2).

We must be sure to clearly distinguish between the notions of ongoing progressive deformation (straining, progressive strain) and the end product of the progressive deformation (strain, finite strain, total strain). Whereas we

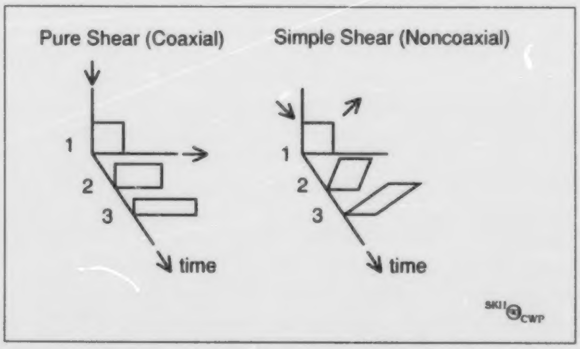

Figure 2. Deformation paths are sequences of accumulating progressive deformation. Two paths are illustrated: progressive pure shear and progressive simple shear. The instantaneous stretching axes are indicated (arrows). The sequence of rotations and changes in length of material lines is a reflection of the nature of the flow type. In pure shear the strain accumulates coaxially, whereas in simple shear it accumulates noncoaxially.

can often observe the latter, we are usually required to deduce the former. It is this process of deduction which is central to the analysis of shear-sense.

Rather than referring to particle velocities and displacements, *it is more practical to refer to the stretching rates* and *angular velocities* of material lines. During progressive deformation, both the lengths and the orientations of material lines may change, according to their orientation in the flow. Consider two flow types commonly referred to in the geological literature: *pure shear* and *simple shear*. In Figure 2, deformation paths due to these two flow types are illustrated: an initial square is progressively deformed, either into a rectangle (pure shear), or a parallelogram (simple shear). In each case the finite deformation state can be considered as the result of the accumulation of an infinite number of infinitesimally small increments of infinitesimal shape change and rotation of the material lines making up the deforming object (Fig. 3, 4).

Coaxial and noncoaxial flow

The nature of the infinitesimal deformation increments is a reflection of the type of the flow (Fig. 4). However, as geologists, we are often confronted with the final state of the material lines (*total strain*). If we know the initial configuration of the deformed material (i.e. its shape expressed as lengths and angles), then we can determine the magnitude and orientation of the total strain, but without supplementary information we can say nothing about the deformation path

Figure 3. Flow types in 2D. In any flow type, the instantaneous shape-change or distortion can be described by an ellipse (X_i, Z_i), symmetrically divided into extensional (1 and 3, large arrows) and shortening *quadrants* (2 and 4, small arrows) by two *lines of zero stretching rate*, or instantaneous change in length. Quadrants are numbered in the direction of the shear-sense. They correspond to fields of instantaneous extension (1 and 3) and instantaneous shortening (2 and 4). Ideally these ellipses should represent infinitesimally small distortions from an initial circle and the lines of zero stretching rate should cross each other at 90°. For clarity, the representations of instantaneous shape change have been slightly exaggerated. A second ellipse can be drawn representing the finite shape-change (X_f, Z_f) resulting from progressive deformation, assuming an invariant flow type. In this illustration we have assumed a constant ratio of the instantaneous stretching axes (X_i/Z_i). *Lines of zero finite change in length* separate material lines which have only undergone extension (white) from lines which have undergone some shortening (shaded). The lines of zero stretching rate maintain a constant angle with respect to X_i, whereas the lines of zero finite change in length rotate towards X_i.

In *progressive pure shear,* the lines of zero finite change in length rotate away from the lines of zero stretching rate. In *progressive simple shear,* the following boundary conditions apply:

(1) All directions within the shear plane, including the axis of rotation of the deformation, are directions of zero stretching rate.

(2) At any instant, the maximum and minimum instantaneous stretching axes of the flow make fixed angles of 45° with the flow plane.

(3) The principal directions of finite strain rotate away from the maximum and minimum instantaneous stretching axes of the flow, with the same sense as that of the imposed shear; in other words the *strain accumulates noncoaxially.*

(4) All markers and inclusions, material and non-material lines, rotate with the same sense as the imposed shear.

Moreover, in the simple shear model, one of the lines of zero stretching rate is materially attached to the shear plane of the deformation. It follows that the corresponding line of zero finite change in length is also fixed to the same material plane. Therefore, the decrease in the angle between the lines of zero finite change in length and X_f results in the rotation of X_f towards the shear plane.

The simplest deviation from simple shear is a two-dimensional general noncoaxial flow, where a contemporaneous shortening across the shear plane is accommodated by extension along the shear direction. Flow remains two-dimensional since there is no instantaneous change in length along the direction of the rotation axis of the deformation. The flow can be considered in terms of two main components; a component of simple shear and a component of pure shear. The instantaneous flow can be represented by an ellipse derived by combining the ellipses representing the pure and simple shear components. The orientations of the resultant X_i ($45^\circ < \alpha < 90^\circ$) and the lines of zero instantaneous change in length ($0^\circ < \alpha < 45^\circ$ and $90^\circ < \alpha < 135^\circ$) are intermediate between those for the simple shear and pure shear cases, and depend on the flow type.

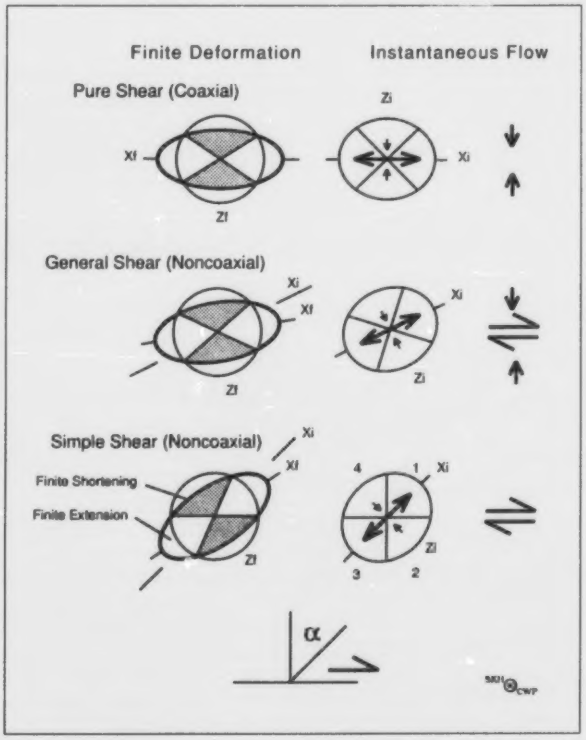

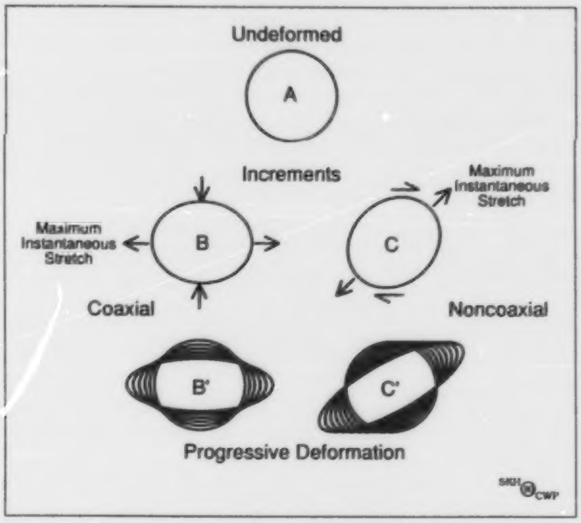

Figure 4. Progressive deformation results from the accumulation of small increments of deformation. Two deformation paths are illustrated here, based upon two flow types: pure shear (coaxial) and simple shear (noncoaxial). The finite deformation states are obtained by sequentially deforming the previous state by the distortion represented by the instantaneous increment characteristic of that flow type. Note that the progressive strain accumulates coaxially in pure shear, but noncoaxially in simple shear. As a consequence, the finite strain ellipsoid rotates with respect to the instantaneous stretching axes in progressive simple shear, but not in progressive pure shear.

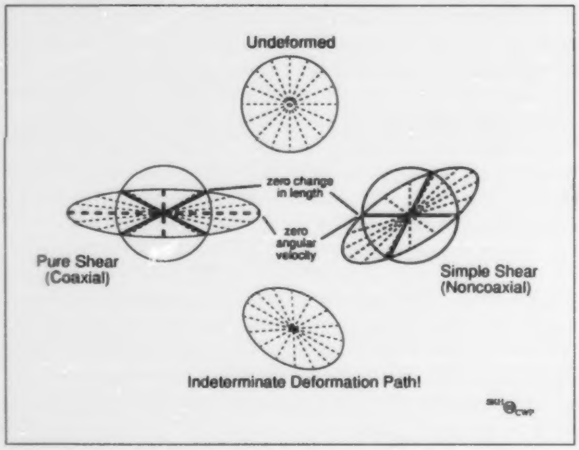

Figure 5. Material lines in flow. Most material lines rotate and change in length with progressive deformation. However, there are exceptions. In each flow type, there are lines which do not rotate. In progressive pure shear, a pair of such lines lies parallel to the instantaneous stretching axes of the flow. In simple shear, only the flow plane is a *direction of zero angular velocity*. At any instant during progressive deformation, there are lines whose finite length is the same as it was in the initial state. In progressive pure shear, there are two such *lines of zero finite change in length*. In progressive simple shear, one of those two lines is fixed to the flow plane. Notice that this is one of the fundamental distinctions between pure and simple shear. Note also that without information concerning the directions of zero angular velocity and of zero finite change in length, the deformation path is kinematically indeterminate.

(Fig. 5). Herein lies the nub of the problem, since it must be borne in mind that many different deformation paths may lead to the same end result (Fig 6).

While it is obvious that one can measure the change in length of a line by comparing it to its original length (Fig. 5), the concept of the rotation of a line requires some thought. In order to be able to describe rotation, a *frame of reference* is required. Although lacking in mathematical elegance (see Ramberg (1975) and Passchier (1987a) for more mathematically lucid alternatives), we feel that the classical reference frame for flow is more familiar to geologists (Fig. 7). Moreover, it enables the geologist to set the reference frame parallel to tangible deformation structures. Hence, in any noncoaxial (shearing *s.l.*) progressive deformation, we have chosen to set the abscissa and ordinate of the external reference frame parallel to the flow plane and its normal. Since this contribution will also be concerned with two-dimensional deviations from simple shear by shortening normal to the flow plane, we shall set the abscissa and ordinate of the external reference frame parallel to the directions of maximum and minimum instantaneous stretch of the pure shear component of any flow. ***Note that we take the maximum instantaneous stretch (Xi) to be the direction of maximum instantaneous extension and the minimum instantaneous stretch (Zi) to be the direction of maximum instantaneous shortening.*** In noncoaxial flows, orientations (α) within the external reference frame are measured from the ordinate, in the direction of shear, unless otherwise specified.

Consider a 2D velocity field, such as that corresponding to pure shear (Fig. 1). It is symmetrically divided by two mutually perpendicular directions corresponding to the *principal directions of instantaneous extension and shortening*, commonly referred to as the instantaneous stretching axes or the principal stretches. These are the directions of maximum and minimum rates of change in length (strain rate) of material lines, referred to as the *maximum and minimum instantaneous stretching axes*. Within this velocity field, the rotation of material lines can be measured with respect to the instantaneous stretching axes.

Rather than the rotation of individual material lines within a velocity field, consider now the averaged angular velocity of all material lines. This can be determined by taking the average of the angular velocities for any two perpendicular lines and applying the convention that the angular velocity of a clockwise rotation is of opposite sign to that of an anticlockwise rotation (Fig. 8). In the case of pure shear, the averaged angular velocity of material lines, measured with respect to the instantaneous stretching axes, is clearly zero. This flow type is *coaxial*. The term derives from the fact that the averaged angular velocities of the two perpendicular material lines which coincide with the instantaneous stretching axes is zero (Fig. 8); therefore they must remain parallel to the instantaneous stretching axes from one instant to the next during progressive deformation (Fig. 3, 4).

Consider now another type of flow, commonly referred to in the geological literature. The velocity field for simple shear is much simpler than that for pure shear (Fig. 1). Although the flow pattern is very different to that for pure shear, the two are nevertheless related. A finite deformation resulting from progressive simple shear can be considered as an increment of pure shear combined with an increment of rigid body rotation (Fig. 3, 4). It is the component of rigid body rotation that transforms the complex velocity field of pure shear into the simple pattern for simple shear.

We can also express the difference between the pure and simple shear flow types by considering the orientation of material lines of zero angular velocity with respect to the velocity field (Fig. 5). Whereas in pure shear such lines lie parallel to the instantaneous stretching axes, in simple shear they lie parallel to the flow plane. In other words, in progressive pure shear the instantaneous stretching axes are fixed to material points, whereas in progressive simple shear, the flow plane is fixed to material points (Fig. 9). Given that the angular velocity of the material line normal to the flow plane is non-zero, the averaged angular velocity of all material lines in progressive simple shear must be non-zero (see Fig. 8). As a consequence, material lines rotate through the direction of the fixed instantaneous stretching axes, towards the direction of the flow plane. Because the same material lines do not remain parallel to the instantaneous stretching axes (Fig. 3, 4), the flow is *noncoaxial*. The rotational component of the flow reflected by the averaged angular velocity of material lines with respect to the instantaneous stretching axes is referred to as the *shear-induced vorticity* ('internal vorticity' of Means et al., 1980; Fig. 10). This vorticity can be either positive or negative; the 'sign' of the vorticity of the flow is more generally referred to as the *sense of shear*.

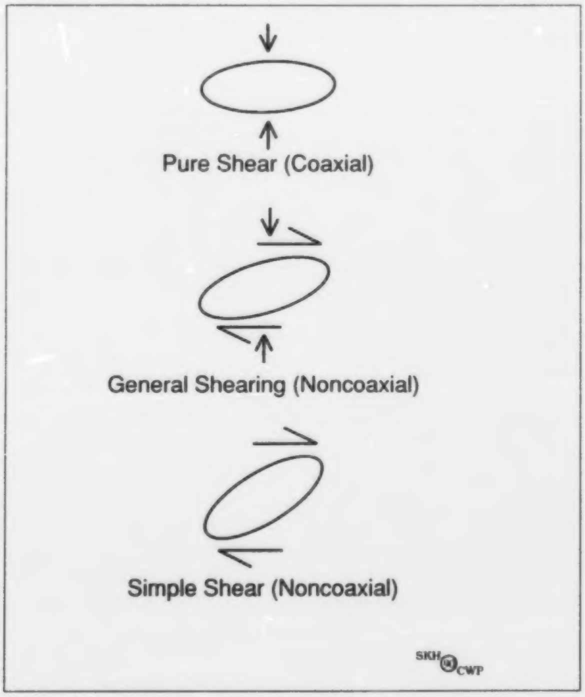

Figure 6. Kinematically indeterminate strain. Shape-change or distortion (strain) is not, of itself, significant with respect to shear-sense. Exactly the same shape of finite strain ellipsoid can be produced from an initial circle by any of a number of deformation paths, coaxial or noncoaxial.

Kinematical vorticity number (W_k)

Having introduced the term *vorticity*, it is now possible to precisely characterize the nature of an homogeneous flow by referring to a quantity known as the *kinematical vorticity number*, defined in terms of the stretching rates and angular velocities of material lines. This can be illustrated graphically

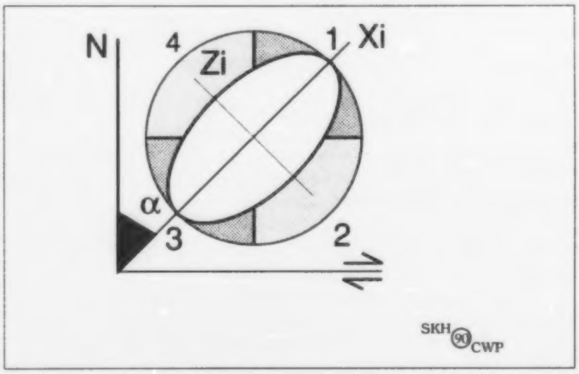

Figure 7. A frame of reference. Schematic representation of the 2D kinematic reference frame for noncoaxial simple shear flow used in this paper. The shear plane of the flow and its normal (N) represent the abscissa and ordinate of the *external reference frame*. The instantaneous stretching axes (X_i,Z_i; ratios exaggerated for clarity) represent the internal reference frame. Orientations (α) are measured with respect to N, in the same direction as the sense of shear. The numbered quadrants are fields of infinitesimal extension (1 and 3) and shortening (2 and 4) delimited by the lines (planes in 3D) of zero instantaneous stretch, shown here in positions corresponding to the special case of simple shear. The order of the quadrant numbers follows the direction of the sense of shear.

Rotations are expressed in terms of angles measured with respect to a reference frame. The observer may select several reference frames and can allow for the rotation of one with respect to another. However, of the several reference frames, one must be fixed with respect to the observer; throughout this contribution, the fixed reference frame is parallel to the flow plane and its normal. Rotations described with respect to the fixed, or external, reference frame are 'external rotations'. Rotations described with respect to the *internal reference frame* are 'internal rotations'.

This contribution is concerned with two-dimensional general noncoaxial flows; in other words, simple shear plus a component of shortening across the flow plane, accommodated by extension along the flow direction. Therefore, we set the abscissa and ordinate of the external reference frame parallel to the directions of maximum and minimum instantaneous extension of the pure shear component of any flow. In continuum mechanical terms, the flow planes of both the coaxial and the noncoaxial components of any flow are set parallel to the abscissa. The interested reader will find a more detailed discussion of, and a different perspective on, reference frameworks in structural geology in Passchier (1987a).

as follows. Consider again the velocity field for pure shear (Fig. 1). The rate at which material lines change length and their angular velocity are both a function of orientation with respect to the instantaneous stretching axes of the flow (Fig. 5). If we plot the stretching rates and the angular velocities of material lines against orientation with respect to the directions of zero instantaneous stretching rate of the flow, we see that they plot as two sine curves, out of phase by 45° (Fig. 11). In other words, the faster a material line changes length, the slower it rotates. The two curves each have maximum and minimum values, corresponding to the instantaneous stretching axes in the one case and the directions of maximum and minimum angular velocity in the other. The curves pass from negative space into positive space, representing extension and shortening on the one hand and clockwise and anticlockwise rotations on the other. Note also that, since both curves cut the abscissa twice, there are two directions of zero angular velocity and two direction of zero instantaneous change in length in the flow (see also Fig. 5). In pure shear, material lines parallel to the instantaneous stretching axes do not rotate at all.

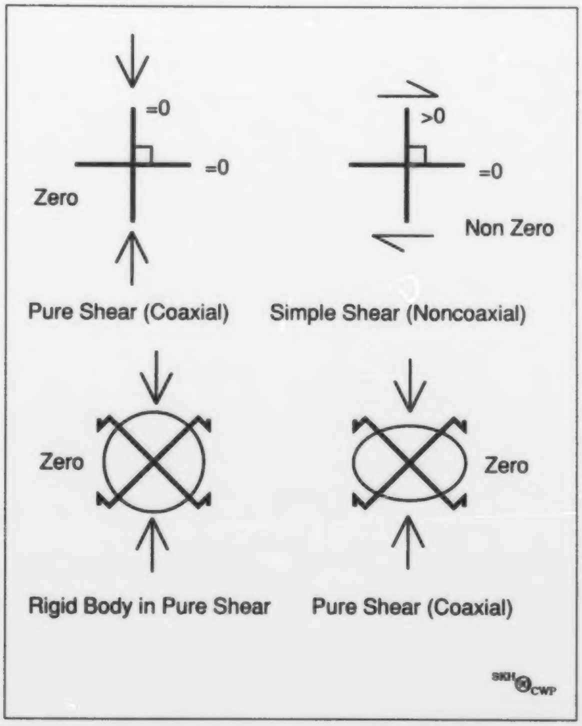

Figure 8. Averaged angular velocity. Taking the margins of the page as the external reference frame, the averaged angular velocity of any flow is the sum of the angular velocities of any two mutually perpendicular lines. In this illustration, we have assumed zero spin (see Fig. 10 and 13). In pure shear, the angular velocities of all such pairs of lines sum to zero, be they parallel (top left) or oblique (bottom row) to the instantaneous stretching axes. This is true whether the volume in question deforms (bottom right) or not (bottom left). In noncoaxial flow, such as simple shear (top right), the line parallel to the flow plane has zero angular velocity, but its normal rotates with the same sense as the bulk shear. Therefore, the averaged angular velocity is non-zero.

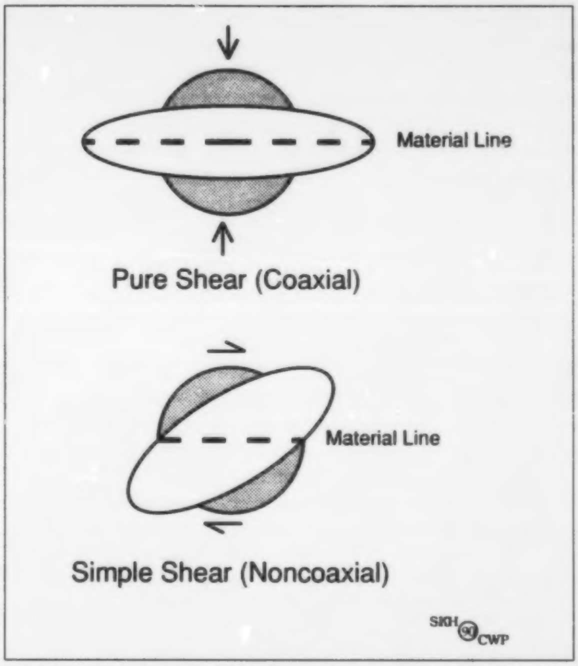

Figure 9. Fixed material lines. Most material lines rotate with progressive deformation, towards the direction of zero angular velocity which lies within the extensional quadrants of the flow. In each flow type there are diagnostic exceptions. In progressive pure shear, the instantaneous stretching axes are fixed to material points (lines) within the deforming material. In progressive simple shear, the flow plane is fixed to material points (lines). It is this difference which determines that, with progressive shape change, the finite strain ellipsoid rotates in simple shear, but not in pure shear (see text).

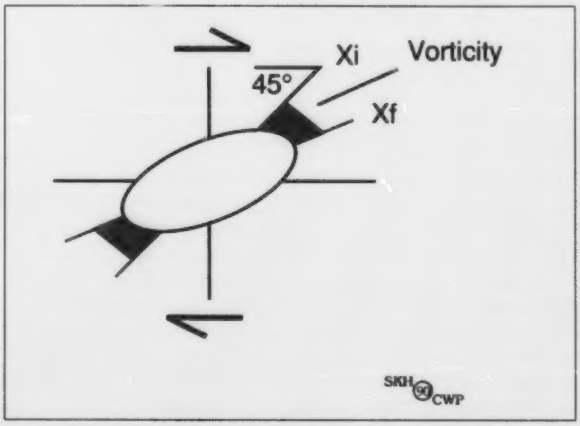

Figure 10. Shear-induced vorticity. In noncoaxial flows, such as simple shear, material lines rotate with respect to the instantaneous stretching axes during progressive deformation. This is termed shear-induced vorticity. In the illustration, the principal finite extension (X_f) has rotated with respect to the maximum instantaneous stretching axis (X_i), in the same sense as the bulk imposed shear (arrows). X_i remains fixed at 45° to external reference frame, represented by the flow plane.

Let us now perform the same operation for simple shear, noting that in this case plotting the stretching rates and angular velocities of material lines against orientation with respect to the directions of zero instantaneous stretching rate is equivalent to plotting with respect to the normal to the flow plane (Fig. 11). We find that the curve representing the stretching rates of material lines has the same form as that for pure shear, but the curve of angular velocities now lies entirely in positive space. This reflects the fact that, in simple shear, lines rotate in one direction only. Graphically, the curve of angular velocities of material lines has been shifted vertically compared with the case of pure shear. Notice that

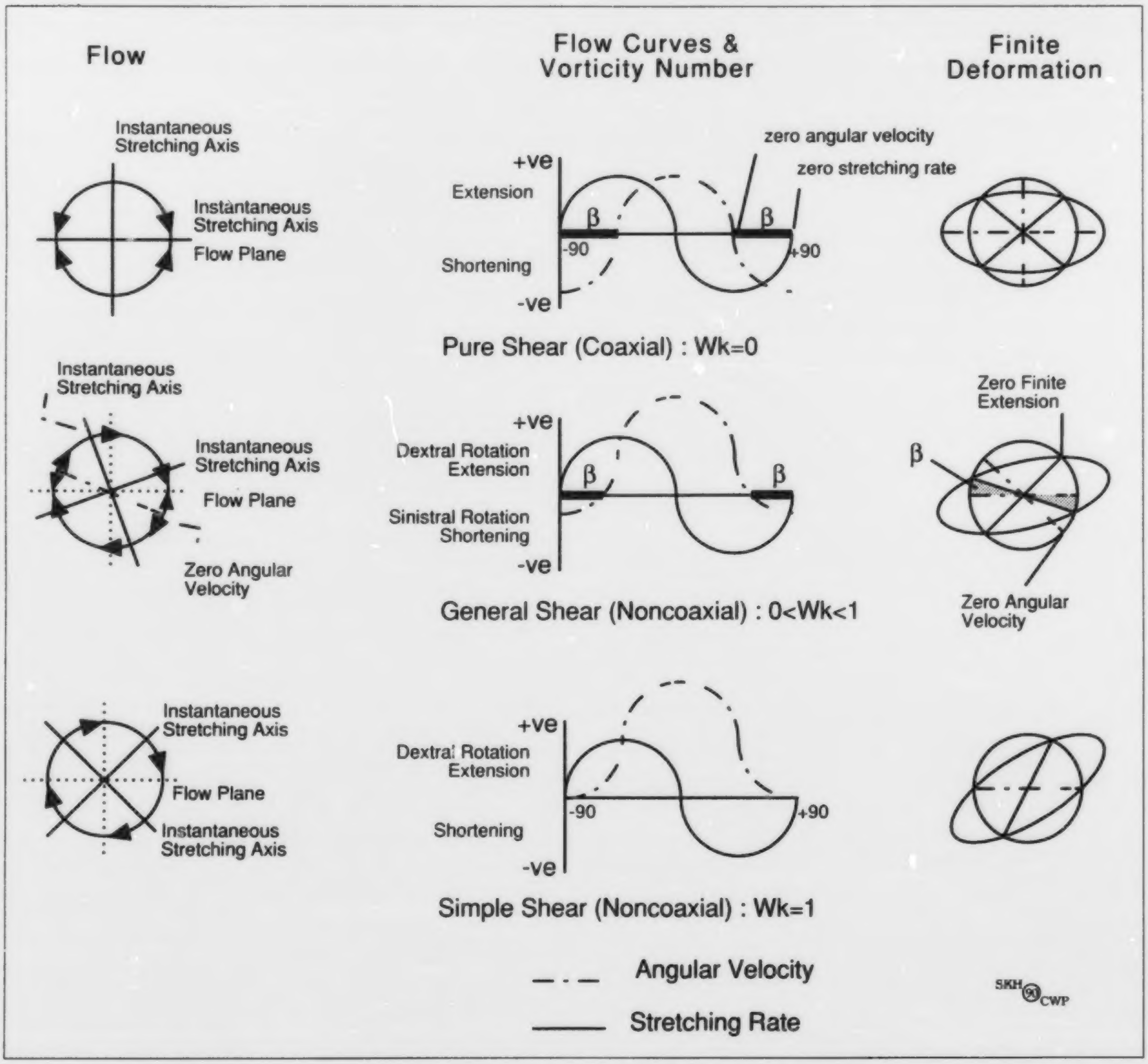
Flow
Flow Curves & Vorticity Number
Finite Deformation
Instantaneous Stretching Axis
Instantaneous Stretching Axis
Flow Plane
zero angular velocity
zero stretching rate
+ve
Extension
β
β
-90
+90
Shortening
-ve
Pure Shear (Coaxial) : Wk=0
Instantaneous Stretching Axis
Instantaneous Stretching Axis
Flow Plane
Zero Angular Velocity
+ve
Dextral Rotation Extension
β
β
Sinistral Rotation Shortening
-ve
General Shear (Noncoaxial) : 0<Wk<1
Zero Finite Extension
β
Zero Angular Velocity
Instantaneous Stretching Axis
Flow Plane
Instantaneous Stretching Axis
+ve
Dextral Rotation Extension
-90
+90
Shortening
-ve
Simple Shear (Noncoaxial) : Wk=1
Angular Velocity
Stretching Rate
SKH 90 CWP

Figure 11. Kinematical vorticity number (W_k). Flow types can be described in terms of the angular velocity and stretching rate (instantaneous change in length) of material lines as a function of orientation with respect to the direction of zero stretching rate. For each flow type, curves for angular velocity and for stretching rate of material lines are drawn (centre). With increase in noncoaxiality, the angular velocity curve migrates upwards, while that for stretching rate remains fixed and the minimum angular distance β between orientations of zero angular velocity decreases (thick line). The kinematical vorticity number $W_k = \cos(\beta)$ is therefore a direct measure of the noncoaxiality of the flow. Note that the symmetry of coaxial pure shear flow is orthorhombic, while all noncoaxial flows are monoclinic (left). Note also that for general noncoaxial flows ($0 < W_k < 1$), there exists a subsidiary angular field of rotation antithetic to the bulk imposed shear-sense (middle left). The orientations of the directions of zero angular velocity and zero finite change in length with respect to the finite strain ellipsoid are also shown for various deformation paths (right). Note that the flow plane is also a direction of zero angular velocity in all flow types.

the single direction of zero angular velocity of material lines now lies at 45° to the instantaneous stretching axes of the flow, and coincides with one of the directions of zero change in length (Fig. 5).

Assuming no change in the area of the deforming surface of observation, we can now use the variable form of the angular velocity curve to precisely identify different flow types. In Figure 11, because of the vertical shift of the curve of angular velocity, the minimum angular distance (β) between the two directions of zero angular velocity varies from 90° to 0°. In pure shear, β is 90°. In simple shear β is 0°. Now it is possible to define the quantity

$$W_k = \mathrm{Cos}(\beta)$$

as the kinematical vorticity number (Means et al., 1980; Passchier, 1986, 1987a), where $W_k=0$ for pure shear and $W_k=1$ for simple shear. Intermediate values of W_k ($0<W_k<1$) describe *general noncoaxial flows*. This flow type may also be referred to as a general flow, general shearing flow, rotational flattening (e.g. Choukroune and Lagarde, 1977), noncoaxial bulk inhomogeneous flattening (Bell, 1981, 1985) or non-ideal flow (Hanmer, 1990); we will confine ourselves to the term general noncoaxial flow. It can be considered as a combination of the two end-member flow types, i.e. simple shear plus a variable component of pure shear (Fig. 3), wherein the maximum instantaneous stretching axis of the pure shear component is set parallel to the flow direction of the simple shear component. Some authors have adopted a different method to express the combination of pure and simple shear in a general noncoaxial deformation path. Ghosh and Ramberg (1976) describe a pure shear/simple shear strain rate ratio (Sr), where Sr = 0 for simple shear and Sr = ∞ for pure shear.

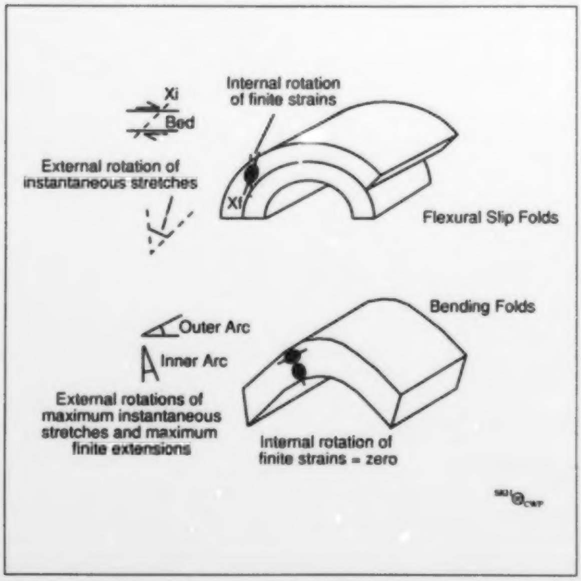
Xi
Bed
Internal rotation of finite strains
External rotation of instantaneous stretches
Xi
Flexural Slip Folds
Bending Folds
Outer Arc
Inner Arc
External rotations of maximum instantaneous stretches and maximum finite extensions
Internal rotation of finite strains = zero

Figure 12. Internal versus external rotation. The rotational behaviour of the finite strain ellipsoid within the fold limbs of two common types of fold, derived at the expense of initially horizontal layers, serves to illustrate the concept of internal and external rotations. In a bending fold, the instantaneous stretching axes in the inner and outer arcs of the fold remain fixed with respect to the boundaries of the deforming layer. However, as the fold develops, the fold limb itself rotates with respect to the Earth's surface. We can say that while the finite strains show no internal rotation with respect to the instantaneous stretching axes, the latter show an external rotation with respect to the horizon. In the case of a flexural slip fold, the finite strains do rotate with respect to the instantaneous stretching axes. Thus we can say that the internal rotation of the finite strains is to some degree countered by an opposing external rotation of the instantaneous stretching axes.

Spin

In the foregoing discussion of vorticity, we have implicitly taken the instantaneous stretching axes of the flow as our frame of reference, against which to measure the rotation of material lines (Fig. 3). However, this ignores the possibility of rotation of material lines with respect to an *external reference frame*. Therefore, let us now suppose that the flow is itself rotating with respect to an external reference frame; the length and width of the page for example. We could now describe the rotation of material lines in two ways: an *internal rotation* with respect to the instantaneous stretching axes of the flow and an *external rotation* with respect to an external reference frame (Fig. 12). The external reference frame is usually taken to be fixed with respect to the observer. Rotation of the instantaneous stretching axes of the flow with respect to the sides of the page would add a uniform angular velocity to all material lines, even in the case of coaxial pure shear. The technical term for the rotation of the instantaneous stretching axes with respect to an external reference frame is *spin* (Fig. 13).

From Figure 12, it is obvious that coaxial flows can spin. Accordingly, material lines have a non-zero averaged angular velocity with respect to the external reference frame; in this case the horizontal and the vertical. Such a flow or progressive deformation path is referred to as *rotational*. Note that the rotational component ('external vorticity' of Means et al. (1980)) of the flow can be accommodated either by shear-induced vorticity, by spin, or a combination of the two (Fig 13). Let us now consider two geological examples by way of illustration of these concepts. In Figure 14, a volume of rock on the flat of a ductile thrust zone is subjected to progressive noncoaxial, non-spinning deformation. Material lines rotate with respect to the instantaneous stretching axes (shear-induced vorticity), but the instantaneous stretching axes remain fixed with respect to the thrust plane and the observer. Figure 15 on the other hand illustrates a case of spinning, noncoaxial progressive deformation. We have chosen the case of a fold limb dominated by flexural flow, wherein the clockwise shear-induced vorticity is more or less balanced by the anticlockwise rotation of the evolving fold limb. Ideally, this could result in an *irrotational*, noncoaxial, spinning deformation path.

Let us now summarize the foregoing discussion. Noncoaxial deformation paths, except under very special circumstances, are rotational. Coaxial deformation paths may be irrotational. However, unless the geologist can be certain of all the boundary conditions, it must be borne in mind that coaxial deformation paths may well be rotational. It is the rotational component of a deformation path which now concerns us. The rotational component of a progressive coaxial deformation can only be due to the spin of the instantaneous stretching axes with respect to the external reference frame. In a non-spinning progressive simple shear deformation, the rotational component is entirely due to the shear-induced rotation of material lines, or shear-induced vorticity. The important point here is that, in progressive deformation, the averaged angular velocity of material lines with respect to an external reference frame (rotational component) can be accomplished either by shear-induced vorticity or by spin.

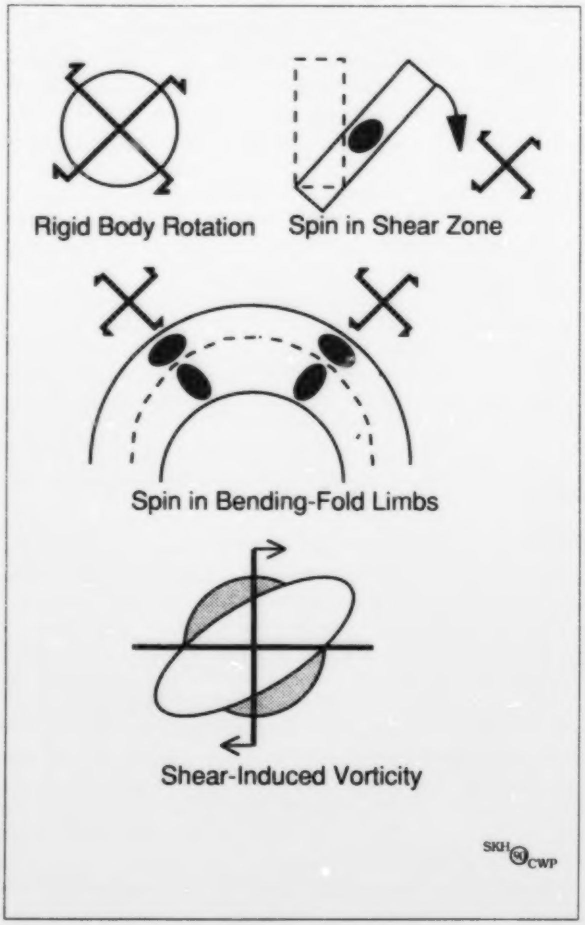
Rigid Body Rotation
Spin in Shear Zone
Spin in Bending-Fold Limbs
Shear-Induced Vorticity
SKH CWP

Figure 13. The rotational component of the flow is the averaged angular velocity of material lines with respect to an external reference frame. This can be accommodated in a number of ways. Spin is the rotation of the instantaneous stretching axes with respect to the external reference frame, whereas shear-induced vorticity is the rotation of material lines with respect to the instantaneous stretching axes. Consider some geological examples. A rotating rigid body spins, but its constituent material lines undergo no shear-induced vorticity. A set of deformable domino-like blocks in a shear zone may spin without shear-induced vorticity. The limbs of a bending fold develop with spin, but little or no shear-induced vorticity (see Fig. 12). However, material lines in a ductile shear zone deformed by progressive simple shear are subjected to shear-induced vorticity without spin (see Fig. 10).

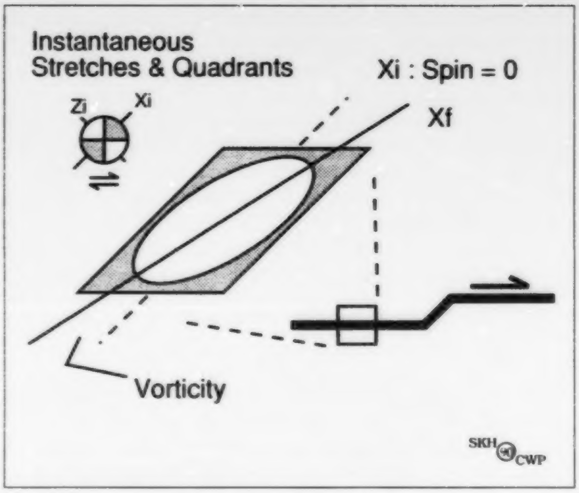
Instantaneous
Stretches & Quadrants
Xi : Spin = 0
Zi
Xi
Xf
Vorticity
SKH CWP

Figure 14. Noncoaxial non-spinning flow. Material lines (X_f) subjected to progressive simple shear on the non-rotating flat of a linked ductile thrust system rotate with respect to instantaneous stretching axes (X_i) which are fixed with respect to the horizon. The rotational component of the flow is entirely accommodated by shear-induced vorticity with zero spin.

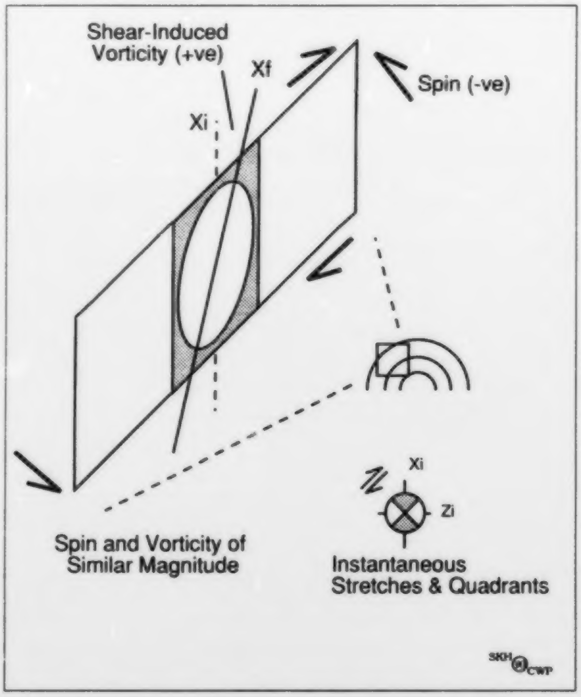
Shear-Induced
Vorticity (+ve)
Xf
Spin (-ve)
Xi
Xi
Zi
Spin and Vorticity of
Similar Magnitude
Instantaneous
Stretches & Quadrants
SKH CWP

Figure 15. Noncoaxial spinning flow. Material lines (X_f) subjected to progressive simple shear on the limb of a flexural slip fold rotate clockwise with respect to instantaneous stretching axes (X_i) which are fixed with respect to the deforming layers (shear-induced vorticity). However, as the fold develops, the limb and the instantaneous stretching axes rotate anticlockwise with respect to the horizon (spin). If the two rotational components cancelled each other, the material lines would have zero angular velocity with respect to the external reference frame and the deformation path would be irrotational.

In most flows, the velocity field is divided into separate domains of clockwise and anticlockwise rotation of material lines by the directions of zero angular velocity (Fig. 5, 11). The domain of clockwise rotation is equal in size to that of anticlockwise rotation in pure shear, whereas only one rotation sense pertains in simple shear. However, in general noncoaxial flows, although most material lines will rotate with the same sense as the vorticity of the bulk flow, material lines oriented in the acute angular field bounded by the two directions of zero angular velocity rotate antithetically. The size of the field of antithetic rotation increases with increasing deviation from simple shear; in other words as W_k increases from 0 to 1. Clearly the geologist must understand the relationship between orientation and flow type in order to successfully deduce the shear-sense of the bulk flow from local observations of the rotational behaviour of material lines.

Progressive deformation

So far we have concentrated on the instantaneous velocities and stretching rates of material lines in flow. Now consider what happens to material lines subjected to an invariant, volume-constant flow type over a finite period of time. In all flow types we can identify directions of zero angular velocity of material lines as well as directions of zero instantaneous stretch (Fig. 5, 11). Directions of zero instantaneous stretch separate quadrants of instantaneous extension (e.g. boudinage)

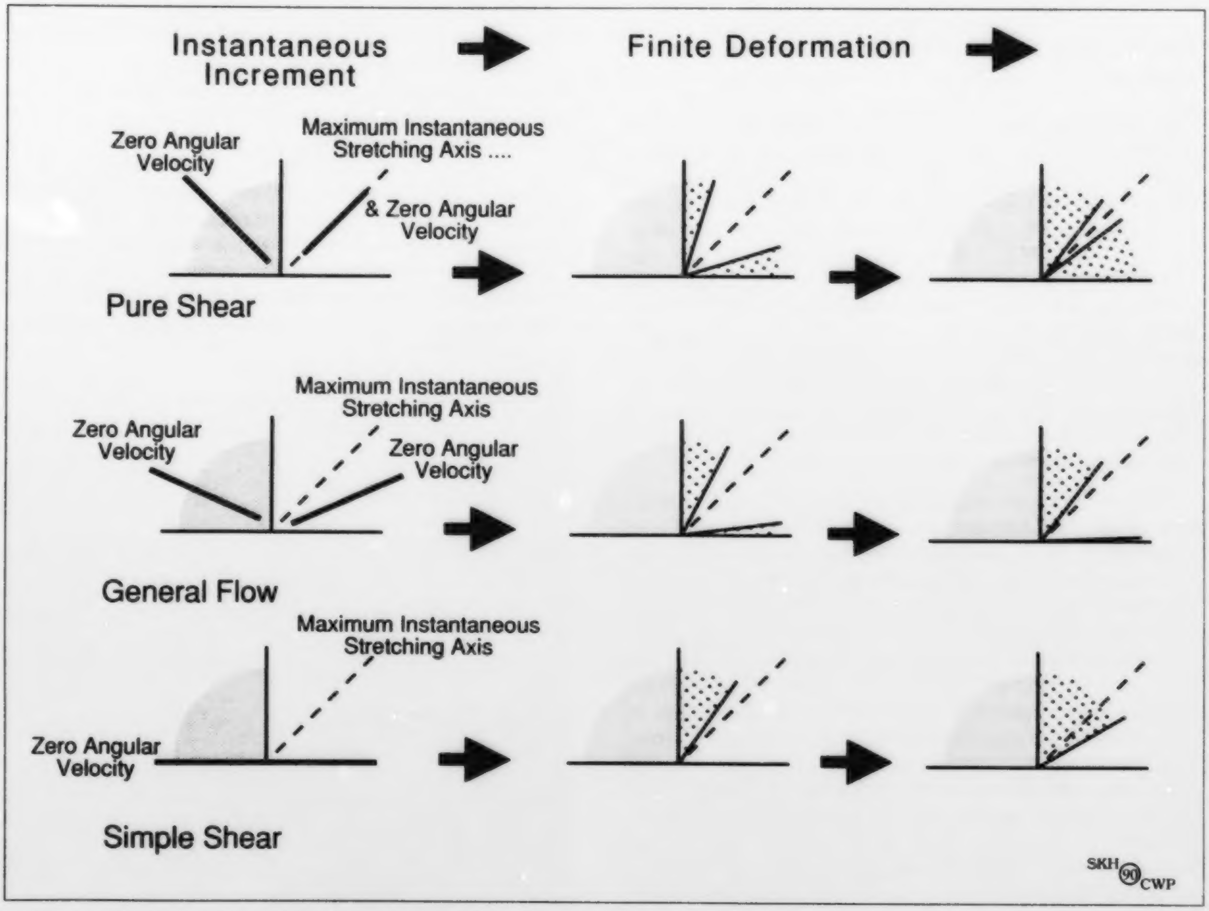
Instantaneous Increment
Finite Deformation
Zero Angular Velocity
Maximum Instantaneous Stretching Axis ....
& Zero Angular Velocity
Pure Shear
Maximum Instantaneous Stretching Axis
Zero Angular Velocity
Zero Angular Velocity
General Flow
Maximum Instantaneous Stretching Axis
Zero Angular Velocity
Simple Shear
SKH 90 CWP

Figure 16. Progressive extension and shortening. At any instant in flow, there are two quadrants of instantaneous shortening (fine dots) and two quadrants of instantaneous extension (white; see Fig. 3 and 7). In the three flows illustrated here (left), only two quadrants are shown, separated by the directions of zero stretching rate (vertical and horizontal lines). All of the flow types are oriented such that their maximum instantaneous stretching axis (dashed) is fixed with respect to the reader. For each flow type, two increments of finite strain are drawn (centre and right). Since, for any flow, lines rotate from the shortening quadrants to the extensional quadrants of the flow, the angular width of the latter decreases with progressive deformation as a third field opens up comprised of lines which, having initially been shortened, are subsequently extended (coarse dots). This is the field of boudined folds. *Note the absence of a field of folded boudins.* In noncoaxial flows, material lines rotate with respect to the instantaneous stretching axes (lower right). Hence, with respect to the instantaneous stretching axes, the finite deformation resulting from noncoaxial deformation paths reflects the monoclinic symmetry of the flow types, whereas progressive pure shear reflects the orthorhombic symmetry of coaxial flow. Directions of zero angular velocity are shown for passive markers (left).

and shortening (e.g. folding). Since material lines rotate with progressive deformation from the instantaneous shortening quadrant into the instantaneous extensional quadrant, there exists an intermediate domain wherein lines which were initially shortened have subsequently been extended, but not vice versa (Fig. 16). In progressive pure shear, the disposition of the directions of zero angular velocity and of zero finite change in length is symmetrical about the instantaneous stretching axes (Fig. 11). Such a flow has orthorhombic symmetry. On the other hand, the symmetry of all noncoaxial flows is monoclinic. The symmetry of the flow type is directly reflected in the symmetry of the finite deformation (Fig. 16) and *it is by identifying the symmetry of the flow from that of the the finite deformation structures and fabrics available to us as geologists that we deduce the sense of shear.*

Partitioning of the rotational component of the flow

Pure and simple shear are two ideal end-members of a range of more general flow types. This range of flow types represents a spectrum from irrotational to more rotational flows. Alternatively, we could consider the range of flow types as representing a spectrum of ratios of shear-induced vorticity to spin. In other words, shear-induced vorticity may be converted into spin (and vice versa) to produce the same rotational component in progressive deformation. Thus we can speak of the rotational component of the flow being *partitioned* between shear-induced vorticity and spin. Moreover, we can consider situations where, due to changes in material properties and boundary conditions, the nature of the partitioning may change such that the rotational component is *repartitioned* between shear-induced vorticity and spin.

Why is the notion of partitioning of the rotational component of the flow between shear-induced vorticity and spin important to us as geologists? Geologists often deal with tectonic features whose boundaries are determined at a scale very much broader than that at which their observations are made. This has undoubtedly drawn geologists to continuum mechanics, of which a principal axiom is that in a continuous, homogeneous isotropic medium, flow at all scales must reflect the displacements at the boundaries of the system in order to satisfy the requirements of strain compatibility. However, rocks are not continuous media. They are granular aggregates, with discontinuities and layers of different rheological properties represented at a variety of scales. As we shall now see, deviations from material ideality influence the partitioning of the rotational component of the flow and hence determine what the geologist will observe at any given scale.

KINEMATIC FRAMEWORK

Orienting the flow in the field

Most field geologists are familiar with the axiom that slaty cleavage lies subparallel to the XY plane of the finite strain ellipsoid and is therefore perpendicular to the principal direction of finite shortening. While there are grounds for questioning the simple identity of cleavage and extension lineation with principal planes (XY) and directions (X) of the finite strain ellipsoid (e.g. Schwerdtner, 1973a; Williams, 1976, 1977; Hobbs et al., 1976), the closeness of the approximation (Ghosh, 1982; Treagus, 1983), coupled with its practical usefulness in the field, lead many to find it an acceptable compromise.

Kinematic indicators are structures from which the geologist can make reliable inferences about flow in rocks during progressive deformation. As an example, consider the response of quartz veins to deformation as a function of their orientation with respect to the instantaneous stretching axes of the flow (Fig. 17). Veins oriented within the instantaneous extensional quadrants will boudin, whereas those oriented in the shortening quadrants will be shortened, perhaps by folding. In reality the situation is complicated by the fact that, with progressive deformation, material lines rotate from orientations where they are being actively shortened to orientations where they are being actively extended. One cannot always tell from the geometry of a folded vein whether or not it has been subjected to extension.

Shear-sense indicators are a subset of kinematic indicators which indicate the sense of shear in a progressively noncoaxially deformed material. Somewhat more technically, a shear-sense indicator is *a structure, resulting from progressive deformation, whose geometry is indicative of the progressive rotation of the finite strain axes with respect to the instantaneous stretching axes and/or the flow plane, at the scale of observation.* The reader will recognize that this is the same thing as saying that a shear-sense indicator is a structure whose geometry indicates the sense of averaged angular velocity of material lines, in other words the vorticity of the flow.

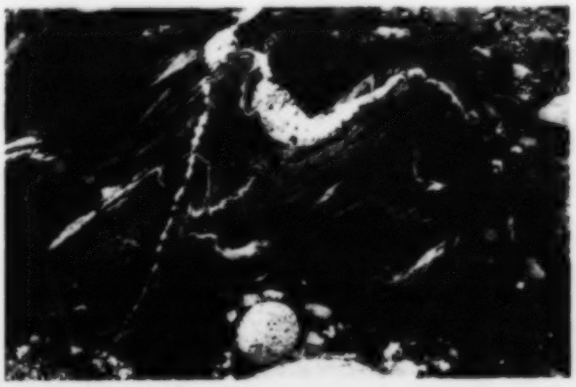

Figure 17. Kinematic indicators are structures from which the geologist can make reliable inferences about the displacement field of material particles (flow) in the rock during progressive deformation. The response of quartz veins to progressive deformation in a folded slate is a function of their orientation with respect to the extensional and shortening quadrants of the flow. Boudined veins have extended, whereas folded veins have shortened. In reality the situation is complicated by the fact that, with progressive deformation, material lines rotate from orientations where they are being actively shortened to orientations where they are being actively extended. (GSC 203942-G)

Shear plane and shear direction

As geologists dealing with the finite end-products of progressive deformation, we should not forget the essential distinction between the instantaneous flow plane and the *shear plane* of the finite deformation. Whereas the flow plane is the plane of zero angular velocity towards which most other planes rotate at any instant (Fig. 3, 4, 11), the shear plane is the mean position of the flow plane during progressive deformation. Similarly, the shear direction is the mean position of the flow direction.

How does the geologist identify the shear plane and the shear direction in the field? The problem may be fairly trivial when deflected markers are available (e.g. Ramsay, 1980a) or when the shear plane is materially manifested in the rock, as in C/S fabrics (see section *Strain-sensitive fabrics*). Until quite recently, geologists have tended to describe most, if not all, natural shearing flows in terms of simple shear. Accordingly, it is often assumed that (i) the extension lineation measured on the ground closely tracks the shear direction in strongly strained rocks (e.g. Escher and Watterson, 1974), and (ii) that shear-sense observations should be made in the XZ plane of the finite strain ellipsoid (Fig. 18). Rather than starting from such assumptions, the geologist can determine the approximate orientation of the shear plane if a strain gradient can be identified, since the one must lie perpendicular to the other (Fig. 19; Ramsay and Graham, 1970). Alternatively, if the rocks in question are known to have undergone noncoaxial progressive deformation and if it can be demonstrated that the total finite strain is of significant magnitude, as for example in many mylonites, one may utilize the fact that all planar features rotate towards the flow plane to deduce that the shear plane is subparallel to the mylonitic foliation. In many of the illustrations in this contribution, the shear plane was identified in the field in just this manner (see Fig. 18).

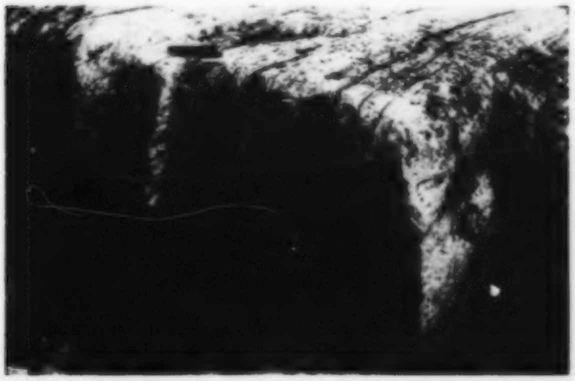

Figure 18. Kinematic framework in the field. A subhorizontal extension lineation developed on vertical foliation planes in a highly strained mylonite. Since lines rotate towards the direction of maximum extension of the finite strain ellipsoid, the orientation of the isoclinal fold (right), representing a significant increment of finite strain, confirms that the streaked-out polycrystalline aggregates and ribbons which it parallels do indeed constitute an extension lineation. Thus, the foliation is taken to lie approximately parallel the XY plane of the finite strain ellipsoid, the lineation is taken to mark the X direction. According to the simple shear model (Fig. 3 and 4), the extension lineation measured on the ground is taken to closely track the shear direction in strongly strained rocks. Therefore, if deformation results from progressive simple shear, the mylonitic foliation lies very close to the shear plane of the deformation and the lineation indicates the shear direction. Accordingly, shear-sense data should be sought on the top (XZ) surface of this outcrop. (GSC 204775-P)

There are many instances of natural deformation where the application of the principle that the observed extension lineation marks the shear direction is warranted (e.g. Michard et al., 1984; Choukroune et al., 1986; Takagi, 1986; Lacassin, 1987; Malavieille, 1987; Bossart et al., 1988; Hanmer, 1988a,b). It has been shown to apply in some complex dip-slip/strike-slip movements (Brun and Burg, 1982; Van den Driessche, 1986a; Mattauer and Collot, 1986; Burg et al., 1987; Schmid et al., 1987). Indeed, it has been demonstrated in natural examples of flow in salt (Talbot, 1979) and in ice (e.g. Hudleston, 1983). Some workers have even attempted to show that the extension lineation can track drastic changes in the shear direction during progressive deformation (Merle and Brun, 1984; Harris, 1985; Dietrich and Durney, 1986). However, contrary to the assumption made in many of the cited studies, confirmation of this simple relationship between finite extension lineation and shear direction does not demonstrate that the deformation histories studied correspond to simple shear; the extension lineation would tend to track the shear direction even in a two-dimensional general noncoaxial flow (Fig. 3, 11). Furthermore, it is the experience of a number of workers that, at least locally, the extension lineation measured on the ground lies at an high angle to the

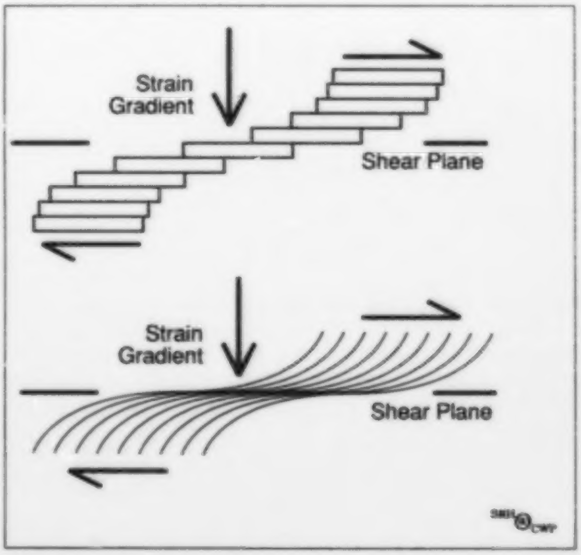

Figure 19. Strain gradient and shear plane. In a 'card-deck' model of a shear zone, corresponding to progressive simple shear, it is intuitively obvious that the strain gradient must lie normal to the shear plane . Now replace the 'card-deck' with a set of strain trajectories, and the same relationship between strain gradient and shear plane still holds true.

shear direction; a phenomenon often attributed either to systematic *three-dimensional transpression* (Harland, 1971; Sanderson and Marchini, 1984; L. Nadeau and S. Hanmer, unpub. data, 1990) or to more ad hoc explanations (e.g. Lister and Price, 1978; Ave Lallemant, 1983; Bouchez et al., 1984; Hanmer and Ciesielski, 1984; Lagarde and Michard, 1986).

The foregoing serves to emphasize that it is essential that the geologist confirm (i) that the linear structure observed is truly an extension lineation and (ii) that the lineation is subparallel to the direction of transport.

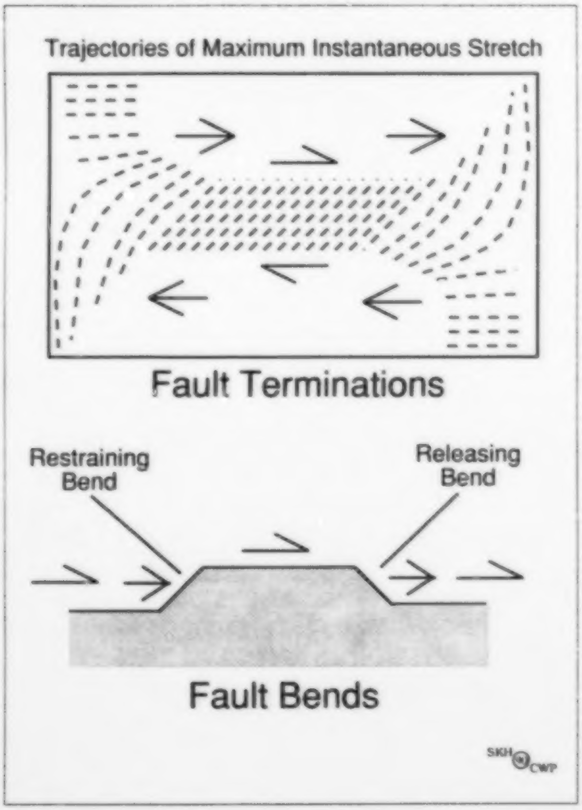

Figure 20. Fault bends and terminations. If a shear zone terminates at both ends within a continuous medium, the finite displacement characteristic of its central part must attenuate to zero at the tips. In the dextral example illustrated, this creates domains of extension normal (upper right and lower left) and parallel (lower right and upper left) to the shear plane. Even if flow in the central part of the shear zone corresponds to simple shear, flow must be of a general noncoaxial type near the terminations (see Ramsay and Allison, 1979; Ramsay, 1980a). Similarly, fault bends are analogous to fault terminations because of the decrease in slip rate at the deflection compared with the master fault plane. Bends across which a component of compression is exerted at an high angle to the local shear plane are analogous to the upper right and lower left domains of the example of fault terminations. Since this impedes slip, they are known as restraining bends. Releasing bends are analogous to the lower right and upper left domains of the fault terminations (see Sibson, 1986).

Fault bends, terminations and flow type

It is well known that, even in the simplest shear zones, flow only corresponds to simple shear in their central portions (Fig. 20). This is because most shear zones terminate within continuous media rather than at at free face, such as the Earth's surface or a tectonic plate boundary (cf. transform faults (Freund, 1974)). Therefore, the finite offset across the shear zone must attenuate to zero at its terminations. As a consequence, domains of shear-parallel compression and extension develop on either side of the terminal segments of the shear zone (Fig. 20), in violation of the boundary conditions of simple shear flow (Chinnery, 1969; Coward, 1976; Ramsay and Allison, 1979; Ramsay, 1980a; Ramsay and Huber, 1987, p. 619). Given that deflections in the trend of the shear plane lead to restraining and releasing bends (Fig. 20; Sibson, 1986) which are kinematically very similar to termination segments, in that they cause the magnitude of displacement to vary along the shear plane, we might expect that flow types and deformation paths in most shear zones will be variable.

ROTATION

Why do finite strains rotate in noncoaxial flows?

Ideal simple shear (Fig. 3, 4) is a mathematically convenient, two-dimensional representation of noncoaxial flow, which is well illustrated by the 'card-deck' model (Fig. 21). The deformation resulting from such a flow can be described as a distortion accompanied by a rigid-body rotation of the principal directions of finite strain (Fig. 4). The instantaneous stretching axes remain fixed at 45° to the flow plane (Fig. 3). *Why, with progressive deformation, do the principal directions of finite strain rotate in the sense of the imposed bulk shear, away from the instantaneous stretching axes and towards the flow plane?* (Fig. 4). There are many ways to explain this rotation, but the following is particularly materialistic. In simple shear, one of the two lines of zero stretching rate is materially attached to the flow plane (Fig. 9, 22), as in the 'card-deck' model (Fig. 21). It follows that the corresponding line of zero finite change in length is also fixed to the same material plane. Therefore, the decrease in the angle between the lines of zero finite change in length and the direction of maximum finite extension (X_f), which occurs during any finite distortion (Fig. 5, 11, 16), results in the rotation of X_f towards the flow plane.

Rotation : rate and direction

Many shear-sense indicators are composed of geometrical elements of various shapes, such as porphyroclasts, or tectonic inclusions, with attached 'wings' or tails. Since the kinematic significance of a structure is generally deduced from the relative rotations of its component parts, we shall now examine rotational behaviour of rigid inclusions in a viscous fluid in some detail (Fig. 23). For more detailed and quantitative treatments, the reader is referred to Ramberg (1975), Ghosh and Ramberg (1976), Ghosh (1977) and Passchier (1987b, 1988).

The relationship between the rotation rate of an inclusion and its orientation is partly a function of the flow type. However, the rotation rate of an inclusion is also a function of its aspect ratio. Let us consider Figure 23. In progressive simple shear all inclusions rotate with the same sense as the bulk flow. Although the rotation rate for all non-circular inclusions decreases as the long axis of the inclusion approaches the flow plane, only passive markers and inclusions of high aspect ratio come to rest in the flow plane. Since passive markers rotate both towards and away from the flow plane, their rest position is one of *unstable equilibrium*.

Deviation from simple shear introduces an angular field of *back-rotation*. In progressive general noncoaxial flow, inclusions whose long dimensions are oriented in this field rotate antithetically with respect to the bulk shear-sense (see also Fig. 11). However, the introduction of an angular field of back-rotation means that it must be separated from the field of forward rotation by positions of zero angular velocity or rotation rate (see also Fig. 11). The orientation (α) at which an inclusion can stop rotating during progressive noncoaxial deformation is a partial function of its shape (Fig. 23). Inclusions of *critical aspect ratio* (R_c) can only stop rotating at a single critical orientation (α_c). Inclusions of aspect ratio greater than R_c will rotate antithetically when their long dimensions are oriented in the angular field of back-rotation. The curves describing their rotational behaviour cut across the zero rotation rate abscissa at two orientations ($90° < \alpha < \alpha_c$ and $\alpha > \alpha_c < 180°$), representing two rest positions for each different inclusion shape. Because inclusions rotate towards aac, such orientations are positions of stable equilibrium; the latter are therefore positions of unstable equilibrium. Inclusions of aspect ratio less than R_c have no rest position and rotate continuously with the same sense as the imposed bulk shear.

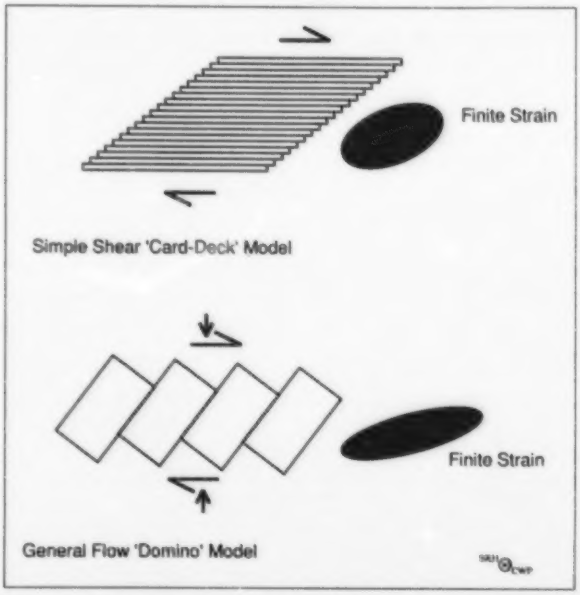

Figure 21. Rheologically controlled flow. Idealised model analogues, where the bulk deformation is entirely accommodated by slip on discrete surfaces bounding incompressible blocks or cards. Both examples represent the same angular shear (45°), but the finite strain ellipsoid in the 'domino' model results from a deformation path representing simple shear plus a component of pure shear, with consequent extension of the shear plane along the shear direction. In the 'card-deck' model, slip along the close-spaced, shear-parallel discontinuities satisfies the boundary conditions of simple shear flow. Note that the cards do not change dimension. The 'domino' or 'book-shelf' model (Freund, 1974; Mandl, 1987) involves slip along spaced discontinuities, oblique to the bulk shear plane and satisfies the boundary conditions of two-dimensional general noncoaxial flow. The illustration presented here represents the special case of discontinuities initially oriented at 90° to the bulk shear plane. Frequently, the discontinuities initiate at 70° to the bulk shear plane, in which case the 'dominoes' could rotate antithetically with respect to the imposed bulk shear. The domino model also illustrates the importance of the scale at which the flow is considered. At the scale of the boundaries between the individual dominos, the deformation path can be described as a spinning simple shear, whereas at the bulk scale the deformation path corresponds to a non-spinning general noncoaxial flow type.

The field of back-rotation, bounded by the two zero intercepts of the rotation rate curve for passive markers, opens within the angular range $90° < \alpha < 135°$, adjacent to the flow plane, and widens with decrease in W_k. The field of back-rotation opens up as the curves of rotational behaviour migrate

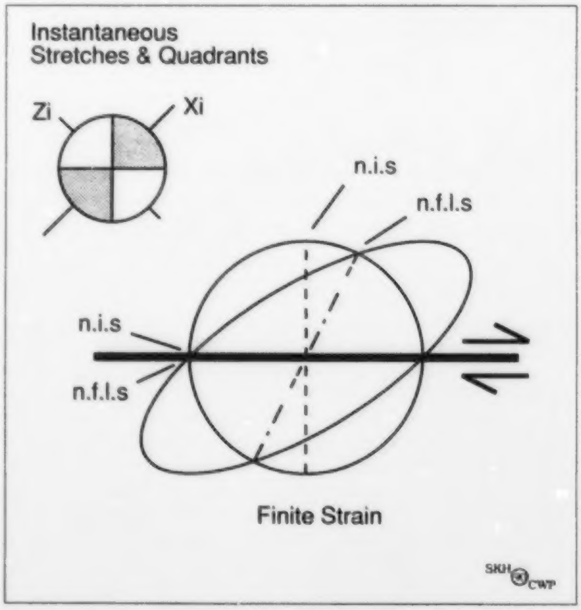

Figure 22. Zero stretching rate in the flow plane. In simple shear, one of the directions of zero stretching rate (no *instantaneous* stretch = n.i.s) lies parallel to the flow plane. Directions of zero stretching rate separate the instantaneous extensional (shaded) and shortening quadrants (white) of the flow. Given that this direction is fixed to material points within the deforming medium, it must also coincide with one of the two directions of zero finite change in length (no *finite* longitudinal strain = n.f.l.s). With progressive deformation, the angle between the two n.f.l.s decreases. Since one of them is attached to material points, the entire finite strain ellipsoid must rotate towards the flow plane as the angle decreases.

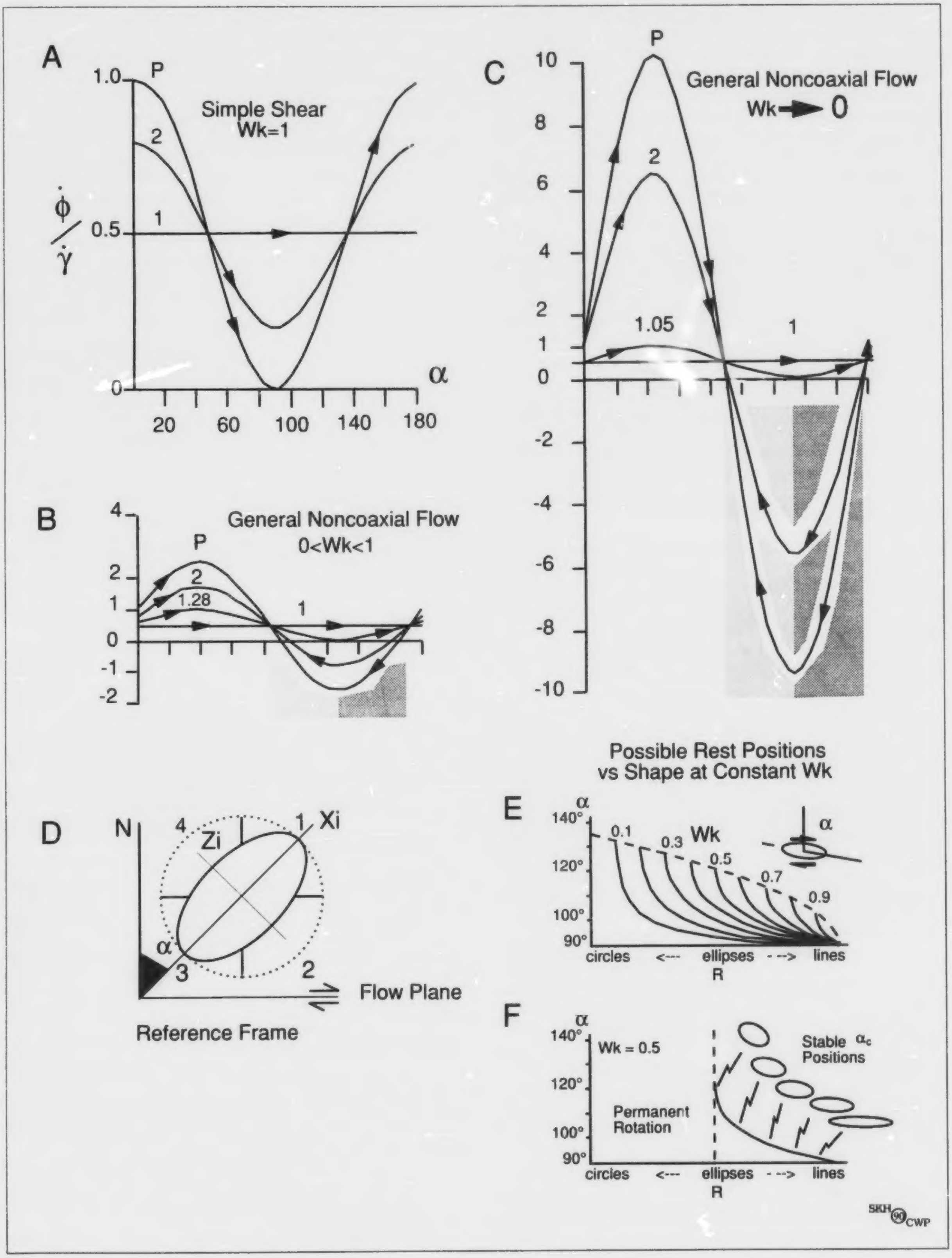
A
Simple Shear
Wk=1
φ̇/γ̇
1.0
0.5
0
P
2
1
α
20
60
100
140
180
B
General Noncoaxial Flow
0<Wk<1
P
2
1.28
1
4
2
1
0
-1
-2
C
General Noncoaxial Flow
Wk → 0
P
2
1.05
1
10
8
6
4
2
1
0
-2
-4
-6
-8
-10
D
N
4
Zi
1
Xi
α
3
2
Flow Plane
Reference Frame
E
Possible Rest Positions vs Shape at Constant Wk
α
140°
120°
100°
90°
0.1
0.3
Wk
0.5
0.7
0.9
α
circles <--- ellipses ---> lines
R
F
α
140°
120°
100°
90°
Wk = 0.5
Permanent Rotation
Stable αc Positions
circles <--- ellipses ---> lines
R
SKH 90 CWP

in $\dot{\phi}/\alpha$ space, downward and toward the right (Fig. 23). Note that the migration of the rotation rate curves is such that the left-hand rest-position for passive markers always lies at $\alpha=90°$. Consequently, with decreasing noncoaxiality of the flow, the rotational singularity for inclusions of critical aspect ratio migrates from α_c= circa 90° towards α_c= circa 135°, and the critical aspect ratio Rc approaches 1. Whereas the wavelength of the rotation rate curves is the same as that for simple shear, their amplitude is inversely proportional to W_k. Let us illustrate the consequences of this by considering two cases of flow characterized by *identical components of simple shear*. A passive marker in simple shear attains its maximum rotation rate when oriented at $\alpha=0°$. In contrast, a passive marker subjected to a general noncoaxial flow of $0<W_k<<1$, attains an order of magnitude greater maximum rotation rate, but when oriented at α= circa 45°. Note the "flight from $\alpha>\alpha_c$": the rotation of inclusions is such that they rotate away from positions of unstable equilibrium $\alpha>\alpha_c$) towards positions of stable equilibrium $\alpha<\alpha_c$).

The fact that, for a given flow type, the rotation rate ($\dot{\phi}$) of an inclusion is a function of both its aspect ratio (R) and its orientation (α), has very important geological consequences (Fig. 23). For example, the apparent or relative rotation of an equant inclusion with respect to the foliation of its enclosing matrix is taken by some geologists to directly indicate the bulk shear-sense of the progressive deformation; but consider Figure 23. In any given flow, all of the rotation rate curves pass through two common cross-over or inflection points, the orientations of which are a function of the flow type. Thus in simple shear ($W_k=1$), a passive marker oriented at $0°<\alpha<45°$ rotates faster than an equant inclusion, whereas the relative rotation rates are inverted if the passive marker lies at $45°<\alpha<90°$. However, now compare the preceding observation with the relative rotation rates for inclusions and markers at $0°<\alpha<45°$ and $45°<\alpha<90°$ for a general noncoaxial flow ($0<W_k<<1$, Fig. 23); the relative rotation rates ($\dot{\phi}$) of inclusions and markers, for most orientations ($0°<\alpha<90°$), are inverted. The tangible consequence of this is that, in a structure composed of geometrical elements of different shapes, *the relative or apparent finite rotation observed between the elements is not only a partial function of their aspect ratios (R) and of the flow type, but also of their initial orientations and subsequent rotation history.*

PARTITIONING AND REPARTITIONING

The foregoing theoretical review of flow should convey the message that intuitive or empirical deduction of the kinematic significance of a structure from its geometry alone is an hazardous undertaking (cf. Choukroune et al., 1987). However, the discussion has so far focused only on rotational behaviour in homogeneous deformation. We shall now examine the situation where the distribution of the components of the flow within the deforming material is heterogeneous. In this discussion, as elsewhere in this paper, we shall refer to deforming media as 'continuous' or 'discontinuous' (Berthé et al., 1979a; Vialon, 1979; Sirieys, 1984; Cobbold et al., 1984). These terms refer to the presence or absence of material discontinuities which permit or provoke discontinuities in the particle velocity field during progressive deformation.

Isotropic media

In cases where the bulk flow deviates from simple shear, the rotational component can be locally *partitioned* between shear-induced vorticity and spin (Fig. 24, 25), to the point where either

Figure 23 (opposite). **Rotation of inclusions and markers**. Calculated curves and pictorial illustrations of the ideal rotational behaviour of rigid inclusions and passive markers set in a Newtonian viscous matrix. The idealized curves should only be taken as a guide to the behaviour of natural examples where the inclusions may not be rigid and the matrix viscosity may not be Newtonian. The rotational behaviour is represented in terms of rotation rate $\dot{\phi}$ (normalized to the shear strain rate $\dot{\gamma}$) and orientation (α) with respect to the flow plane normal. Curves are presented for three flow types; simple shear (A) and two general noncoaxial flow types, $0<W_k<1$ (B) and $0<W_k<<1$ (C). Aspect ratios of inclusions (R) are indicated on the curves; the rotational behaviour of a rigid inclusion whose aspect ratio is greater than about 6 is essentially the same as that of a passive marker (P). Arrows on curves indicate the sense of rotation of the inclusions. (D) shows the kinematic reference frame for the graphs; X_i and Z_i are maximum and minimum instantaneous stretching axes, the ellipse is an exaggerated representation of instantaneous strain ellipse. (E) and (F) are graphs showing the possible rest positions of inclusions as a function of R, W_k and α.

In progressive simple shear (A), all inclusions rotate with the same sense as the imposed shear. The rotation rate for all non-circular inclusions decreases as the long axis of the inclusion approaches the flow plane ($\alpha=90°$) and only passive markers and inclusions of high aspect ratio (curve P) come to rest in the flow plane at positions of unstable equilibrium. In general flow types ($0<W_k<1$), there is an angular field of back-rotation, wherein inclusions rotate antithetically with respect to the bulk shear-sense. There is a *'critical'* aspect ratio, below which inclusions rotate permanently and above which they cease rotating at positions of either stable or unstable equilibrium (E and F). The R_c values for the general noncoaxial flow types illustrated here are 1.28 (B) and 1.05 (C) respectively. The stable positions are unique for specific R_c and W_k values (F). For material lines (passive markers), they coincide with the directions of zero angular velocity, one of which is parallel to the flow plane ($\alpha=90°$). For elliptical objects with R exceeding R_c, they lie between the two directions of zero angular velocity. Note that whereas the wavelength of the curves is the same as that for simple shear, their amplitudes are inversely proportional to to W_k. Note also that the rotational pattern in general shearing flow is such that inclusions rotate away from rest-positions of unstable equilibrium (darker shading) towards the rest-positions of stable equilibrium (lighter shading). Adapted and modified from Ghosh and Ramberg (1976), Hanmer (1984a) and Passchier (1987b).

one of these two components may tend towards a zero value. *Repartitioning* can occur in nature if the local conditions of flow change with time. Consider three hypothetical examples.

(i) First, if a layer of material were to weaken with respect to slip, while it lost its ability to accommodate shortening across the flow plane, it would no longer be able to accommodate a flow which deviated from simple shear. A geological example might be the concentration of aligned phyllosilicates by preferential removal of more soluble quartz through a process of mass transfer (e.g. White and Knipe, 1978; see Fig. 21).

(ii) Alternatively, if a layer were to develop the ability to accommodate extension parallel to the flow plane, its response to the imposed bulk flow could change such that W_k decreased. A geological example might be the development of fractures or discrete shears oblique to the bulk flow plane (e.g. White et al., 1980; Hanmer, 1989; see Fig. 21).

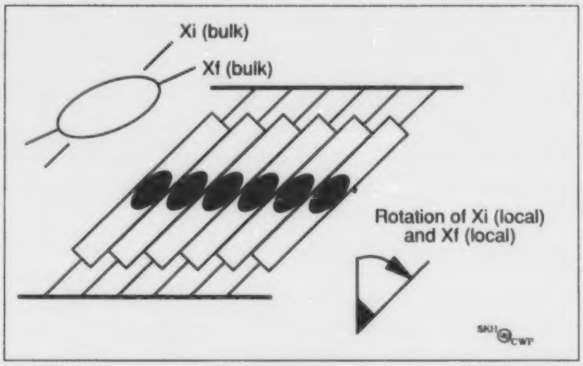

Figure 24. Rotating anisotropy and flow partitioning. A model shear zone with a set of internal, inclined planes of easy slip (anisotropy) to illustrate the principles of repartitioning of the rotational component of the flow between shear-induced vorticity and spin. Deformable sheets are attached by swivel joints to rigid walls. The walls are displaced dextrally according to the boundary conditions of bulk ideal simple shear. Had the shear zone comprised an isotropic, homogeneous material, the kinematics of local flow would have reflected those of the bulk flow (upper left), i.e. a finite value for shear-induced vorticity, but zero spin. This is reflected in the orientation of the maximum instantaneous stretching axis (X_i(bulk)) and the rotation of the direction of maximum finite extension (X_f(bulk)) with respect to X_i(bulk).

In the anisotropic case, the sheets were initially oriented perpendicular to the bulk flow plane. As they rotate in the bulk simple shear flow, they stretch so as to preserve the constant width of the shear zone. If their contacts are planes of zero resistance to slip, the sheets will extend by internal coaxial flow with zero shear-induced vorticity. Within the sheets, the principal directions of finite strain (black ellipses) remain parallel to the instantaneous stretching axes of the local flow. Compared with the homogeneous, isotropic case, the rotational component of the bulk flow is entirely repartitioned into spin. This is reflected in the rotation of the direction of the instantaneous stretching axes within the sheets (X_i local), with respect to the bulk shear plane of the deformation. Note that X_i local tracks the rotation of the anisotropy (lower right). Adapted and modified from Lister and Williams (1983).

(iii) Thirdly, if the pattern of bulk boundary displacements imposed upon a layer of material changed with time, the local flow type would similarly evolve. A geological example might be the intersection of a propagating shear zone with an unconstrained boundary (e.g. Tapponier et al., 1982; Peltzer and Tapponier, 1988).

Consequently, in all three examples, compensatory adjustment of the flow type (increase or decrease of Wk) would be required in the adjacent material in order to maintain material continuity and strain compatibility. All of these changes in flow type can be described in terms of repartitioning of the rotational component of the flow between shear induced vorticity and spin.

Geologists often make spot observations at scales several orders of magnitude smaller than those at which they seek to apply their deductions (e.g. Schwerdtner, 1973b). One obvious geological consequence of repartitioning is that the geologist may be confronted with deformation, resulting from a bulk noncoaxial flow, where the local observations only record a coaxial deformation history. It is therefore necessary to review the concept of the distribution of flow and its coaxial and noncoaxial components in space and the role of material properties that influence that distribution.

In homogeneous simple shear in an isotropic, homogeneous medium, the instantaneous stretching axes of the flow do not rotate with respect to the external reference frame (Fig. 3, 4). Accordingly, the spin component of the deformation is zero and the rotational component of the deformation is entirely represented by the shear-induced vorticity (Fig. 10). *How can the rotational component of a deformation be repartitioned into spin?*

Rotating anisotropy

Consider now a deforming medium which, while statistically homogeneous, is strongly anisotropic. Geologically such an anisotropy might represent discrete rheological layering or a schistosity. Lister and Williams (1983) utilize the simple, but highly effective, analogue model of a shear zone subjected to progressive simple shear, comprised of deformable sheets attached by swivel joints to either wall (Fig. 24). A geological equivalent might be represented by shearing across bedding or layering, or across a set of fractures (e.g. Hanmer, 1989). In Figure 24 the sheets were initially oriented perpendicular to the flow plane. As they rotate with the bulk imposed shear, they stretch so as to preserve the constant width of the shear zone (a condition of simple shear; see Fig. 21). If their contacts are planes of zero resistance to slip, the sheets will extend coaxially with zero shear-induced vorticity. Within the sheets, the principal directions of finite strain remain parallel to the local instantaneous stretching axes of the flow. Compared with an homogeneous, isotropic material, the rotational component of the bulk flow is entirely repartitioned into spin. This is reflected in the rotation of the instantaneous stretching axes within the sheets, with respect to the bulk flow plane (Fig. 24). Clearly, the rotation of discrete surfaces of easy slip can accommodate part or all of the rotational component of the flow. The geological consequence is that observations made at a finer scale than that of the spacing of discrete planes or zones of easy slip in rocks may lead the

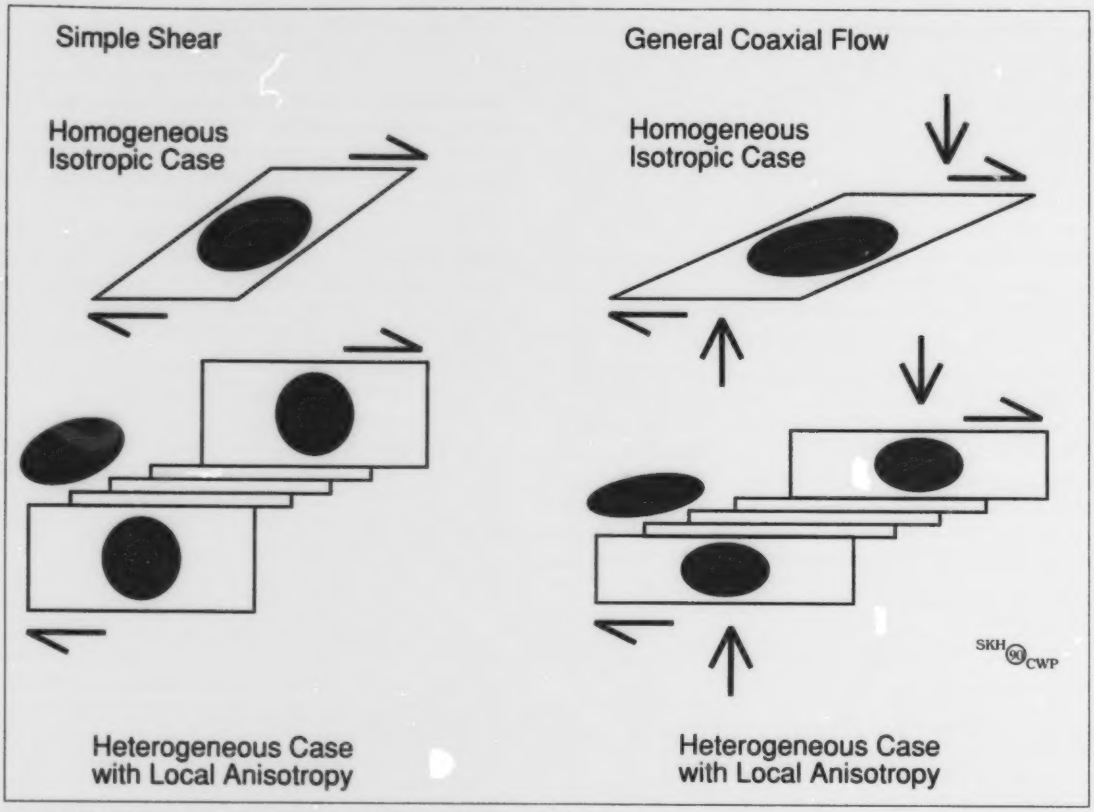
Simple Shear
General Coaxial Flow
Homogeneous Isotropic Case
Homogeneous Isotropic Case
SKH 90 CWP
Heterogeneous Case with Local Anisotropy
Heterogeneous Case with Local Anisotropy

Figure 25. Non-rotating anisotropy and flow partitioning. Idealised model shear zones with sets of internal, shear-parallel planes of easy slip. If, in bulk simple shear (left), progressive deformation were to lead to the development of an incompressible, inextensible, well lubricated, anisotropic 'card-deck' (lower left; see Fig. 21) within an initially isotropic, homogeneous simple shear zone (upper left), the flow would be redistributed such that more intense simple shear occurs in the anisotropic zone, but less deformation is accommodated in the adjacent isotropic part of the model. This is reflected in the greater strain ratio and the greater rotation of the finite strain ellipsoid in the 'card-deck', with respect to the instantaneous stretching axes. However, the orientation of the maximum instantaneous stretching axes in both the homogeneous case and the anisotropic case must be identical. Note that, for clarity, this illustration represents the idealized case where the anisotropic zone corresponds to a perfect 'card-deck' model and the slip-surfaces are planes of zero shear stress; hence the isotropic volume experiences no strain at all.

In the case of two-dimensional general noncoaxial flow (right), the deformation induced development of a similar 'card-deck' would result in repartitioning of the rotational component of the flow. The anisotropic zone is incapable of shortening normal to the flow plane, but can accommodate all of the simple shear component of the bulk progressive deformation. The result is a progressive repartitioning of the rotational component of the bulk imposed deformation. In the anisotropic insert, a counterclockwise spin accompanies an increase in the clockwise shear-induced vorticity (W_k) as the local flow changes from general noncoaxial flow to simple shear. In the isotropic part of the model, the shear-induced vorticity decreases to zero as the rotational component of the flow is entirely repartitioned into clockwise spin.

unwary geologist to draw erroneous kinematic conclusions. Look again at Figure 24: observation of only the central area could lead to the mistaken conclusion that bulk progressive deformation corresponded to a sinistral general noncoaxial flow, wherein the flow plane was inclined at a significant angle to what we know to be the true orientation. Observations confined to the interior of one of the sheets would only indicate coaxial flow.

What differences would be introduced into this model by replacing the bulk boundary conditions with those of a general noncoaxial flow? Quite simply, extension along the flow direction allows the shear zone to behave as a *book-shelf* or *domino* model (Fig. 21). Whether or not this occurs depends on the relative roles of slip and distortion of the anisotropic material in accommodating the deformation. The lower the resistance to slip, or the stiffer the sheets, the greater the tendency to accommodate the bulk flow by slip.

Non-rotating anisotropy

Consider now the case of surfaces of easy slip which are already parallel to the flow plane and can no longer rotate (Fig. 25; Schwerdtner, 1973a). The 'card-deck' model of homogeneous simple shear is one possible analogue (Fig. 21), whereas a strongly foliated, phyllosilicate-rich schist represents a possible geological example. Clearly in this trivial case the spin is zero and the rotational component of the deformation is entirely accommodated by the shear-induced vorticity (Fig. 10). In fact, this case is essentially the same as that of an homogeneous, isotropic medium subjected to ideal simple shear (Fig. 25).

In order to examine a case of non-zero spin, first consider the deformation of an homogeneous, isotropic medium, such as a non-foliated granite, subjected to a general noncoaxial flow (Fig. 25). The pure and simple shear components of the flow are each homogeneously distributed throughout the material, at both the bulk and local scales. Now introduce a narrow zone of thin sheets of incompressible material, parallel to the bulk flow plane, each sheet being bounded by surfaces of easy slip (Fig. 25). Geologically, this could be approximated by an elongate xenolithic raft, particularly rich in aligned phyllosilicates, flanked by the isotropic granite. Alternatively, it could represent a microscopic micaceous lamina which developed with progressive deformation by localized pressure solution. In the model (Fig. 25), the incompressible zone is only capable of accommodating the simple shear component of the bulk flow; it can not accommodate shortening perpendicular to the slip surfaces. Obviously this shortening must be accommodated within the flanking isotropic material. The result is local repartitioning of the pure and simple shear components of the flow; the kinematical vorticity number (W_k) increases from the bulk imposed value within the anisotropic zone, but decreases within the flanking isotropic material. In terms of repartitioning, the shear-induced vorticity decreases in the isotropic material as the maximum instantaneous stretching axis spins clockwise towards the flow plane. In the anisotropic material, counterclockwise spin occurs as the rotational component of the deformation increases and is accommodated by clockwise shear-induced vorticity.

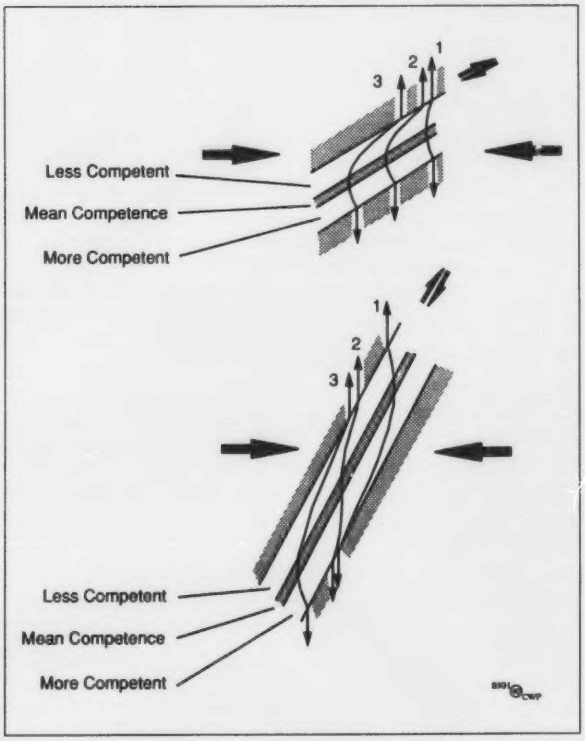

Figure 26. Refraction in multilayers. Local refraction of the principal directions of *bulk coaxial flow* through rheologically layered materials, oriented at 60° (upper) and 30° (lower) with respect to the direction of maximum instantaneous stretch of the bulk flow, such as might occur in a fold limb. Shaded material represents a background mean rheology. White layers are either less competent, or more competent, than the mean rheology. Stiffness in each white layer increases from the upper boundary to the lower boundary such that maximum rheological contrasts occur at the upper boundary of the less competent and the lower boundary of the more competent layers. The oblique angle between layering and the maximum instantaneous stretching axis of the bulk flow results in the resolution of shear along the layering, accompanied by normal stretches operating across the layering. We can describe the flow in the layered material as a general noncoaxial flow. Three trajectories are represented within the layers: the maximum instantaneous stretching axis (1) and the directions of maximum finite extension for moderate (2), and greater (3) magnitudes of finite strain. In particular, note that:

(i) The maximum instantaneous stretching axis (1) refracts across a rheological interface, such that, in the stronger material, the local (1) is deflected towards either the plane of the interface or its normal, whichever is the closer in terms of angular distance. Refraction induced deflection of (1) in the weaker material is just the opposite.

(ii) The local finite extension (2, 3) always tends to lie closer to the plane of the rheological interface in incompetent layers, but rotates with progressive deformation towards the interface normal in competent layers. The degree of rotation is obviously a function of the initial orientation of the maximum instantaneous stretching axis (1) in the same layer.

(iii) Refraction results in the redistribution of the shear components of the flow. The rotational component is redistributed according to the strength of the material; the instantaneous flow in the competent material approaches pure shear while that in the incompetent material approaches simple shear.

The reader will note the similarity between these statements and the description of repartitioning in the text. Adapted from Treagus (1983).

STRAIN AND FLOW REFRACTION

Many rocks are *multilayers* at the scale of an hand specimen, an outcrop or a map unit. A multilayer is simply a volume of rock made of alternating layers of at least two distinct rheologies or degrees of stiffness. Most geologists are familiar with the phenomenon of *strain refraction* at rheological interfaces, usually illustrated in textbooks by examples of cleavage refraction. The common occurrence of cleavage refraction should suffice to indicate the potential pitfalls of extrapolating from local structural observations to the bulk scale. However, relatively few studies have specifically examined the deviation of local deformation histories from that of the bulk structure (e.g. Hobbs et al., 1976, p. 286; Treagus, 1981, 1983, 1988).

Treagus has examined in detail the progressive of deformation of obliquely strained multilayers (Fig. 26). The maximum instantaneous stretching axis refracts across a rheological interface, such that, in the stronger material, it deflects towards either the plane of the interface or its normal, whichever is the closer in terms of angular distance. Refraction induced deflection of the maximum instantaneous stretching axis in the weaker material is just the opposite. The local direction of maximum finite extension always tends to lie closer to the plane of the rheological interface in incompetent layers, but rotates with progressive deformation towards the interface normal in competent layers. The degree of rotation is obviously a function of the initial orientation of the maximum instantaneous stretching axis in the same layer. Clearly, refraction results in the creation of a rotational component in the flow. The rotational component is distributed according to the strength of the material; flow in the competent material approaches pure shear while that in the incompetent material approaches simple shear (Fig. 26).

The point being made here is that, at the scale of observation, deformation structures within multilayers may reflect local deformation histories which deviate in both orientation and flow type from the imposed bulk deformation history. The initiation of essentially symmetrical folds in experimental shear zones (Ghosh, 1966; Manz and Wickham, 1978; Anthony and Wickham, 1978), instead of the asymmetrical folds which some geologists might have intuitively expected, serves as an appropriate illustration.

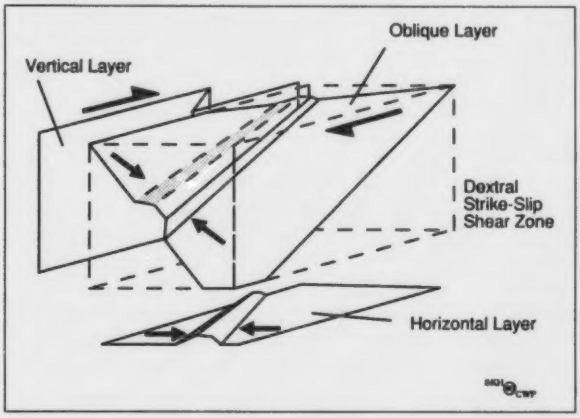

Figure 27. Refraction and folds. Schematic representation of the orientations of folds and refracted minimum instantaneous stretching axis in competent layers lying parallel, perpendicular, and oblique to the flow plane and the direction of flow. The undistorted rectangular box (broken lines) is a cartesian reference frame for the dextral strike-slip shear zone. For simplicity, extreme refraction has been assumed, such that the local minimum instantaneous stretching axis (shortening direction) lies within the layers. Fold axes are generated at high angles to the minimum instantaneous stretching axis *within* each layer. Local instantaneous stretching axes within the initially horizontal layer show the least deviation from the bulk directions and folds initiate at circa 45° to the bulk flow plane. In the initially vertical layer, where the minimum instantaneous stretching axis is refracted towards the flow direction, folds initiate with vertical plunges. In the initially oblique layer, refraction is more complex. Initial folds make low angles with both the flow direction and the trace of the flow plane. Adapted from Marcoux et al. (1987).

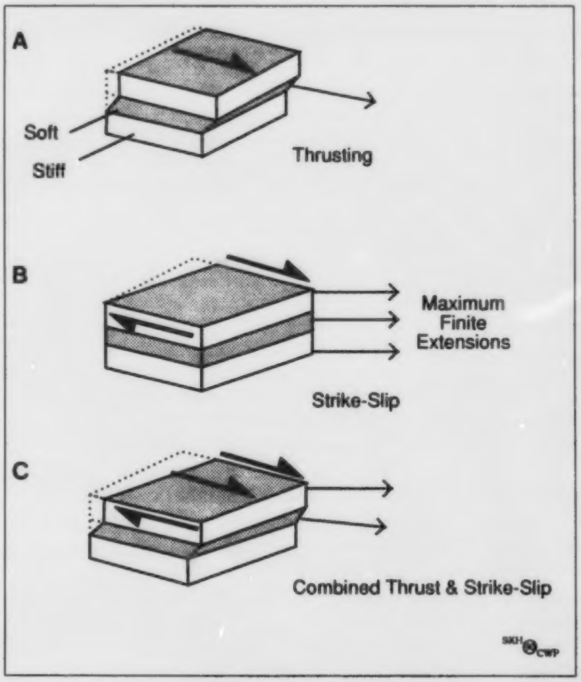

Figure 28. Refraction and shear zones. Schematic representation of the local directions of maximum finite strain (thin arrows) in competent (white) and less competent layers (shaded).

(A) Simple layer-parallel thrusting. Stiff layers are represented as rigid, so deformation is only accommodated in the incompetent layer.

(B) Transcurrent shear on planes normal to layering. Both competent and incompetent layers must participate in the flow in order to preserve material continuity across the rheological interfaces. All layers show the same orientation of maximum finite extension.

(C) Thrusting and transcurrent shear combined. The stiff layers only resolve the wrench component while the incompetent layer resolve both components. In this example only the principal directions of local finite strain in the incompetent layer are parallel to those of the bulk finite strain. After Ridley (1986).

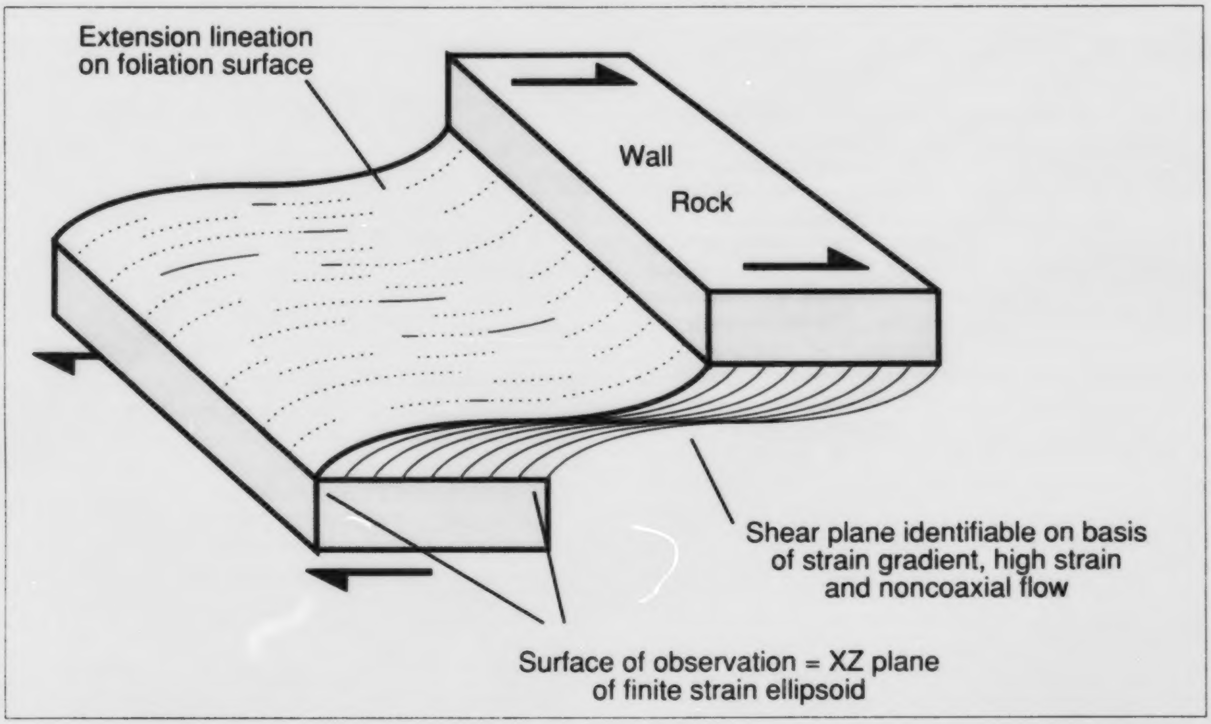
Extension lineation on foliation surface
Wall
Rock
Shear plane identifiable on basis of strain gradient, high strain and noncoaxial flow
Surface of observation = XZ plane of finite strain ellipsoid

Figure 29. Where to look. A self-explanatory illustration of where to look for shear-sense criteria in a shear zone corresponding to either progressive simple shear, or 2D general noncoaxial flows of the type discussed in the text. Valid observations of shear-sense criteria should be made on the surface facing the observer in our illustration: perpendicular to the newly formed foliation and parallel to the extension lineation.

As another example, consider the orientation of the instantaneous stretching axes within a stiff layer, itself inclined obliquely to both the flow plane and the vertical rotation axis of a strike-slip shear zone (Fig. 27). What would be the initial orientation of fold axes generated within that layer, compared with folds generated in a layer initially normal or initially parallel to the rotation axis of the shear zone? (e.g. Treagus and Treagus, 1981; Marcoux et al., 1987). Local instantaneous stretching directions within an initially horizontal layer would show the least deviation from the bulk direction and folds would initiate at circa 45° to the flow plane. In an initially vertical layer, where the minimum instantaneous stretching axis is refracted towards the flow direction, folds would initiate with vertical plunges. In an initially oblique layer, refraction is more complex. Initial folds can make low angles with both the flow direction and the trace of the flow plane (Fig. 27).

As a more complex example, consider the orientation of the directions of apparent maximum finite extension within a multilayer subjected to shear on two mutually perpendicular flow planes, as in the case of combined thrusting and transcurrent shear (Fig. 28). The stiff layers would only resolve the wrench component while the incompetent layers would resolve both components. Only the principal directions of local finite strain in the incompetent layer are parallel to those of the bulk finite strain. Such a situation might characterize the transition from the frontal section of a thrust zone to a lateral ramp (e.g. Coward and Kim, 1981; Coward and Potts, 1983). The lateral ramp may essentially be a transcurrent structure. The bulk flow in the transition zone would therefore represent a complex hybrid of transcurrent and thrust related components. Refraction in a suitably oriented multilayer would result in differential accommodation of the components of the flow according to the rheology of the layers (Ridley, 1986).

WHERE TO LOOK

Having examined flow in some detail, it is perhaps timely to remind ourselves of where we should look to find structures which will enable us to deduce the shear-sense of the flow, before going on to look at the structures themselves. This is summarized in Figure 29.

SHAPE FABRICS (FOLIATIONS)

In this section we shall deal with three aspects of shape fabrics: the development of (i) simple and of (ii) complex fabrics in shear zones and (iii) the deflection of existing fabrics around stiff inclusions, or into shear zones.

Simple shape fabrics

Strain-sensitive fabrics

The modern analysis of shear-sense indicators began in the late 1960s with such studies as Ramsay and Graham's (1970) examination of the variation of the orientation and magnitude of finite strain across zones of concentrated deformation. This study is still an excellent guide to modern students of kinematic analysis in their own endeavors.

Ramsay and Graham (see also Ramsay, 1980a) presented a model, couched in terms of strain variation and strain compatibility within a continuous, ductile material undergoing progressive simple shear, which accounted for the observed geometry of some natural structures. They recognized that the penetrative foliation which formed within a materially continuous shear zone initially made an angle of circa 45° with the shear plane and that, being *strain-sensitive*, it rotated, with the finite strain ellipsoid, towards the boundaries of the shear zone during progressive deformation (Fig. 30; cf. Ingles, 1986). From these observations, they were able to demonstrate that

(i) The initial orientation of the foliation is approximately normal to the minimum instantaneous stretching axis of the flow.

(ii) The progressive curvature of the foliation, from the outer parts of the shear zone to the inner parts, tracks the rotation of the finite strain ellipsoid with respect to the instantaneous stretching axes and reflects the variation in strain intensity and the associated rotation of the finite strain ellipsoid in response to the vorticity of the flow.

(iii) At high magnitudes of finite strain, the extension lineation on the foliation surface marks the approximate movement of the rigid wall rocks bounding the shear zone.

(iv) Assuming an invariant simple shear deformation path, the total displacement across the shear zone can be measured by integration of the finite strains, determined from the orientation of the foliation at points along a transverse profile.

(v) The relationship of the distribution of strain across the shear zone to the displacement of its wall rocks is a consequence of the boundary conditions of the deformation.

Figure 30. Strain-sensitive simple fabrics. A continuous sinistral shear zone, developed in isotropic meta-gabbro by progressive simple shear, from the type locality described by Ramsay and Graham (1970). The term *continuous* refers to the manner in which the shear strain varies across the shear zone. The plane of observation corresponds to the XZ plane of the finite strain ellipsoid. Shear-sense along the shear plane and the inferred instantaneous stretching axes of the simple shear flow are indicated (arrows). Within the shear zone, the foliation has rotated anticlockwise with progressive deformation, recording the rotation of the finite strain ellipsoid with respect to the instantaneous stretching axes. By assuming an invariant simple shear deformation path (a reasonable assumption given the isotropic wall-rock), the total displacement across a segment of the continuous shear zone can be measured by integration of the finite strains, determined from the orientation of the foliation at points along a transverse profile. Castell Odair, N. Uist, looking down. (GSC 203942-E)

Strain-insensitive fabrics

Strain-insensitive fabrics do not closely track the finite strain ellipsoid during noncoaxial progressive deformation. In highly strained rocks, such as some mylonites, compositional layering and highly attenuated polycrystalline ribbons lie subparallel to the shear plane. This fabric component is often referred to as the mylonitic foliation, S_m, or more commonly S_a (Law et al. 1984). A penetrative microscopic shape fabric, S_b, defined by elongate quartz grains lying at an angle of about 20-30° to S_a, is very commonly developed within *monomineralic* quartz ribbons in mylonites formed at all metamorphic grades (Fig. 31; e.g. Brunel, 1980; Lister and Snoke, 1984; Burg, 1986; Law et al., 1986; Law and Potts, 1987; Knipe and Law, 1987). Few examples of *polymineralic* S_b (several minerals participating as foliation-forming elements) have been described in the literature and only from mylonitic rocks formed at amphibolite or granulite facies (e.g. Hanmer, 1984b; Fig. 31D). In monomineralic aggregates, S_b is typically straight and may maintain a fairly constant orientation within a given ribbon.

A theoretical description of the process whereby fabric forming elements, developed in a monomineralic aggregate undergoing noncoaxial progressive deformation, would not track the rotating principal directions of finite strain, was first given by Means (1981; see also Jessel, 1988). He proposed that a shape fabric (S_b) will not rotate in noncoaxial progressive deformation if the *fabric-forming processes are balanced by fabric-weakening processes* (Fig. 31A). Means argued that a grain undergoing strain participates in the definition of a shape fabric (foliation) in the aggregate and begins to rotate as the foliation attempts to track the finite strain ellipsoid. However, in response to the increase in internal strain energy (dislocation density), a distorted grain will dynamically recrystallize to form a sub-aggregate of fine, equant grains (Nicolas and Poirier, 1976; Poirier and Guillopé, 1979; Poirier, 1985). Equant grains do not contribute to the definition of a shape fabric. Moreover, because the aggregate is monomineralic, the outline of the parent grain is no longer visible, given that its neighbours have also recrystallized.

In order to reduce the relatively elevated surface energy inherent to the fine grain size, the sub-aggregate coarsens by *grain boundary migration* (Kerrich et al., 1980; Urai et al., 1986 and references therein). The coarsening grains are subject to on-going deformation and the cycle of strain and participation in the shape fabric of the overall aggregate begins anew (Fig. 31A). We must emphasize that, although our description relates to the history of a single parent grain, all stages of the cycle of deformation and recrystallization will be represented in the aggregate at any given instant. With the next increment of strain, the equant grain will transform to a shape whose long axis lies close to the orientation of the maximum instantaneous stretching axis of the flow. In other words, the degree to which the foliation reflects the instantaneous stretching axes, rather than the principal finite strains, is a function of the relative efficiency of the fabric-weakening processes. The overall orientation of the fabric-forming elements (S_b) will therefore lie within the extensional quadrants of the flow, somewhere between the maximum instantaneous stretching axis of the flow and the position to which a deforming grain rotates prior to dynamic recrystallization. Hence, from the angular relationship between S_b and the strain-insensitive fabric the geologist can determine the shear-sense of the flow.

Strain-insensitive fabrics may also develop in polymineralic aggregates. The outlines of the strained, monomineralic, polycrystalline sub-aggregates should still be preserved after the initiation of dynamic recrystallization and should continue to participate in a recognizable strain-sensitive shape fabric, unless something happens to disperse them. Very little work has been done to determine how such aggregates are destroyed in polymineralic strain-insensitive fabrics. Hanmer (1984b) proposed that, in geological circumstances where the kinetic barriers to mass transfer by diffusion are low, even a relatively mild decrease in the free energy of the aggregate might suffice to drive a process of dispersion of the monomineralic sub-aggregates by mass transfer. The necessary conditions include very fine

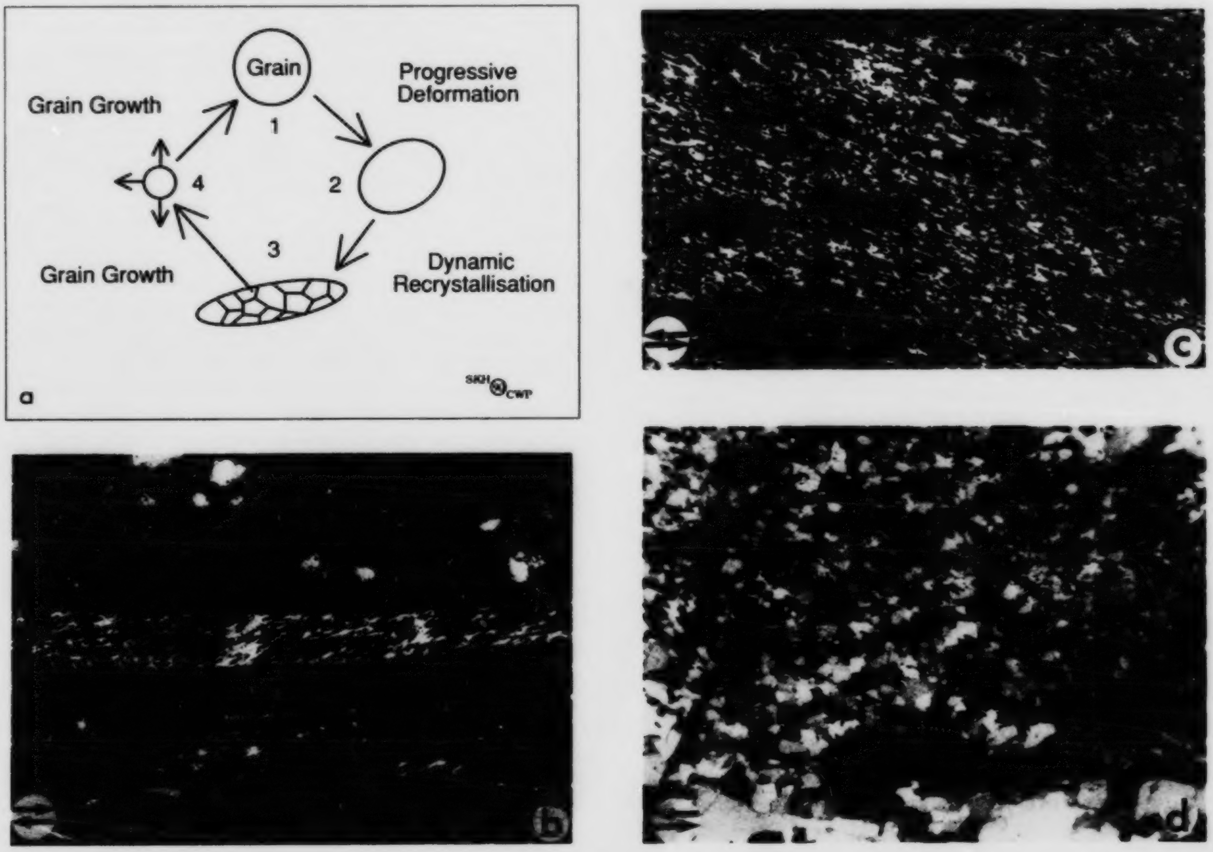

grain size and elevated temperatures and would be enhanced by the (transient?) presence of an aqueous phase in the grain boundary network. Such conditions might apply to mylonites forming under upper amphibolite and granulite facies metamorphic conditions. However, the only 'hard data' derive from 20 year old petrographic studies (Vernon, 1968; Flinn, 1969) which indicate that grain boundaries between phases of the same mineral *('like' boundaries)* have higher *interfacial energies* than those between different minerals (*'unlike' boundaries*). If these optical estimates of relative interfacial energies are valid, enhancement of the occurrence of 'unlike' boundaries at the expense of 'like' boundaries might lead to diffusive dispersal of the monomineralic sub-aggregates and the destruction of their outlines, thus allowing the formation of a strain-insensitive fabric (S_b). Clearly more work is required to accurately assess the magnitude of the energy difference between 'like' and 'unlike' grain boundaries before placing too much weight on Hanmer's (1984b) interpretation. As in the case of monomineralic aggregates, the orientation of Sb with respect to the instantaneous stretching axes of the flow, is a function of the relative efficacy of the fabric-forming and fabric-weakening processes. The occasional occurrence of sigmoid deflections of S_b into local, near monomineralic S_a bands (Fig. 32; Hanmer, 1984b) is a reflection of spatial variation in the relative efficacy of these processes perhaps due, for example, to variation in shear strain rate (Hanmer, 1984b).

Complex shape fabrics

Kinematically significant complex fabrics are comprised of two distinct sets of planes. We shall examine two types of complex fabric. Both comprise one set of planes oriented parallel to the flow plane. However, in one type a penetrative strain-sensitive cleavage

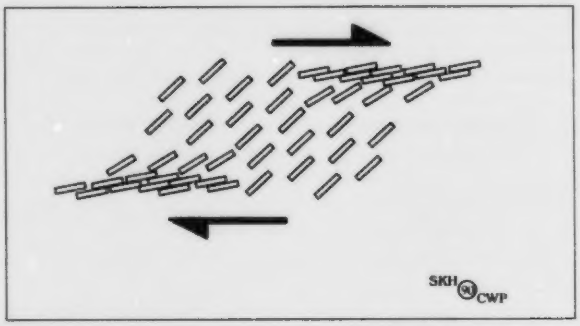

Figure 32. Locally sigmoid strain-insensitive foliation. Homogeneously distributed, isolated laths of e.g. biotite forming a strain-insensitive foliation in a strongly deformed dextral quartzofeldspathic mylonite. In bands where the biotite is more highly concentrated the laths show a greater tendency to attempt to track the rotation of the finite strain ellipsoid with progressive deformation (see text).

Figure 31a (opposite). **Strain insensitive simple fabrics**. Under certain circumstances, a foliation may not rotate with the finite strain ellipsoid during noncoaxial progressive deformation. A grain (1) undergoing distortion (2) participates in the definition of a shape fabric (foliation). In response to the increase in internal strain energy, the distorted grains dynamically recrystallize to form a sub-aggregate of fine, equant grains (3). In order to reduce the relatively elevated surface energy inherent to fine grain size, the sub-aggregate coarsens by grain boundary migration (4). The coarsening grains are subject to on-going deformation and the cycle of distortion and participation in the shape fabric of the overall aggregate begins anew. Hence the overall orientation of the fabric-forming elements lies close to the maximum instantaneous stretching axis of the flow. Adapted and modified from Means (1981).

Figure 31b (opposite). Detail (1800μmx1200μm) of a polycrystalline, monomineralic quartz ribbon, oriented parallel to the shear plane (S_a) in a mylonite, contains an internal oblique strain-insensitive shape fabric (S_b). Observed in the XZ plane of the finite strain ellipsoid. The shear plane is shown (arrows). The fabric-forming elements are elongate quartz grains with sutured margins. The suturing is due to bulges of similar size to the small, equant grains scattered through the microstructure, suggesting that the equant grains are derived by the dynamic recrystallization of the elongate grains (Vernon, 1981; Urai et al., 1986). Note that the ribbon exhibits discrete internal surfaces oriented parallel to the shear plane. Although the structure geometrically resembles a *strain-sensitive* C/S fabric, the strong deformation which the mylonite and the ribbon have undergone would result in a very small C^S angle. On the other hand, the quartz grain shape fabric (S_b) is *strain-insensitive* and indicates the disposition of the extensional quadrants of the flow with respect to the shear plane. From these angular relations we can deduce that the shear-sense here is dextral. Great Slave Lake Shear Zone, N.W.T., looking down. (GSC 205186-C)

Figure 31c (opposite). Detail (1200μm x 800μm) of (S_b) from within a wide polycrystalline, monomineralic quartz ribbon in a mylonite showing many of the microstructural features described in A. Observed in the XZ plane of the finite strain ellipsoid. The shear plane is shown (arrows). The boundary of the ribbon (lower-left and centre) is parallel to the shear plane (S_a). From the angular relations between the shear plane (S_a) and (S_b) we can deduce the disposition of the extensional quadrants of the flow with respect to the shear plane and determine that the shear-sense here is sinistral. Central Metasedimentary Belt boundary thrust zone, Grenville Province, Ontario, looking north-northeast. (GSC 204776-R).

Figure 31d (opposite). Detail (3500μm x 2500μm) of a polymineralic quartz-feldspar-biotite band of mylonite within which the small dark biotites are all aligned at circa 40° (upper left to lower right) to the shear plane. Observed in the XZ plane of the finite strain ellipsoid. The shear plane is shown (arrows). Note how the biotites are isolated single grains, homogeneously distributed throughout the mylonitic band. However, the large biotite lath (bottom) is aligned in the plane of the mylonite band itself and has probably rotated into parallel with the shear plane with progressive deformation. We interpret the fine grained microstructure with its aligned small biotites as a strain-insensitive foliation in a sinistral shear zone; the shear plane and the inferred instantaneous stretching axes of the flow are shown accordingly (arrows). Central Gneiss Belt, Grenville Province, Ontario, looking northeast.

is initially developed oblique to the flow plane, oriented in the extensional quadrants of the flow (Fig. 33A). In the other, a set of discrete shear bands is developed oblique to the flow plane, oriented in the angular range $90^\circ<\alpha<135^\circ$ (Fig. 33B).

C/S fabrics

The standard work on the description and interpretation of complex fabrics composed of (C)isaillement (shear) and (S)chistosité (cleavage) planes (Fig. 33) is that of Berthé et

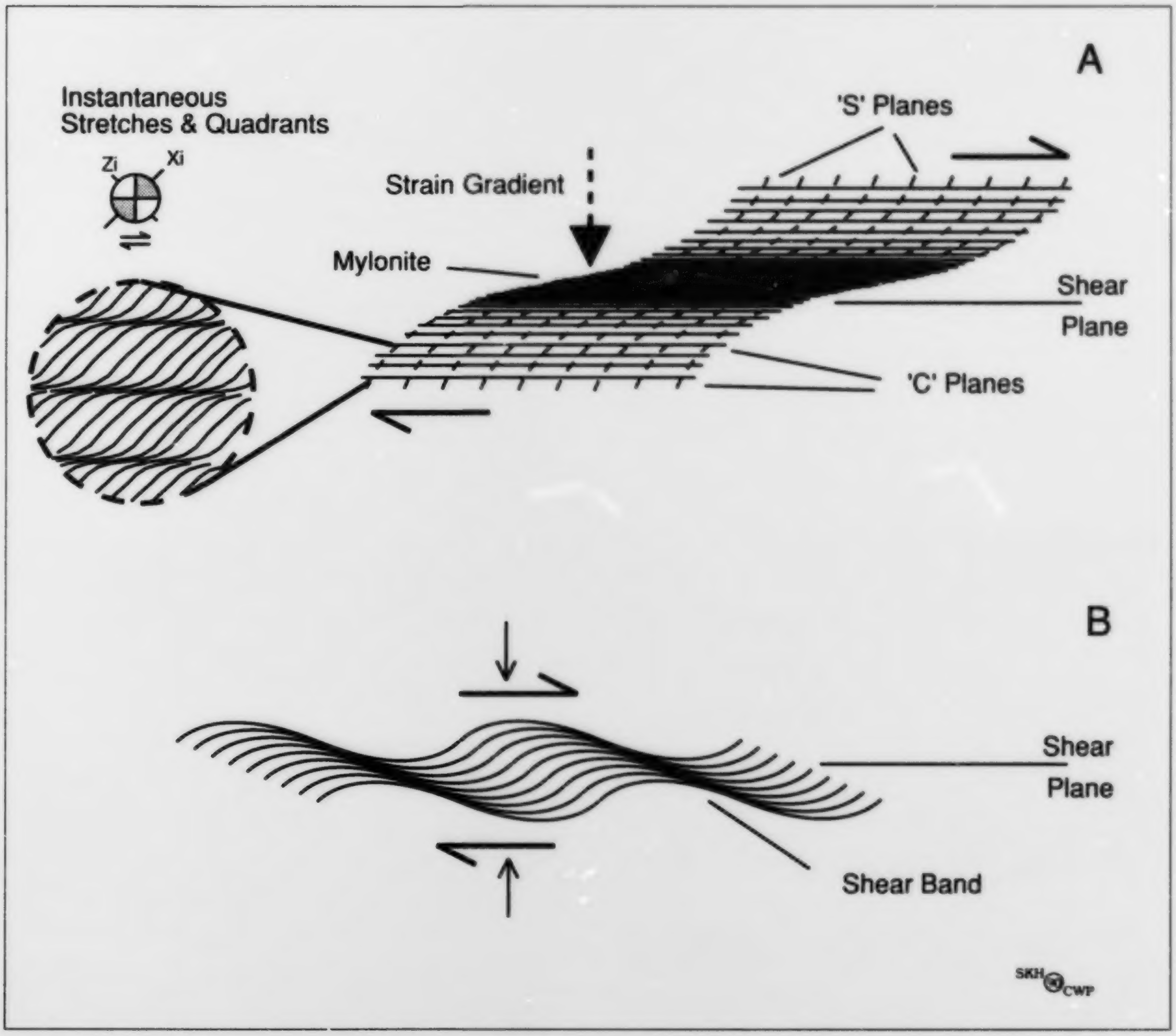

Figure 33. C/S fabrics versus asymmetrical extensional shear bands. (**A**) Zones of C/S fabric are discontinuous shear zones. The term *discontinuous* refers to the manner in which shear strain varies across the shear zone. The extensional (shaded) and shortening (white) quadrants of the flow are shown. C planes are discrete shear zones, up to tens of centimetres in length by a millimetre or so in thickness, spaced at centimetre intervals. The S fabric describes a sigmoid shape within the lithon between any two adjacent C planes (left). Each C plane may be considered as a small scale shear zone, bounded on either side by strain gradients. The sense of rotation of the S planes along the strain gradients is a reflection of the rotation of the finite strain ellipsoid with respect to the instantaneous stretching axes of the flow (shear-induced vorticity). Both this fine scale rotation and the rotation of the average orientation of the S planes (right), with respect to the larger scale shear zone boundaries (rotational component of the flow), reflect the sign of the vorticity (shear-sense) of the flow. Note that at high finite strains, the S and C planes can no longer be separated; to the naked eye, both lie parallel to the shear plane of the deformation. After Berthé et al. (1979a). (**B**) Asymmetrical extensional shear bands oriented within the angular range $90^\circ<\alpha<135^\circ$ in a general noncoaxial flow (see text).

al. (1979a, 1979b; see also Vernon et al., 1983; Lister and Snoke, 1984). S planes represent a penetratively developed strain-sensitive flattening (*sensu lato*) fabric which attempts to track the XY plane of the finite strain ellipsoid during progressive deformation, much like the schistosity developed in a continuous shear zone (Fig. 33A). C planes are discrete narrow shear zones which are taken to lie parallel to the flow plane of the progressive deformation.

In any C/S fabric, it is possible to observe different stages in the progressive accumulation of the finite strain, even within a hand-specimen or a thin section. Each individual C plane is a narrow shear zone, bounded on either side by strain gradients (Fig. 33A, 34) and so resemble continuous shear zones. Continuing the analogy, the sigmoid S surfaces rotate towards the shear plane (C) with increasing strain. Hence, taking the C plane as our reference, the distal segment of an S surface lies closer to the maximum instantaneous stretching axis, while the proximal segment lies closer to the bulk direction of maximum finite extension (Fig. 33). Therefore, the progressive rotation of the finite strain ellipsoid with respect to the instantaneous stretching axes (shear-induced vorticity) can be deduced directly from the distal to proximal curvature of the S surfaces, from which one determines the shear-sense.

C planes form in rocks where the strain distribution is heterogeneous at the grain-scale, such as in granites deformed at temperatures below the crystal-plastic limit for feldspars. Although most workers describe C/S fabrics from granitoids, they have been successfully simulated in laboratory experiments using halite and carbonate (Jordan, 1987). They are rarely developed in granitoid rocks deformed under high temperature metamorphic conditions, where both plagioclase and K-feldspar may recrystallize dynamically (e.g. Hanmer, 1982b; Tullis, 1983; Tullis and Yund, 1985, but see Simpson and Wintsch, 1989). Stiff feldspars act as centimetre-size stress raisers and their boundaries may be the loci of locally high strain rates. Where the grain boundaries of several neighboring feldspars are aligned in a plane parallel to the shear plane of the deformation, a C plane nucleating on one feldspar can readily propagate across to the others (see also Tullis and Yund, 1977, 1979).

Figure 33A is a simplified representation of C/S fabrics developed in progressive simple shear. The range of potential initial C^S angles is a function of two factors. The first is a reflection of the influence of the flow type on the orientation of the instantaneous stretching axes of the flow (Fig. 3). As already discussed, the angle made by the maximum instantaneous stretching axis with the flow plane decreases with increasing shortening across the flow plane. The second factor is the finite strain and accompanying rotation required to form a set of S planes detectable by the human eye (White and Knipe, 1978; Ingles, 1986). Assuming a shortening of about 30% (Ramsay, 1967, p. 180) and progressive simple shear, the finite strain ellipsoid would already have rotated through approximately 15° with respect to the instantaneous stretching axes before the geologist can even see a foliation plane.

Berthé et al. (1979a) described composite C/S fabrics as *continuous-discontinuous* (Fig. 33A; see also Burg and Laurent, 1978), as opposed to the continuous nature of Ramsay and Graham (1970) shear zones (Fig. 30). This implies that the C planes are not simply narrow ductile shear zones. Berthé et al. (1979a) documented discrete brittle slip along some C planes which cut and off-set mica grains. They also described the C planes as zones of comminuted feldspar, recrystallized quartz, mica and insoluble residue. Clearly C planes are shear zones characterized by a complex interplay of crystal-plastic, mass transfer and brittle deformation processes. Some workers have opted to refer to C planes by the non-specific term *shear bands*; that is, thin planar zones along which differential movement has been accommodated. We find this practice unfortunate since it introduces confusion with another type of structure known as 'shear band foliation' (see next section).

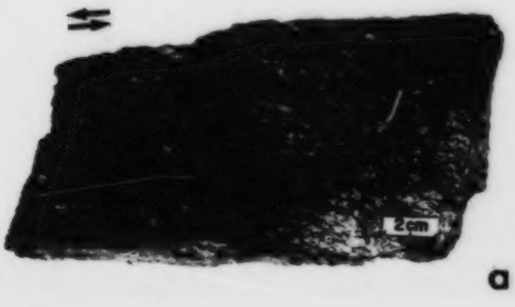

Figure 34a. Natural C/S fabrics. Sinistral C/S fabrics developed in deformed granite, observed in the XZ plane of the finite strain ellipsoid. C planes are discrete shear zones, oriented parallel to the bulk shear plane, spaced at intervals equal to the size of the stiff feldspar grains. S planes form a penetrative cleavage, lying in the extensional quadrants of the flow. Chedabucto Fault Zone, Nova Scotia, looking up, specimen inverted!

Figure 34b. Demonstrates that C planes in a dextral C/S fabric represent discrete micro-shear zones. A thin aplite vein emplaced along the S planes is offset by several millimetres as it crosses certain C planes. The lack of offset across other C planes suggests that the distribution of slip on a population of C planes is heterogeneous. Wopmay Fault Zone, N.W.T., looking down. (GSC 204128-D).

Asymmetrical extensional shear bands

Shear band foliation (White et al., 1980), *C'* Berthé et al., 1979b), and *asymmetrical extensional crenulation cleavage* (Platt and Vissers, 1980) are three terms used in the literature to designate one of the commonest shear-sense indicators. Anisotropic rocks, such as many mylonites, phyllites and micaschists, subjected to noncoaxial flow along the plane of the anisotropy, often respond by developing a set of discrete shear zones or 'shear bands' oriented at about 15-25° to the bulk flow plane (Fig. 33B; e.g. Platt, 1984; Dennis and Secor, 1987). The exact geometry varies from case to case, but an average, representative description can be given (Fig. 35). The shear bands are up to several millimetres thick, by up to 10 centimetres long. As a general rule, they are less continuous than any associated C planes (Berthé.et al., 1979b). They may be homogeneously developed and constitute a foliation or crenulation cleavage, or they may occur sporadically. Ideally, only one set of shear bands is developed, whose sense of slip is synthetic to the shear-sense on the bulk shear plane (Fig. 36). However, it is not uncommon for a conjugate, but numerically subordinate set to form (Harris and Cobbold, 1985; Behrmann, 1987). The shear bands may be composed of the same mineralogy as the rest of the rock (e.g. Gapais and White, 1982), or they may show compositional changes suggestive of retrograde metamorphic reactions (e.g. McCaig, 1987; Norrell et al., 1989) or the concentration of less soluble material by mass transfer.

We have adopted term *asymmetrical extensional shear bands* for this structure in an attempt to avoid the semantic confusion which has entered the structural literature concerning the use of the term 'shear band foliation'. The terms *cleavage* and *foliation* suggest a penetrative fabric and are perhaps injudicious terms to refer to often sporadically developed fabric elements. *Shear band* is a metallurgical and rock mechanics term referring to the concentration of noncoaxial flow in a narrow band of finite thickness. Some authors have used the term to refer to the C plane component of C/S fabrics, which lies parallel to the bulk flow plane of the progressive deformation (e.g Lister and Snoke, 1984; Bell and Hammond, 1984; Platt, 1984; Malavieille and Cobb, 1986; Davis et al., 1987; Behrmann, 1987; Saltzer and Hodges, 1988). Although this is technically correct, such usage leads to confusion since 'shear band' is most commonly used by geologists to designate asymmetrical extensional shears (White et al., 1980). This has perhaps led some authors to confuse composite fabrics with asymmetrical extensional shear bands (e.g. Fig. 5 in Simpson and Schmid, 1983). In an homogeneous, isotropic material, subjected to an homogeneous deformation, *entirely accommodated by slip on discrete slip surfaces*, active extensional slip planes should rotate towards the flattening (X/Y) plane of the bulk finite strain ellipsoid (Freund, 1974). It is therefore quite remarkable that illustrations of asymmetrical extensional shears developed in geographically dispersed anisotropic mylonites, of variable geological age and metamorphic grade, should resemble each other so closely (e.g. White et al., 1980; Platt and Vissers, 1980; Gapais and White, 1982; Simpson and Schmid, 1983; Weijermars and Rondeel, 1984; O'Brien et al., 1987; McCaig, 1987; Blumenfeld and Bouchez, 1988). All show single sets of shears, lying at approximately 15-25° to the mylonite foliation, yet theoretically the shears should back-rotate towards the flow plane, lock and be overprinted by successive sets initiating at circa 25° (Platt and Vissers, 1980).

We are unable to offer a comprehensive explanation for the apparent lack of clearly documented cases of rotated and overprinting sets of asymmetrical extensional shear bands. However, we can at least consider why they work as shear-sense indicators. Slip on extensional shears would result in a component of extension within the bulk flow plane, in a direction perpendicular to the intersection of the extensional shears with the bulk flow plane. Unless there is a component

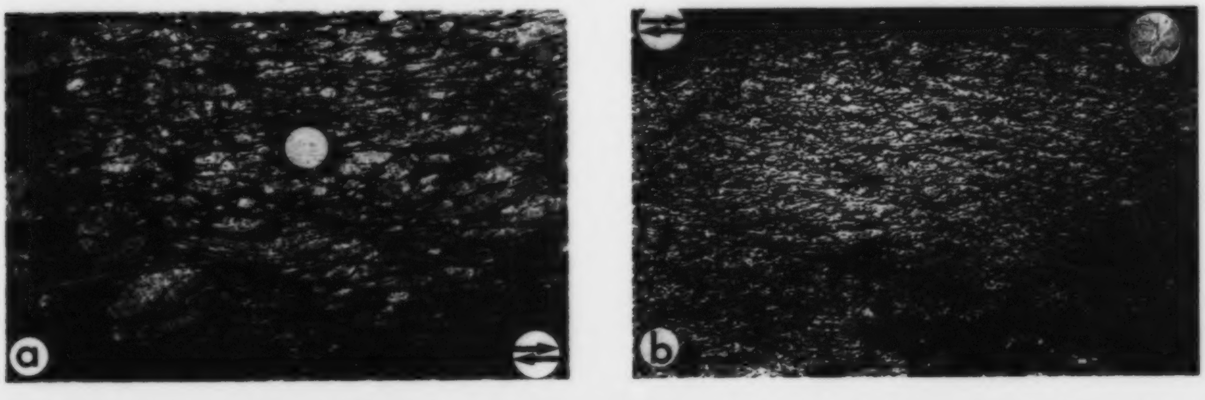

Figure 35. Asymmetrical extensional shear bands developed in protomylonite and mylonite, observed in the XZ plane of the finite strain ellipsoid. The bulk shear plane, here subparallel to the mylonitic foliation, and the bulk shear-sense are indicated (parallel arrows). **(a)** Irregularly distributed, short shear bands indicative of dextral sense of shear on the bulk shear plane. (GSC 204776-Y). **(b)** Long, homogeneously distributed dextral shear bands, indistinguishable in this view from C/S fabrics (compare with Fig. 34). However, the bulk strain gradient within this same outcrop is oriented parallel to the short dimension of the photograph and indicates that these shear bands are oblique to the bulk shear plane of the deformation; hence they can not be C planes (see Fig. 19, 33). (GSC 204776-X). Both are from Great Slave Lake Shear Zone, N.W.T., looking down.

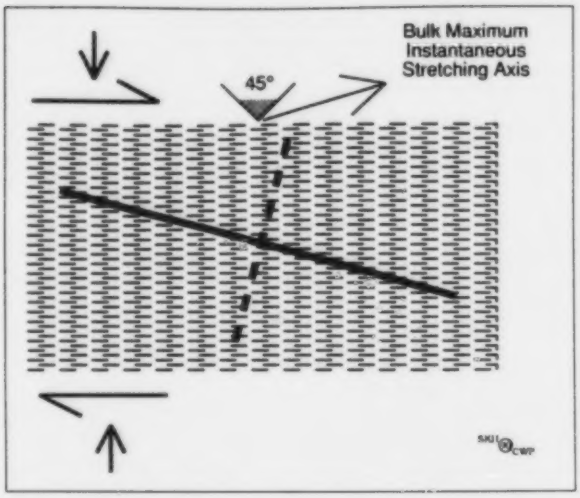

Figure 36. Why are extensional shears bands asymmetrical? Slip on extensional shears results in a component of extension within the flow plane (general noncoaxial flow), in a direction perpendicular to the intersection of the extensional shears with the main mylonitic foliation, itself oriented parallel to the bulk flow plane. At the moment of their initiation, the potential conjugate sets of shear bands are symmetrically disposed about the maximum instantaneous stretching axis of the bulk flow, itself oriented at less than 45° with respect to the bulk flow plane. The set of shear bands whose orientation is closest to that of the rheological anisotropy (e.g. mylonitic foliation) can be expected to be preferentially developed. From this set, the geologist is able to determine the approximate orientation of the kinematic quadrants of the flow with respect to the bulk flow plane and hence deduce the sense of shear.

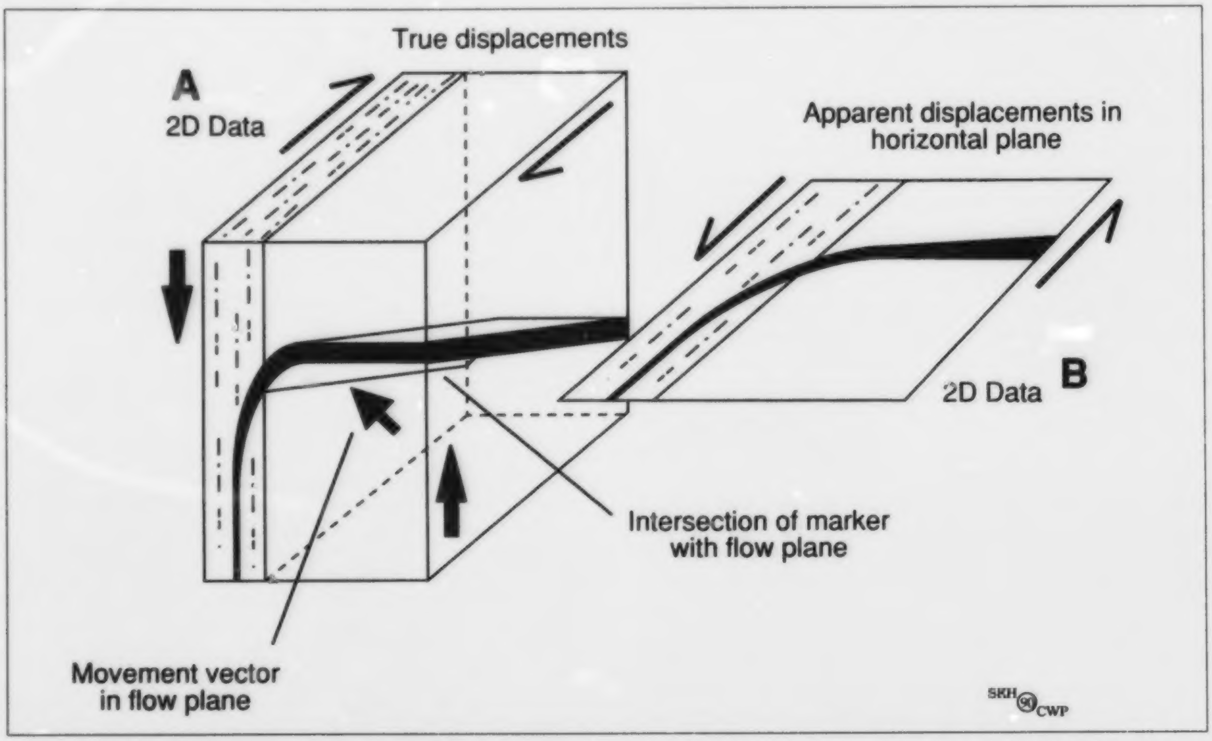
True displacements
A
2D Data
Apparent displacements in horizontal plane
2D Data
B
Intersection of marker with flow plane
Movement vector in flow plane

Figure 37. Deflections and shear zones. Where a pre-existing external marker intersects a shear zone, it is deflected from its original orientation and thinned from its original thickness as it enters the zone of high strain. (**A**) and (**B**) represent a marker layer entering a zone of simple shear. Compare the observed deflection in the plane of observation in (A) with that in (B). The apparent deflection of a marker in two-dimensions will always accurately reflect the bulk shear-sense where the intersection of the marker with the flow plane lies at an high angle to the plane of observation and/or where the true displacement vector lies very close to the plane of observation; the vertical face in A for example. Where the intersection lies close to the plane of observation, and/or makes an high angle with the true displacement vector, as in B, there is a statistically significant probability that the observed deflection of the marker in that plane will be opposite to the sense of the bulk shear.

of shortening along the general direction of the mylonitic foliation within the material between the shear bands, the bulk deformation corresponds to a progressive general noncoaxial flow, which results in extension of the shear plane. The initiation of discrete extensional shear bands in a material which was previously able to deform homogeneously appears to be a response to hardening of the deforming mylonite (e.g. White et al., 1980; Passchier, 1986). *Why does only one set of shear bands develop, as opposed to two conjugate sets?* At the moment of their initiation, the potential conjugate sets of shear bands are symmetrically disposed about the instantaneous stretching axes of the bulk flow (Fig. 36). The mechanism of initiation of shear bands is related to the amplification of perturbations in the planar anisotropy of the foliated host rock (Cobbold et al., 1971; Cobbold, 1976). Accordingly, the set of shear bands whose orientation is closest to that of the anisotropy can be expected to be preferentially developed. From this set, the geologist is able to determine the approximate orientation of the shortening and extensional quadrants of the flow and hence deduce the sense of shear.

Comparison of fabrics

By what criteria can C/S fabrics be identified? Geometrically, C/S fabrics resemble an early penetrative cleavage, cut and crenulated by a second spaced cleavage (polyphase S1/S2; see Fig. 33A, 34). Berthé et al. (1979a) demonstrated that, at the scale of a thin-section, the development of an initial S fabric precedes its deflection into the nascent C planes. However, at the scale of the hand specimen or of the outcrop, they showed that the S and C components of the fabric develop simultaneously. The corollary is that, where the fabric can be traced back along a strain gradient into less deformed protolith, the C and S components should attenuate at approximately the same place. In the case of polyphase S1/S2 this would represent a remarkable coincidence.

By what criteria can asymmetrical extensional shear bands be distinguished from C planes? Geometrically, a mylonitic foliation cut by asymmetrical extensional shear bands bears some resemblance to a C/S fabric (compare Fig. 34B, 35B). Berthé et al. (1979a) point out that the C planes of a C/S fabric lie very close to the shear zone boundary and the shear plane of the bulk deformation. Furthermore they document that, in the presence of a strain gradient, the spacing of the C planes decreases with increasing deformation (Fig. 33A). Since the direction of the strain gradient lies perpendicular to the flow plane (see also Cobbold, 1977), we have only to compare it to the orientation of the discrete shear bands in question. If they are clearly oblique to the deduced shear plane (Fig. 33B), the shear bands are not C planes.

Strain-sensitive C/S and strain-insensitive Sa/Sb fabrics may superficially resemble each other geometrically, although the sigmoid character of the S component in C/S fabrics is the rule, rather than the exception. However, the processes involved in their formation and their relationships to progressive deformation are quite distinct. Unfortunately,

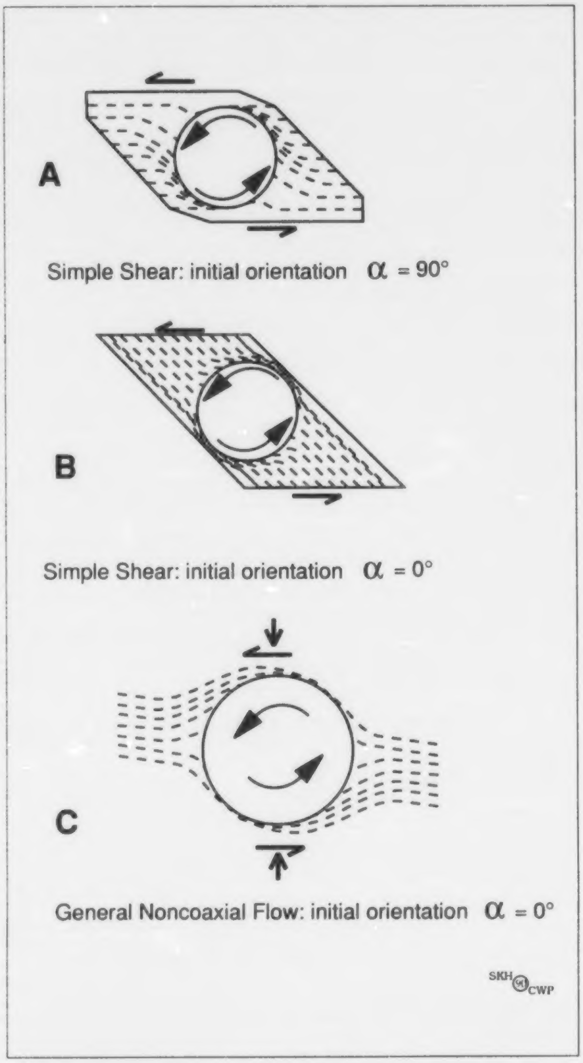

Simple Shear: initial orientation $\alpha = 90°$

Simple Shear: initial orientation $\alpha = 0°$

General Noncoaxial Flow: initial orientation $\alpha = 0°$

Figure 38. Deflection and inclusions. The apparent "drag" of matrix foliation around an equant inclusion reflects the relative rotation rates of elements of different aspect ratio (R; see Fig. 23), the initial orientation (α) with respect to the flow plane and the flow type. *Simple shear:* (**A**) The foliation, initially parallel to the shear plane of the flow, is deflected by the anticlockwise rotation of the equant inclusion. The sense of the deflection directly reflects the shear-sense of the flow (arrows). (**B**) The foliation was initially oriented perpendicular to the shear plane. The inclusion rotated anticlockwise (sinistrally), yet the apparent deflection could be described as a relative clockwise rotation of the inclusion with respect to the foliation. This reflects the fact that in simple shear, a passive marker oriented at $0° < \alpha > 45°$ rotates faster than a circular inclusion. *General shearing flow:* (**C**) Inspection of Fig.23 shows that, with significant shortening across the flow plane, a foliation oriented within the angular range $45° < \alpha < 90°$ may rotate faster than a circular inclusion. Hence, the apparent sense of "*drag*" can be opposite to the bulk shear-sense. (A) and (B) adapted from Ghosh (1975). (C) adapted from Ghosh (1977).

published terminology is rather confusing, since the label 'C/S' has been attached to strain-sensitive fabrics (Berthé et al., 1979a) and the label 'S/C' has been attached to strain-insensitive fabrics (Lister and Snoke, 1984). Although Lister and Snoke were careful to discriminate between strain sensitive *Type I* S/C fabrics and strain-insensitive *Type II* S/C fabrics, some other workers have been less discriminating in their use of the S/C label. If for this reason alone, we strongly suggest that C/S be reserved for strain-sensitive composite fabrics and that strain-insensitive fabrics be described in terms of Sa/Sb components (Law et al., 1984).

Deflection of foliations and layers

The deflection of a planar marker as it enters a shear zone, is often colloquially referred to as "*drag*". Deduction of shear-sense from the resulting geometry is then predicated on the sense of drag. We will examine the kinematic significance of two types of deflection structure which are commonly used as shear-sense indicators; the deflection of markers into shear zones and around stiff inclusions.

Shear zones

It is practically axiomatic that the deflection of a line or a plane into the flow plane is a direct reflection of the sense of shear. While this may well hold true under some circumstances, where the data are two-dimensional there are situations where the geologist would be well advised to exercise caution (see Wheeler, 1987; Fig. 37A, B). Where an external pre-existing layer intersects an ideal simple shear zone, it is deflected from its original orientation and thinned, or thickened, from its original dimensions as it enters the zone of high strain. The apparent deflection of a marker plane in two-dimensions will accurately reflect the bulk shear-sense (i) where the intersection of the marker with the wall of the shear zone lies at an high angle to the plane of observation; and/or (ii) where the true displacement vector of the wall rocks lies very close to the plane of observation (Fig. 37A). Where the intersection lies close to the plane of observation and/or makes an high angle with the true displacement vector, the observed deflection of the marker in that plane may be opposite to the sense of the bulk shear (Fig. 37B).

Inclusions

The asymmetry of the deflection of matrix foliation around approximately equant porphyroclasts has been used as a shear-sense indicator in mylonitic rocks (e.g. Simpson and Schmid, 1983; Takagi, 1986). However, this approach does not yield unique solutions unless the geologist is able to independently establish the initial orientation of the foliation and the nature of the flow regime (Fig. 38). The apparent deflection of matrix foliation around an equant inclusion reflects the relative rotation rates of elements of different aspect ratio (R; see section Rotations). However, while the normalized rotation rate of a circular inclusion is a constant ($\dot{\phi}/\dot{\gamma} = 0.5$), that of a passive marker is dependent on both flow type and orientation (α) of the marker (Ghosh and Ramberg, 1976; Fig. 23). This means that it is necessary to know both the initial, or at least some intermediate orientation of the foliation and the flow type in order to deduce the kinematic significance of the observed deflection.

Consider a foliation initially oriented perpendicular to the bulk flow plane and subjected to sinistral ideal simple shear (Fig. 38B). Without an established kinematic frame of reference, the observed deflection could be described either as a relative clockwise rotation of the inclusion with respect to the foliation, or as a relative anticlockwise rotation of the foliation with respect to the inclusion. This reflects the fact that in simple shear, a passive marker oriented at $0^\circ < \alpha < 45^\circ$ rotates faster than a circular inclusion. Simply assuming that the foliation initially lay parallel to the shear plane (as in Fig. 38A) would lead to incorrect deduction of both the sense of shear and the orientation of the shear plane (Fig. 38B). Experimental work by Ghosh (1977) has demonstrated that similarly equivocal geometries can be readily generated in general noncoaxial flow (Fig. 38C).

INCLUSIONS AND APPENDAGES

We shall now examine seven aspects of inclusions: (i) the rotational behaviour of inclusions; (ii) why many inclusions do *not* rotate at all , even in bulk noncoaxial flows; (iii) the positions in which some inclusions are *'at rest'*, after having rotated; (iv) the rotational behaviour of appendages associated with inclusions; (v) the formation of pressure fringes and pressure shadows; (vi) asymmetrically disposed structures in domains of layer-parallel and layer-normal shortening adjacent to inclusions; and (vii) the 'tiling' of inclusions.

Inclusions of stiff material, included in a relatively soft matrix undergoing noncoaxial progressive deformation, may rotate with respect to the flow plane. The qualified nature of this statement may surprise some readers, but consider for a moment an hypothetical, well exposed outcrop of strongly sheared, mylonitic orthogneiss, laden with large feldspar porphyroclasts, such as might be derived by the deformation of a megacrystic granite. Most of the large feldspars are elliptical, but almost all are oriented with their long axes lying in the mylonitic foliation (shear plane), aligned along the extension lineation (shear direction; see section *Shear plane and shear direction*). However, the outcrop may contain one or two "textbook" examples of *'rotated feldspars'*, upon which the kinematic interpretation of the outcrop is based (see section *Winged porphyroclasts*). Our hypothetical outcrop is fairly representative of many "type" shear-sense locations. Readers may be reminded of their own favorite "show-and-tell" outcrops, or of those they have visited on field trips. The rotated feldspars are indeed of great kinematic interest, but an equally important aspect of the deformation is all too often overlooked: *why do the other feldspars show no apparent evidence of the non-coaxiality of the flow*?

Students of inclusions have tended to consider them under three headings: (1) porphyroblasts, (2) porphyroclasts, and (3) stiff inclusions in general, each of which has been considered in terms of both simple shear and general noncoaxial flows. We shall first look at the theoretical and experimental analysis of the special cases of porphyroblasts and winged porphyroclasts. Then we will consider the general case of stiff inclusions, with and without wings and will apply our discussion to natural examples.

PORPHYROBLASTS

The rotation of porphyroblasts, i.e. crystals which have grown in the solid state, during or after their growth, is well described in the literature and is known to most geologists, at least at an intuitive level (e.g. Spry, 1969; Rosenfeld, 1968, 1970; Wilson, 1971; de Wit, 1976; Dixon, 1976; Schoneveld, 1977, 1978; Ghosh and Ramberg, 1978; Powell and Vernon, 1979; Williams and Schoneveld, 1981; Lister et al., 1986; Vissers, 1987; Jamieson and Vernon, 1987; Mandal and Banerjee, 1987). Porphyroblasts contain trails of inclusions which represent segments of matrix foliation overgrown by, and included in, the porphyroblast. The trails are referred to as the *internal foliation*, as opposed to the *external foliation* of the matrix (Fig. 39). The difference between the orientations of the internal and external foliations can be used to determine the relative rotation of the porphyroblast with respect to the far-field foliation in the matrix. However, as pointed out by T.H. Bell (1981, 1985; Bell et al., 1986), it is not necessarily a simple matter to determine which of the two, porphyroblast or matrix foliation, underwent true rotation with respect to the flow plane (see also Dixon, 1976; Ghosh and Ramberg, 1978). Ideally, at least the later increments of growth of the porphyroblast should have been contemporaneous with the rotation in order to maintain continuity from the internal to the external foliations. Although many porphyroblastic species are deformable (e.g. andalusite), the porphyroblast is usually assumed to be rigid (e.g. garnet) and its rotation is taken to represent the rolling of a rigid body. We remind the reader that while many studies, including the present one, take the foliation, in its present position, to lie close to the shear plane of the deformation in highly strained rocks, this is nevertheless an assumption.

Many rocks comprise large, relatively stiff, weakly anisotropic porphyroblasts set in a finer grained, anisotropic matrix. According to the models of Rosenfeld (1968, 1970) and Schoneveld (1977, 1978), a growing, rotating porphyroblast will incorporate two types of included material (Fig. 39).

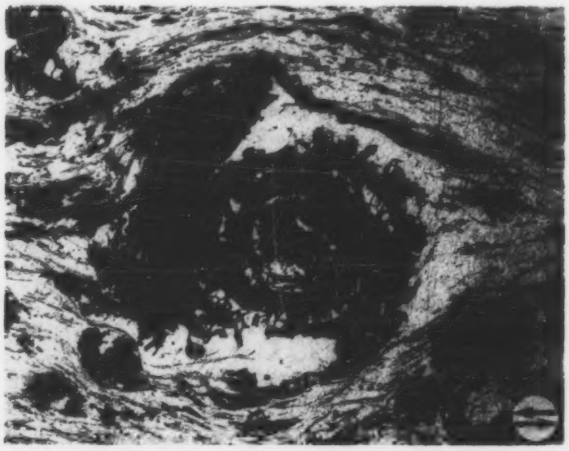

Figure 39. Rotated garnet porphyroblast. An *helicitic* garnet, observed in the XZ plane of the finite strain ellipsoid. The sense of shear along the flow plane is shown. The *internal foliation* is a spiral trail of inclusions of matrix material making three left-handed 360° turns from the centre of the porphyroblast. The porphyroblast has rotated anticlockwise in response to sinistral shear during its growth. Garnet diameter = 5 mm. Specimen #512, Schoneveld collection, University of Utrecht. (GSC 205184).

On faces making an high angle with the maximum instantaneous stretching axis of the flow, inclusions of pressure shadow material (see section *Pressure shadows*) are incorporated into the body of the growing porphyroblast. On those faces making an high angle with the minimum instantaneous stretching axis, grains of matrix material often aligned in the matrix foliation are incorporated. The result is two spiral inclusions trails, each composed of different inclusions and linked across the porphyroblast boundary to the exterior at different places around the porphyroblast perimeter.

In a recent series of papers, Bell has highlighted the role of porphyroblasts, and of material properties in the adjacent matrix, in the repartitioning of the rotational component of a bulk noncoaxial deformation (Bell, 1981, 1985; Bell et al., 1986). Instead of assuming a uniform flow type throughout the flowing material, he considers the nature of the flow as a function of the variably anisotropic character of the deforming rock (Fig. 40). Bell considered the specific case of a genetic spatial relationship between microstructural variation in the matrix and the presence of porphyroblasts. The perturbation represented by the porphyroblasts leads to an heterogeneous strain distribution in the adjacent matrix. During progressive deformation, pressure solution generates strongly anisotropic, phyllosilicate-rich zones adjacent to porphyroblast faces making an high angle with the minimum instantaneous stretching axis. Such a genetic relationship is not essential to our discussion. For our purposes here, it suffices to consider porphyroblasts set in a matrix which contains abundant, phyllosilicate-rich zones, oriented subparallel to the flow plane, some of which lie adjacent to the porphyroblasts.

In the case of bulk general noncoaxial flow, the relatively low resistance to slip in the highly anisotropic, phyllosilicate-rich parts of the matrix enhances their ability to accommodate the simple shear component of the flow. Because phyllosilicates are relatively insoluble compared to quartz, Bell suggests that, depending on the orientation of the anisotropy with respect to the bulk flow plane, phyllosilicate-rich zones will not readily accommodate the pure shear component of the flow. On the other hand, the porphyroblasts and the less anisotropic parts of the matrix do not efficiently accommodate simple shear. Rather, unless they are rigid, they may respond to the imposed deformation by a more or less coaxial local flow (compare Fig. 41 with the right-hand side of Fig. 25). The result would be a repartitioning of the rotational component of the bulk flow. If we now apply the same arguments to the case of bulk simple shear, it follows that the more efficiently the anisotropic zones are able to accommodate slip, the lower the strain rate in the porphyroblast and its adjacent matrix. The result is a special case; redistribution of the flow, without repartitioning of its rotational component (see left-hand side of Fig. 25).

When considering some natural examples of supposedly rotated helicitic garnets, Bell (1985) accounts for the sigmoid geometry of the internal foliation as an asymmetrically

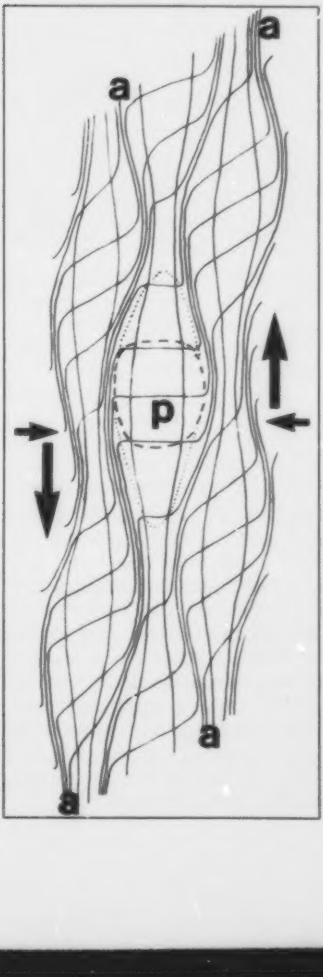

Figure 40. To rotate, or not to rotate... .Variation in microstructure can lead to a systematic partitioning of the rotational component of the flow such that the local flow type nowhere corresponds to that of the bulk flow (see Fig. 25). Consider an 'island' of isotropic, relatively stiff material, enclosed in a foliated matrix within which there are *highly anisotropic zones* (a) whose resistance to slip is low and which cannot readily accommodate layer-normal shortening. This might correspond to a porphyroblast (p) with pressure shadows, flanked by phyllosilicate-rich zones. The *local flow*, contributing to the accommodation of a bulk general noncoaxial flow, would be variable within such a differentiated microstructure. The anisotropic zones can efficiently accommodate the noncoaxial simple shear component by slip. Rotation of the anisotropy towards the local shear plane may make a minor contribution towards accommodating the shortening normal to the bulk flow plane. The contribution of the isotropic 'island' to accommodating the simple shear component of the flow will be relatively minor. It will depend on the stiffness of the material, as will the ability of the 'island' to accommodate shortening normal to the bulk flow plane. For example, the central 'island' in the accompanying illustration is drawn as if it contained a rigid porphyroblast. The other four 'islands' are represented as stiff, but deformable volumes, either of matrix or of deformable porphyroblast material. In any case, relative to the bulk regime, flow in the 'islands' tends to be more coaxial, while in the anisotropic zones it tends towards simple shear. Modified after Bell (1985).

micro-folded or crenulated foliation, whose hinge zones are overgrown and preserved by the stiff porphyroblast (Fig. 41). According to Bell, the micro-fold closures are sites of preferential nucleation and growth of the porphyroblasts (Bell et al., 1986). Metamorphic segregation during the folding process tends to concentrate phyllosilicates in the fold limbs. Hence, the limbs are predestined to become zones of easy slip. Continued deformation leads to the total transposition of the micro-fold limbs into a new foliation which wraps around the porphyroblasts. The crenulation fold closures are obliterated, except where they are fossilized as sigmoid trails in the stiff porphyroblasts. The repartitioning of the rotational component of the flow is such that 'islands' of coaxial, irrotational progressive deformation nucleate about the porphyroblasts. In other words, many "helicitic" porphyroblasts may not have rotated at all.

Bell's perceptive analysis and reinterpretation of sigmoid inclusion trails in some porphyroblasts is supported by similar analysis of micas (Vernon, 1988). It offers an elegant explanation of the all too often overlooked absence of rotated porphyroclasts in many sheared rocks. However, it does not explain why the geometry of curved inclusion trails is usually symmetrical with respect to the core of the porphyroblast (M.R. St-Onge, pers. comm., 1989). *We do not consider that all sigmoid internal foliations formed without rotation of the porphyroblast during growth.* For example, Bell's model does not predict continuous spiral inclusion trails which curve through angles much greater than 180° (Fig. 39). The point here is that these kinds of studies clearly demonstrate that geologists must carefully weigh the evidence before determining shear-sense from such microstructures.

STIFF INCLUSIONS

Theoretical prelude

Before considering natural examples of stiff inclusions set in a matrix which has undergone noncoaxial progressive deformation, let us first examine the predictions which can be made based on ideal theoretical models (e.g. Ghosh and Ramberg, 1976; Hanmer, 1984a; Passchier, 1987b). As discussed in the section Rotation: rate and direction, the rotational behaviour of inclusions and passive markers, in a given flow type, is a partial function of their aspect ratio (Fig. 23). Inclusions of circular section rotate continuously at a constant angular velocity, except in coaxial flow when they do not rotate at all. Passive markers rotate towards the flow plane at an angular velocity whose magnitude depends upon their orientation

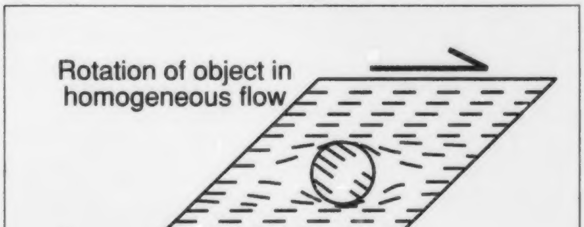
Rotation of object in homogeneous flow
A
B
'Apparent' rotation: object stationary
SKH 90 CWP

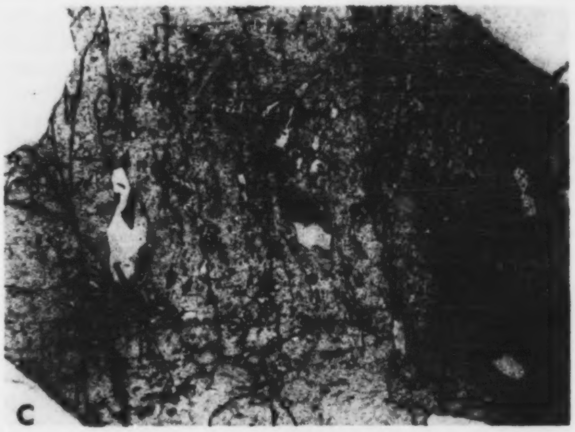

Figure 41. Rotated porphyroblast or fossilized crenulation? (A) and (B) represent two models of porphyroblasts with an included internal foliation oblique to the external foliation. In (**A**), a component of simple shear flow along the external foliation results in rotation of the porphyroblast. If the porphyroblast grew during rotation then it may include and preserve a sigmoid internal foliation from whose geometry one can deduce the shear-sense of the flow. However, in (**B**), the porphyroblast is shown overgrowing an older foliation which in the matrix is seen to be tightly crenulated by a second dominant foliation (enlargement). The presence of the stiff porphyroblast provokes a repartitioning of the rotational component of the flow such that local flow adjacent to the porphyroblast is more coaxial, whereas the flow in the matrix away from the porphyroblast is more noncoaxial than the bulk flow. Without the boundary displacements shown in the illustration, the deformation histories of (A) and (B) could not be unequivocally distinguished. (**C**) An euhedral 'helicitic' garnet in a paragneiss, observed in the XZ plane of the finite strain ellipsoid. The 'internal foliation' is an 'S'-shaped sigmoid trail of quartz and biotite inclusions. Has the garnet rotated sinistrally through some 90° during porphyroblast growth, or is the internal foliation a fossilised pre- to syn-growth microfold closure? Central Metasedimentary Belt boundary thrust zone, Ontario, looking northeast.

with respect to the flow plane. Upon reaching the flow plane, they cease rotating. Elliptical inclusions rotate at an angular velocity which depends upon their orientation, their shape and the flow type. In progressive simple shear, the angular velocity is 'pulsating'. In a general noncoaxial flow type, elliptical objects whose aspect ratio is greater than the critical aspect ratio (R_c) can come to rest at positions partly determined by their shape.

'Naked' inclusions

By *naked*, we simply mean that the inclusions are discrete objects, without lateral appendages, or *wings*. The statistical analysis of the orientation frequency of a population of such inclusions could reflect both the sign of the vorticity (shear-sense) of the flow and the flow type (Fernandez et al., 1983; cf. Hooper and Hatcher, 1988). Several recent studies have attempted to address this question (Hanmer, 1984a, 1986a, 1990; Passchier, 1987b).

From the symmetrical distribution of the rotation rate curves for simple shear in Figure 23, it follows that the orientations of stiff inclusions should constitute a *normal distribution*, symmetrical about the flow plane. On the other hand, in general noncoaxial flows, the rotation rate curves are displaced towards higher values of α. Given that inclusions of aspect ratio $R>R_c$ have stable positions in the flow, and given the "flight" of inclusions from unstable rest-positions oriented at $\alpha>\alpha_c$ (Fig. 23), histograms of the orientation frequency should be skewed such that their modes lie within the angular range $90^\circ<\alpha<\alpha_c$.

Few data on inclusion aspect ratio (R) versus orientation (α) are available for natural populations of rotated inclusions (Hanmer, 1986a; Passchier, 1987b; Tagaki and Ito, 1988). Such measurements would be most easily obtained in porphyroclast-bearing mylonites. In the data sets from two studies presented in Figure 42, the skewness towards the angular range $90^\circ<\alpha<135^\circ$ in both populations is subtle, but systematic. We would suggest that this skewness of the data reflects the general noncoaxial nature of the flow and that the sense of skewness reflects the sign of the vorticity (shear-sense) of the flow. However, we must stress here that the natural data do not conform very closely to the theoretical predictions outlined above (Fig. 42E, F). This probably reflects deviation of the natural case from the ideal model due to non-Newtonian behaviour of the matrix, ductility of the inclusions, deviation from elliptical inclusion shape and interference between inclusions, as well as possible variation in flow type during progressive deformation.

Winged porphyroclasts

A winged porphyroclast, observed looking along the rotation axis of the flow, comprises a circular to elliptical monocrystalline core attached to thin, planar, polycrystalline, wing-like appendages, often similar in composition to the porphyroclast itself. The wings may be *in-plane*, that is they may lie in a single material plane which passes through the centre of the porphyroclast and lies subparallel to the flow plane, except immediately adjacent to the porphyroclast, which itself may be markedly oblique to the flow plane. The long dimension of the elliptical porphyroclast often lies within the angular range $90^\circ<\alpha<180^\circ$ of the flow (Fig. 43A). Alternatively, the structure forms a *stair-step* wherein the wings are flats, linked by the porphyroclast. Triangular volumes of matrix are generally entrained between the porphyroclast and its wings. Winged porphyroclasts are often derived by the mechanical degradation of granitic pegmatite in a strongly sheared mylonitic host rocks and often occur as trains of objects aligned along the mylonitic foliation (Fig. 43C). It is important to note that, since fold structures are absent in the mylonitic foliation

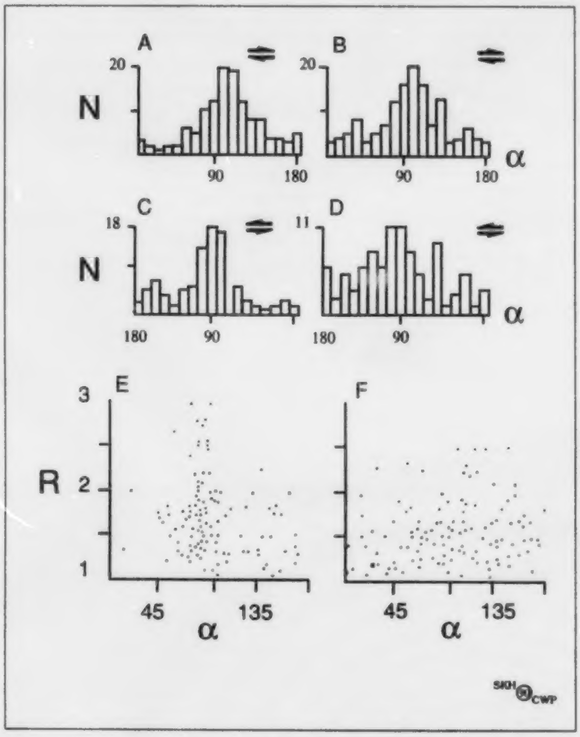

Figure 42. 'Naked' inclusions. The frequency distribution of orientations in a population of inclusions should be a partial function of the flow type. A naked inclusion is a discrete elliptical object, without lateral appendages or wings. (**A**) and (**B**) are data for porphyroclasts in mylonites from the dextral transcurrent Great Slave Lake Shear Zone, N.W.T. (Hanmer, 1986a, 1988). (**C**) and (**D**) are data for porphyroclasts in mylonites of the sinistral transcurrent Median Tectonic Line, Japan, taken from Takagi and Ito (1988). These data were measured in the XZ section of the finite strain ellipsoid. Each population is mildly, but systematically, skewed towards the angular range $90^\circ<\alpha<180^\circ$, in agreement with theoretical prediction for general noncoaxial flows (see Fig. 23).

Theory predicts that the orientations of those inclusions *at rest* are a partial function of the aspect ratio (Fig. 23). However, two populations of data from Great Slave Lake Shear Zone (**E** and **F**) do not show a detectable correlation between R and α. This presumably reflects deviation of the natural case from the ideal model due to (i) non-Newtonian behaviour of the matrix, (ii) ductility of the inclusions, (iii) deviation from elliptical inclusion shape and (iv) interference between inclusions.

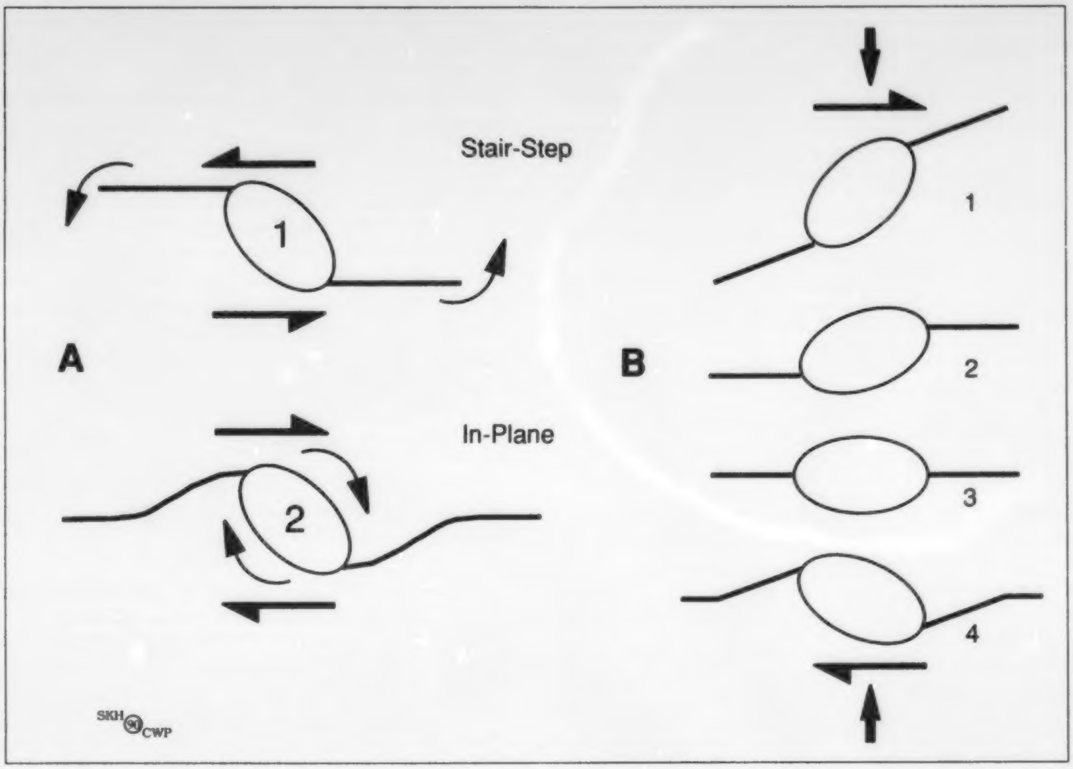

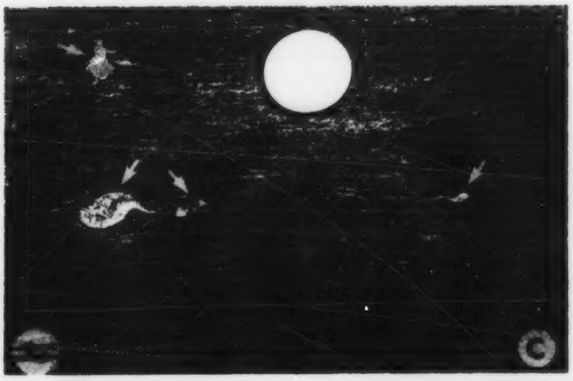

Figure 43. Winged inclusion geometry. The geometry of an elliptical winged inclusion, observed looking along the rotation axis of the flow, may correspond to any one of a number of developmental stages. Shear-sense along the flow plane is shown. (**A**) The *stair-step* (#1) and *in-plane* (#2) geometries of two winged inclusions superficially resemble each other. However, inclusion #2 has rotated dextrally through the flow plane. Its wings lie in a single material plane which passes through the centre of the inclusion and lies parallel to the flow plane, except immediately adjacent to the inclusion. Inclusion #1 has rotated sinistrally. Its wings have rotated into parallel with the flow plane, while the long dimension of the inclusion is still markedly oblique. The structure forms a right-stepping stair-step wherein the wings are flats linked by the inclusion. (**B**) In general, mature *in-plane* geometries imply a component of extension in the flow plane. Here a sequence of geometries (1-4) is developed from an inclusion and its wings, initially oriented in the extensional quadrants of the flow (see Simpson and Schmid, 1983), but undergoing a *general noncoaxial flow*. Because objects of high aspect ratio rotate faster in general noncoaxial flow ($0<W_k<<1$) than stubby objects oriented in the range $45^\circ<\alpha<90^\circ$, the wings of the structure show a *stair-step* configuration in the less mature stages of development (B2). In simple shear, the inclusion would have rotated faster than the wings (see Fig. 23). Furthermore, the sequence from B1 to B3 could not occur in simple shear, because it requires that the flow plane extend in the shear direction in order to allow the wings to approach the in-plane configuration (B3). Note however that, although in-plane geometries reflect total deformations corresponding to progressive general noncoaxial flow, the instantaneous nature of the flow remains unknown; the same geometry could result from a variety of sequences of simple shear and pure shear flows. A mature winged inclusion will only preserve a stair-step geometry where the progressive deformation path was simple shear. (**C**) Four natural examples of inclusions (white arrows), very similar to A2 and B4, derived by the mechanical degradation of granitic pegmatite in an ultramylonite, observed in the XZ plane of the finite strain ellipsoid. The sense of shear is sinistral. All four inclusions lie at with their long dimensions oriented within the angular range $90^\circ<\alpha<180^\circ$. Note the absence of fold structures in the mylonitic foliation; the porphyroclasts are not simply the short limbs of asymmetrical folds. Parry Sound, Grenville Province, Ontario, looking northeast. (GSC 204337-J)

of the host rock in the examples illustrated in this study, the porphyroclasts are clearly not simply the short limbs of asymmetrical folds (Fig. 43C).

The way in which a porphyroclast responds to progressive deformation distinguishes it from stiff inclusions comprised of rock fragments (see section *General winged inclusions*). When a relatively large single crystal deforms by crystal-plastic processes, the concentration of lattice distortion in its outer parts is relaxed by dynamic recrystallization (e.g. Nicolas and Poirier, 1976; Poirier and Guillopé, 1979; Poirier, 1985; Tullis and Yund, 1985). This results in a *core-and-mantle* microstructure; a relatively stiff relic monocrystalline *core*, surrounded by a relatively soft polycrystalline *mantle* (White, 1976). The soft mantle may deform into a pair of lateral appendages or *wings*, drawn out on either side of the inclusion. In a series of physical experiments, Passchier (Passchier and Simpson, 1986) and Van den Driessche and Brun (1987) have successfully modelled the evolution of the geometry of core-and-mantle structures subjected to bulk progressive simple shear (Fig. 44, 45).

By varying the ratio of the recrystallization rate to the shear strain rate ($\dot{R}/\dot{\gamma}$), Passchier was able to produce a range of different geometries with increasing strain (Fig. 44). The basis of the experiment is that when a stiff crystal, circular in section, progressively recrystallizes at its periphery it feeds new grains into a soft, polycrystalline mantle capable of undergoing shape change. For experimental convenience, the deformation was performed in steps; an increment of recrystallization followed by an increment of imposed bulk simple shear. The geometry which results is in part dependent upon the $\dot{R}/\dot{\gamma}$ ratio. Recrystallization feeds new daughter grains into

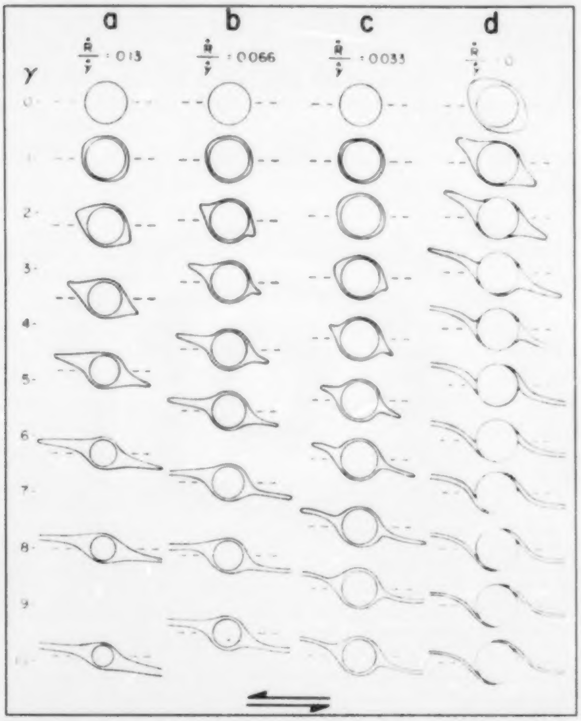
a
b
c
d
$\dot{R}/\dot{\gamma}$ = 0.13
$\dot{R}/\dot{\gamma}$ = 0.066
$\dot{R}/\dot{\gamma}$ = 0.033
$\dot{R}/\dot{\gamma}$ = 0
γ
0
1
2
3
4
5
6
7
8
9
10

Figure 44. Experimental 'winged' porphyroclasts I. In the deformation experiments of Passchier (Passchier and Simpson, 1986), a rigid cylinder of circular section was set in a soft matrix. A passive marker circle inscribed on the matrix around the cylinder, subjected to sinistral simple shear, simulates a soft polycrystalline *mantle* about a rigid *core*. The maximum instantaneous stretching axis runs from top left to bottom right. By incrementally transferring the shape of the deformed passive marker to a new model, into which is set a cylinder of smaller diameter, the experiment sequentially simulates progressive recrystallization of the core, as well as deformation and rotation of the mantle. Accordingly, the experimentalist can vary the ratio of the recrystallization rate ($\dot{R}$) to the shear strain rate ($\dot{\gamma}$). In all cases, the soft polycrystalline mantle is initially drawn out along the direction of maximum finite extension. With progressive deformation, the distal part of the deformed mantle flows along the direction of maximum finite extension and tracks its rotation towards the flow plane. The geometry which results is in part dependent upon the $\dot{R}/\dot{\gamma}$ ratio. At high normalized recrystallisation rates ($\dot{R}/\dot{\gamma}$), a full mantle is maintained around the porphyroclast and the overall core-and-mantle geometry resembles the Greek letter sigma (σ). At low normalized recrystallisation rates, the geometry of the structure resembles the Greek letter delta (δ). Taken from Passchier and Simpson (1986).

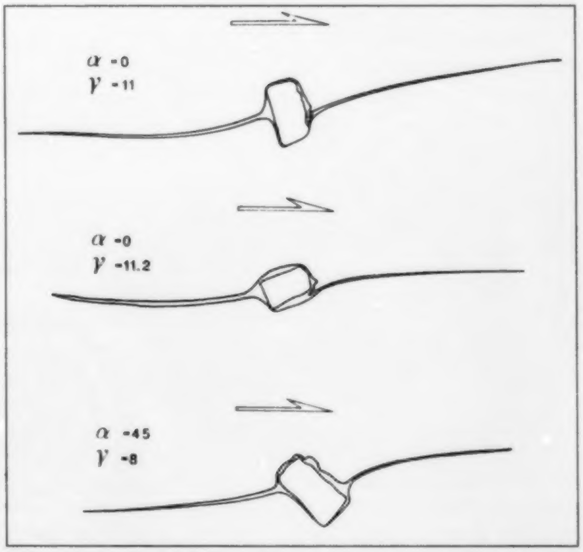

Figure 45. Experimental 'winged' porphyroclasts II. In the deformation experiments of Van den Driessche and Brun (1987) a relatively stiff, rectangular core was set in a soft matrix. Colour added to the matrix immediately adjacent to the core simulated a soft polycrystalline mantle, rheologically indistinct from the enclosing matrix. The mantle was initially of even thickness all around the inclusion. Prior to deformation, the inclusion was oriented with its long dimension at α=90° (upper and middle) or α=45° (lower). The initial configuration was subjected to progressive simple shear. The mantle flowed with the matrix and the resulting wings attempted to track the direction of maximum finite extension. In keeping with progressive simple shear, the inclusion has rotated faster than the attenuated mantle wings (Fig. 23). The overall structure shows a marked stair-step geometry (Fig. 43). With one exception (middle-right), the wings are curved along much of their length, despite the high shear strain values (γ). Taken from Van den Driessche and Brun (1987).

the proximal parts of the deforming polycrystalline mantle and attempts to compensate the attenuation of the mantle shape. At high normalized recrystallization rates ($\dot{R}/\dot{\gamma}$), a full mantle is maintained around the porphyroclast and the overall core-and-mantle geometry resembles the Greek letter sigma (σ). At low normalized recrystallization rates, the mantle is rapidly depleted at the edge of the porphyroclast and most of the porphyroclast is in direct contact with the rock matrix (d in Fig. 44). The core-mantle contacts are reduced to two small zones, one on either side of the porphyroclast. Initially these zones lie in the extensional quadrants of the flow, but rotate progressively to lie in the shortening quadrants. At this stage, the geometry of the structure resembles the Greek letter delta (δ).

In natural examples, the deflection of the attenuated mantle adjacent to the core occurs due to viscous drag as the circular porphyroclast rotates. Because the mantle is effectively uncoupled from the core, the point of contact between the rotating porphyroclast and the mantle can only migrate to the point where the mantle makes a tangent with the porphyroclast outline. Further rotation of the porphyroclast does not modify the geometry of the structure. Note that both σ and δ structures result in a stair-step geometry (Fig. 43), wherein the attenuated mantle flats are linked by a core step.

The boundary conditions of the experiments performed by Van den Driessche and Brun (1987) were very similar to those of Passchier (Passchier and Simpson, 1986) for low $\dot{R}/\dot{\gamma}$ ratios. However, these experiments were carried to greater shear strains than those of Passchier, and the initial core was rectangular. Van den Driessche and Brun showed that even at shear strains of $\gamma>11$, the wings of the structure are strikingly curved, clearly oblique to the flow plane all along their length and show a marked stair-step geometry (Fig. 45).

In their initial stages of development, the shear-sense significance of natural σ and δ structures is readily deduced, since the direction of elongation of the polycrystalline mantle is clearly close to that of the maximum infinitesimal extension (Fig. 44). However, even assuming that the orientation of the bulk flow plane is known, does the sense of obliquity between the deformed mantle and the flow plane give an unambiguous sense of shear in the more mature stages of mantle development? (e.g. a8 and b8 in Fig. 44). Clearly not, since a single example of such a geometry does not enable the geologist to observe evidence for a rotation of the principal directions of finite strain with respect to the instantaneous stretching axes of the flow, or with respect to the flow plane. Moreover, the geometry of a mature σ structure bears a resemblance to a rotated pressure shadow (see section *Rotated pressure shadows*); yet, kinematically the two structures represent opposite senses of shear (compare a5-a10 and b5-b10 in Fig. 44 with Fig. 63B). *The kinematic significance of mature σ structures is only apparent when a number of examples are present in the rock,* representing several stages of development, from which to reconstruct the progressive deformation history.

By way of contrast, a single example of a mature δ structure contains all of the information required to determine the sense of shear. The shear-sense is directly read from the sense of drag of the polycrystalline wing in the vicinity of the porphyroclast. While this is intuitively obvious, the technical explanation may be read in the rotational behaviour curves for simple shear (Fig. 23). Referring to Figure 44, in simple shear, a passive marker oriented at an angle of $\alpha>45°$ (d1) rotates more slowly than an inclusion of circular, or sub-circular section. As its shape becomes attenuated with strain, the rotational behaviour of the mantle wing approaches that of a passive marker, hence its rotation rate slows to zero as it approaches the flow plane (d3-d10). Note that, beyond the initial stages of development (d2), the rheology of the polycrystalline mantle is not pertinent to the discussion, since even rigid elongate appendages would show the same rotational behaviour as a passive marker. The core continues to rotate with progressive deformation at a constant rate and, due to the viscous drag at its boundary, deflects the proximal part of the mantle wing (d3-d7). The deflection reflects the rotation of the porphyroclast, which directly reflects the shear-sense of the flow.

General winged inclusions

In addition to winged porphyroclasts, where the wings are derived by recrystallization of the central inclusion, it is possible to define a more general set of winged structures. We use the term *winged inclusion* to refer to any stiff inclusion attached to relatively thin, planar, external wing-like appendages (Hanmer, 1984a). Others have used the term *rolling structure* (Van den Driessche, 1986b). Independently of their internal structure, the overall geometry of winged inclusions generally conforms to the following geometry, as observed looking along the rotation axis of the flow (Fig. 43):

(1) The inclusion is *elliptical;* only rarely is it circular in section.

(2) The long dimension of the inclusion can make any angle (a) with the normal to the shear plane. Nonetheless, we are struck by the frequent occurrence of field examples where the long dimension of the inclusion lies within the angular range $90°<\alpha<180°$ of the flow (Fig. 43C, 47A, 48, 49 and 50). Given the small number of examples in any given outcrop, it is difficult to support this contention statistically. However, quantitative support is derived from the analysis of 'naked inclusions' (section Naked inclusions).

(3) In the mature structure, the wings are often straight and *in-plane* (Fig. 43C, 46A, 47B, 48, 49 and 50). The wings of the structure may show a *stair-step* geometry in the less mature stages of development, though some mature examples preserve the stair-step (Fig. 46B, 47A).

Some inclusions are comprised of porphyroclasts of feldspar, often the relics of once very coarse pegmatite which has suffered extensive dynamic grain size reduction. The fine grained, polycrystalline wings attached to these inclusions may be either monomineralic feldspar or quartzo-feldspathic aggregates. There is no *prima facie* reason to suppose that the wings were derived from the porphyroclast with which they are now spatially associated (Fig. 46A, B). Other inclusions are polycrystalline

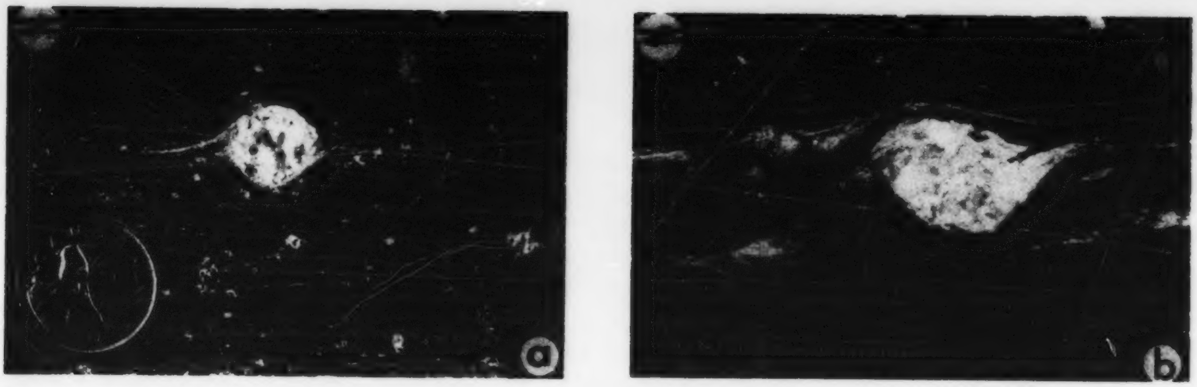

Figure 46. Natural winged porphyroclasts. Dextrally rotated 'δ-type' winged feldspar porphyroclasts in mylonite, observed in the XZ plane of the finite strain ellipsoid. Derived by the mechanical degradation of pegmatite. Shear-sense along the shear plane is shown. Note the triangular volumes of matrix entrained between the inclusion and the wings. (**a**) The porphyroclast is circular in cross section. The wings are straight, except adjacent to the porphyroclast, and show an in-plane geometry, implying that the flow plane was significantly extended during part or all of the progressive deformation. (**b**) The long dimension of the elliptical porphyroclast lies in the angular range $90^\circ<\alpha<180^\circ$. The wings are straight, except adjacent to the porphyroclast, and show a subtle stair-step geometry, stepping to the left. While the orientation of the inclusion could indicate general noncoaxial flow, the preservation of the 'stair-step' geometry suggests that extension of the shear plane was probably minor. Both examples are from Great Slave Lake Shear Zone, N.W.T., looking down. (GSC 204776-P and GSC 204337-I)

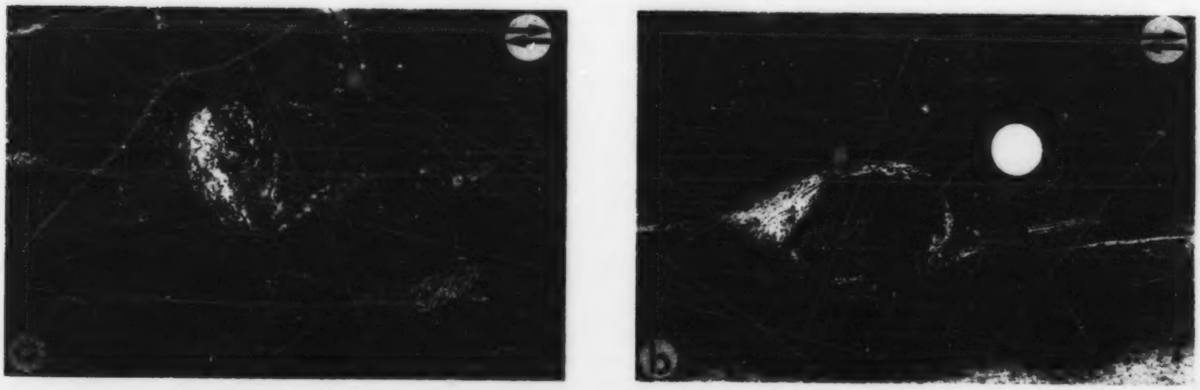

Figure 47. Natural winged inclusions I. Elliptical, dextrally rotated winged quartzite inclusions in a marble mylonite, observed in the XZ plane of the finite strain ellipsoid. Shear-sense along the shear plane is shown. Triangular volumes of matrix were entrained between the inclusions and their wings. The white marble of the wings is similar to marble bands within the mylonite matrix; it was not derived from the silicious inclusions. (**a**) The wings show a subtle stair-step geometry. Away from the inclusion, the right-hand wing shows a similar sweeping curve to those produced experimentally in ideal simple shear (Fig. 45). The marble wings are composed of relatively coarse, graphite-poor material, initially formed in pressure shadows in the extensional quadrants of the flow (see section *Pressure shadows*). The pressure shadows, the right-hand one of which is particularly well preserved, have rotated toward the shear plane with progressive deformation. An imaginary line linking the proximal parts of the pressure shadows has been rotated into the angular range $90^\circ<\alpha<180^\circ$. Whereas the orientation of the inclusion is probably not kinematically significant, the preservation of the stair-step geometry of the wings suggests that extension of the flow plane was relatively minor. (**b**) The wings show an in-plane geometry. Unlike (a), there is no evidence to suggest that the wings were derived by the deformation of pressure shadow material. Note the entrained triangular volume of matrix between the wing and the inclusion (right). The combined features of the structure suggest that extension of the shear plane of the deformation was important during some part of the deformation.

Both examples from the Central Metasedimentary Belt, Grenville Province, Ontario, looking northeast. (GSC 204775-F and GSC 204776-M).

and often polymineralic. Their wings may be deformed pressure shadows (Fig. 47A) or they may be bands of matrix material, entrained by the rotating inclusion (Fig. 47B). Several of the examples of inclusions illustrated here are simply thicker segments of otherwise thin rock layers and are not necessarily rheologically distinct from their wings (Fig. 48, 49). The salient points to retain here are that a general model for the rotational behaviour of winged inclusions (i) cannot be specific to a given process of wing differentiation (cf. Passchier and Simpson, 1986), (ii) must account for both *stair-step* and *in-plane* geometries (cf. van den Driessche and Brun, 1987), and (iii) it must allow for cases where the wings are *materially continuous* with the inclusion, as well as cases where the wings and the inclusion are *uncoupled*.

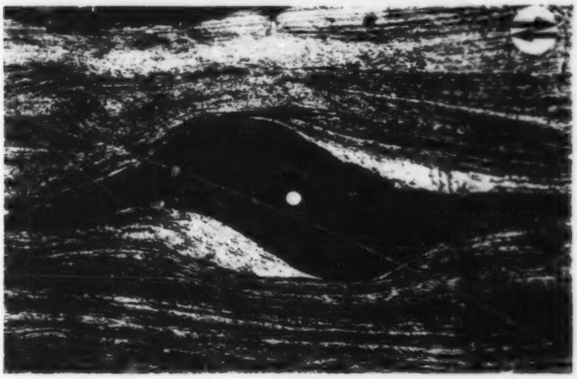

Figure 48. Natural winged inclusions II. A dextrally rotated *swell* in an heterogeneously extended amphibolite dyke in a mylonite matrix, observed in the XZ plane of the finite strain ellipsoid. Shear-sense along the shear plane is shown. The long dimension of the inclusion lies in the angular range $90^\circ<\alpha<180^\circ$. The wings are materially continuous with the inclusion and show an in-plane geometry. Note the development of pegmatite (light grey) in the extensional quadrants of the flow, adjacent to the inclusion (upper right and lower left). The orientation of the inclusion and the in-plane geometry of the wings imply that the flow plane was significantly extended during part, or all, of the deformation history. Great Slave Lake Shear Zone, N.W.T, looking down. (GSC 204337-N)

Instead of a stair-step configuration (Fig. 46B, 47A), the overall geometry of many natural examples of well developed winged inclusions is one of in-plane straight wings, deflected out of their far-field orientation in the vicinity of the inclusion (Fig. 43C, 46A, 47B, 48, 49 and 50). There are two possibilities: either the stair-step was never present, or it has been destroyed during progressive deformation.

First consider the case where an initial stair-step may have been destroyed. In order for an initial stair-step to transform to a mature structure wherein the wings lie in-plane, both the inclusion and the wings must have lain in-plane at some intermediate stage of the deformation (Fig. 43B). This can only occur if the entire structure is extended in the flow plane, such as would be the case in general noncoaxial flow. Further progressive shearing will have no effect on the orientation of the attenuated wings in the mature structure, since they are at rest in the flow plane (Fig. 23). Only the stubby inclusion will continue to rotate forwards (Fig. 43B) and, in doing so, it will deflect the proximal part of the wings. From a comparison of Figure 23 and the section *Naked inclusions*, the overall geometry of an in-plane winged inclusion structure, wherein the inclusion itself has attained a rest position within the angular range $90^\circ<\alpha<135^\circ$, can be readily explained in terms of a progressive general noncoaxial flow. A natural example showing many of the above mentioned stages of development is described in detail in Figure 50. A corollary to the foregoing model is that those mature winged inclusions which preserve a stair-step in their overall geometry (Fig. 46B, 47A) must have formed in flow approximating simple shear.

Now consider under what circumstances an in-plane winged inclusion might form without passing through a stair-stepped stage. The structure could have been heterogeneously extended along the shear plane of the deformation prior to rotation of the inclusion (Fig. 51A). This implies that

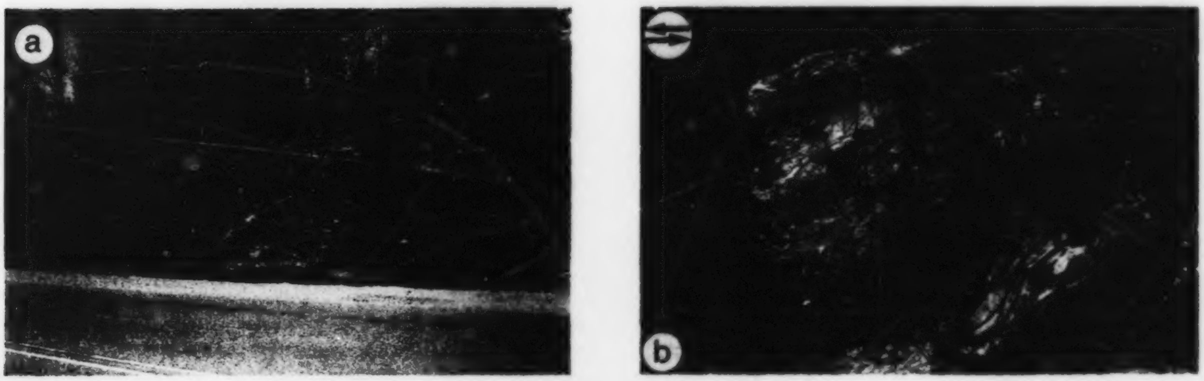

Figure 49. Natural winged inclusions III. Setting and detail of a sinistrally rotated, thick segment of quartzo-feldspathic gneissic layering, materially continuous with the stretched and thinned part of the same layer, observed in the XZ plane of the finite strain ellipsoid. Shear-sense along the shear plane is shown. The strongly attenuated layering is parallel to the shear plane. The long dimension of the inclusion lies in the angular range $90^\circ<\alpha<180^\circ$, suggesting general noncoaxial flow. Central Metasedimentary Belt boundary thrust zone, Grenville Province, Ontario, looking north-northeast. (GSC 204775-A)

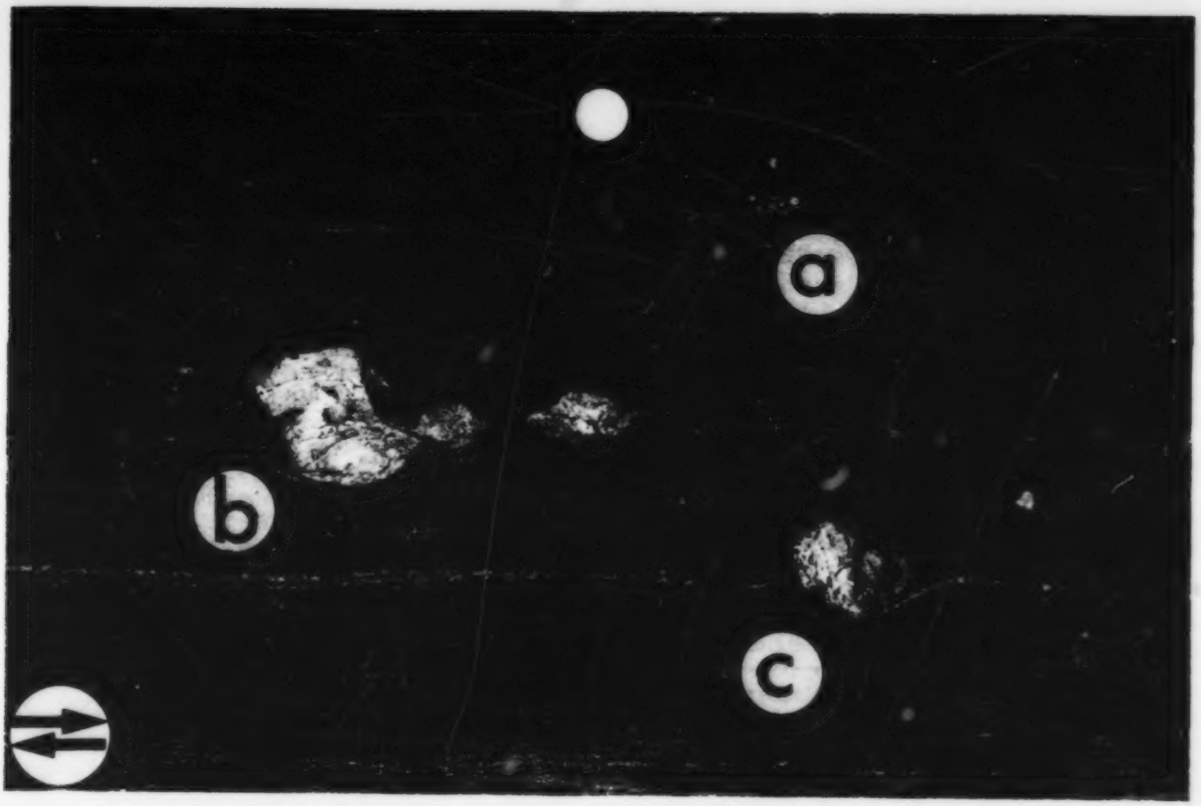

Figure 50. Fast wings and slow inclusions. Occasionally, the rotational behaviour of the component parts of natural winged inclusions can be observed at various stages of structural development. This illustration is of feldspar inclusions and polycrystalline feldspar wings, derived by the mechanical degradation of granitic pegmatite in an ultramylonite with a dextral sense of shear. The observation surface is the XZ plane of the finite strain ellipsoid. Shear-sense along the shear plane is shown. The *stair-step* geometry of the immature structure (**a**) can be described in terms of two elements: (i) an inclusion of moderate to low aspect ratio, oriented with its long dimension lying in the extensional quadrants of the flow at approximately α=80° and (ii) straight wings of *very high aspect ratio*, attached to the apices of the inclusion and oriented in the extensional quadrants of the flow at α=85°.

In simple shear, within the range $45° < \alpha < 90°$, the wings would rotate towards the shear plane more slowly than the inclusion, because of the sensitivity of the rotation rate to the aspect ratio of the object (see Fig. 23). Hence, an *ad hoc* explanation would be required to account for the observed geometry. However, in a general noncoaxial flow, where $0 < W_k << 1$, the relative rotation rates of the inclusion and the wings could be used to predict the observed geometry (see Fig. 43B). Had deformation continued, example a would have progressed to an 'S' shaped stair-step geometry, wherein each straight wing would be parallel to the shear plane along its length, even adjacent to the inclusion. (**b**) and (**c**) represent more advanced stages. Note that their wings lie *in-plane* and that the inclusions both lie with their long dimension oriented within the angular range $90° < \alpha < 180°$. Compare these with the geometries in Figures 43C, 48 and 49. The in-plane geometries of (b) and (c) can only be derived from initial stages such as a if there is a component of extension along the flow direction; in other words in general noncoaxial flow. Central Metasedimentary Belt boundary zone, Grenville Province, Québec. Taken from Hanmer and Ciesielski (1984). (GSC 204105-Q)

the inclusion was initially subjected to coaxial flow prior to rotation, or that it was insufficiently differentiated from its incipient wings in the earlier stages of a general noncoaxial flow. This is probably a fairly common occurrence in nature. Another possibility is that the wings and the inclusion formed by inhomogeneous extension of a layer which initially lay in the extensional quadrants of progressive simple shear at α=45°. Such a layer may initially extend inhomogeneously in its own plane (Fig. 51B). Within the angular range $45° < \alpha < 90°$, the stubby swells rotate faster than the attenuated pinches with progressive deformation (Fig. 23). When the line of centres of the swells has rotated to subparallel to the flow plane, the long dimensions of the swells will have rotated into the shortening quadrants of the flow. There would of course be a limit to the degree of separation between the swells. This scenario, while theoretically possible, represents a serendipitous set of fortuitous circumstances; it is only included here for completeness.

In some examples, the high angle made by the wing with the border of the inclusion at the symmetrical stage is preserved in the mature stage. This indicates good cohesion between the inclusion and its rock matrix, resulting in a *contact strain area* (Ramsay, 1967, p. 416) which rotates

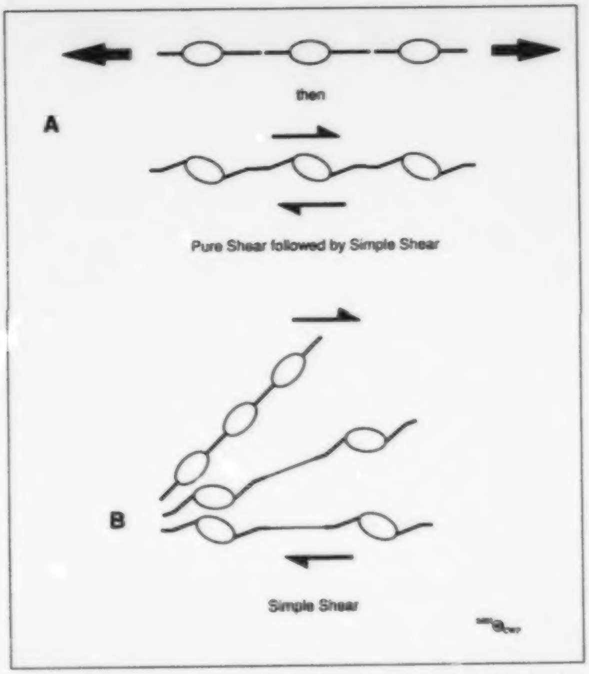

Figure 51. In-plane winged inclusions in simple shear. Rather than forming by progressive general noncoaxial flow, in-plane winged inclusions could form as a result of rotation in response to simple shear. (**A**) A layer initially subjected to coaxial inhomogeneous extension, is subsequently subjected to simple shear along its own plane. The stubby *swells* rotate with the same sense as the vorticity of the simple shear, but the attenuated *pinches* remain in the flow plane. (**B**) Alternatively, a layer oriented at $\alpha = 45°$ in simple shear may initially extend inhomogeneously in its own plane. However, within the angular range $45° < \alpha < 90°$, the stubby swells rotate faster than the attenuated pinches with progressive deformation (see Fig. 23). When the line of centres of the swells has rotated to sub-parallel to the flow plane, the long dimensions of the swells will have rotated into the angular range $90° < \alpha < 180°$. In light of the relative rotation and extension rates, this scenario is rather unrealistic. It is only included for completeness.

with the inclusion. The fact that the wings are continuous from the contact strain area into the far-field matrix, indicates that the inclusion does not necessarily uncouple from the wings (cf. Fig. 44, 45).

We wish to re-emphasise the difficulties and complexities involved in trying to interpret the rotational behaviour of inclusions and their attendant appendages. The models described above, predicated on the assumption of homogeneous flow, are easier to present than to apply unequivocally to rheologically heterogeneous natural examples. Other complexities will become even more apparent as we now turn to examine (i) the problem of antithetic rotation and (ii) the internal structure of pressure fringes.

BACK-ROTATED STRUCTURES

The kinematic significance of many shear-sense indicators is directly inferred from the sense of rotation of their component parts, as in the case of winged inclusions (see section *General winged inclusions*) or C/S fabrics (see section *C/S fabrics*). However, there is a category of shear-sense indicators which rotate *antithetically* with respect to the sense of the bulk flow.

As we have already seen in the case of *apparent deflection* of foliation wrapping around stiff inclusions, to cite but one example (see section *Inclusions*), geometry alone does not suffice to distinguish true rotation from apparent rotation. Clearly, before proposing that a given structure has not only undergone a true rotation, but an antithetic one at that, the onus is on the geologist to demonstrate that other possible interpretations can be reasonably discounted. *In order to identify true back-rotation of a structure the geologist must be able to reasonably infer the orientation of the structure in question, with respect to the instantaneous stretching axes and the flow plane, prior to the rotation of the structure*. Let us therefore begin with an examination of some natural examples of demonstrably apparent back-rotation, with respect to the flow plane (Fig. 52), before turning to consider possible examples of true antithetic rotation.

Apparent back-rotation

Consider a soft matrix subjected to coaxial progressive deformation. Set a stiff layer into the matrix such that it makes an initial angle of just under 45° with the maximum instantaneous stretching axis of the bulk flow and lies, therefore, within the extensional quadrants of the flow (Fig. 52B top). Flow within the soft matrix transmits stresses into the stiff layer across the cohesive rheological interface. If we now continue to subject the stiff layer to progressive deformation following an invariant deformation path, it will extend heterogeneously and breakup into a train of boudins. In our illustration, we have set the rheological contrast between the stiff layer and its matrix high enough that the boudins are blocky (Fig. 52B top). Prior to boudinage, strain refraction across the matrix/layer interface (see section *Strain and flow refraction*) causes the maximum instantaneous stretching axis within the stiff layer to lie parallel to the interface, oblique to the extension in the matrix. Thus, the resulting train of boudins is initially symmetrical.

Now, consider the flow pattern after the initiation of boudinage. Instead of a stiff layer, the soft matrix now contains a train of discrete stiff objects of relatively low aspect ratio, whose rotational behaviour is a function of their shape, their orientation with respect to the instantaneous stretching axes of the flow and the flow type (Fig. 52B top; see also section Rotation). However, the line of centres of the individual boudins represents a passive marker which must also rotate. From Figure 23, it is obvious that the rotation of the individual boudins with progressive deformation will lag behind that of the line of their centres (Fig. 52B top).

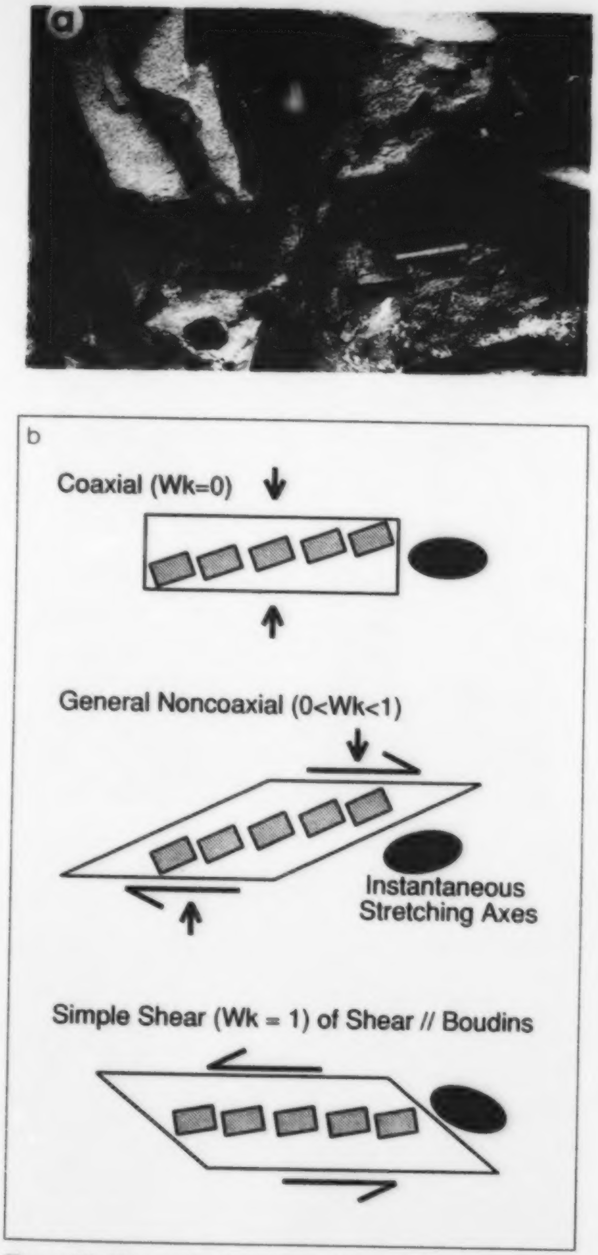
a
b
Coaxial (Wk=0)
General Noncoaxial (0<Wk<1)
Instantaneous Stretching Axes
Simple Shear (Wk = 1) of Shear // Boudins

Figure 52. Kinematically equivocal rotated boudinage. The photograph (**a**) illustrates a natural occurrence of boudins whose long dimensions are oblique to the line of their centres. The line drawings (**b**) illustrate three different models capable of producing that geometry. The case of *rotated boudinage* by coaxial progressive deformation is adapted from Ramsay (1967). The general noncoaxial case is indistinguishable from the first without independent knowledge of the flow type and the orientation of the layer with respect to the flow. The third case illustrates the application of simple shear along the length of a train of already extended stubby boudins. Clearly, it is not possible to determine shear-sense from (A) without additional data. (A) is from the Central Metasedimentary Belt boundary thrust zone, Grenville Province, Ontario, looking southwest. (GSC 204128-C)

The result of the above experiment is well known and has been termed *rotated boudinage* (Ramsay, 1967, p. 108-109). Now extend this example to a case of general noncoaxial flow (Fig. 52B middle). Here, the stiff layer was initially set at an angle of just less than 45° with respect to both the maximum instantaneous stretching axis of the coaxial component of the flow and the flow plane of the simple shear component. The result is geometrically very similar to that for the previous pure shear case, except that now we can describe the *apparent* anticlockwise rotation of the boudins as *apparently* antithetic with respect to the shear-sense of the bulk flow. However, in the absence of independent information concerning the flow type and, if appropriate, the orientation of the shear plane of the deformation, the unwary geologist might be tempted to see in our illustrations a train of inclusions which had undergone a real anticlockwise rotation with respect to the line of their centres. Clearly the anticlockwise rotation is only apparent, in both of our examples (compare with 52B bottom).

The foregoing leads us to reiterate: in order to identify true back-rotation of a structure the geologist must be able to reasonably infer the orientation of the structure in question, with respect to the instantaneous stretching axes and the flow plane, prior to the rotation of the structure. Although this is often easier said than done, let us now consider the possibility of real back-rotation of geological structures.

Back-rotated foliation segments

The geometry of several naturally occurring structures has been attributed by some workers to back-rotation with respect to the flow plane, antithetic to the shear-sense of the bulk flow. These include *foliation fish*, back-rotated anisotropic *pinch-and-swell* structures (Type IIa pull-aparts of Hanmer, 1984a, 1986b) and *mica fish* (Lister and Snoke, 1984).

These structures all share the following common features when observed in the XZ plane of the finite strain ellipsoid:

(1) They comprise volumes which are elongate in cross-section.

(2) They contain an *internal planar anisotropy*, oriented approximately parallel to the long dimension of the volume.

(3) The trace of the internal anisotropy and of the long dimension of the volume make a consistent angle of 5-10° with the bulk flow plane in the surrounding, external material. In a population of such structures, the sense of obliquity is constant.

Mica fish and back-rotated pinch-and-swell structures represent volumes of material of different composition and/or grain size compared with their enclosing matrix. In contrast, foliation fish are simply segments of the same foliated material as the surrounding rock, distinguished only by the orientation of their internal anisotropy. Hanmer (1986b) considered back-rotated swells and foliation fish in two subsets: (i) those associated with discrete asymmetrical extensional shears (see section *Asymmetrical extensional shear bands*; Fig. 53) and (ii) those without (Fig. 54). In the former

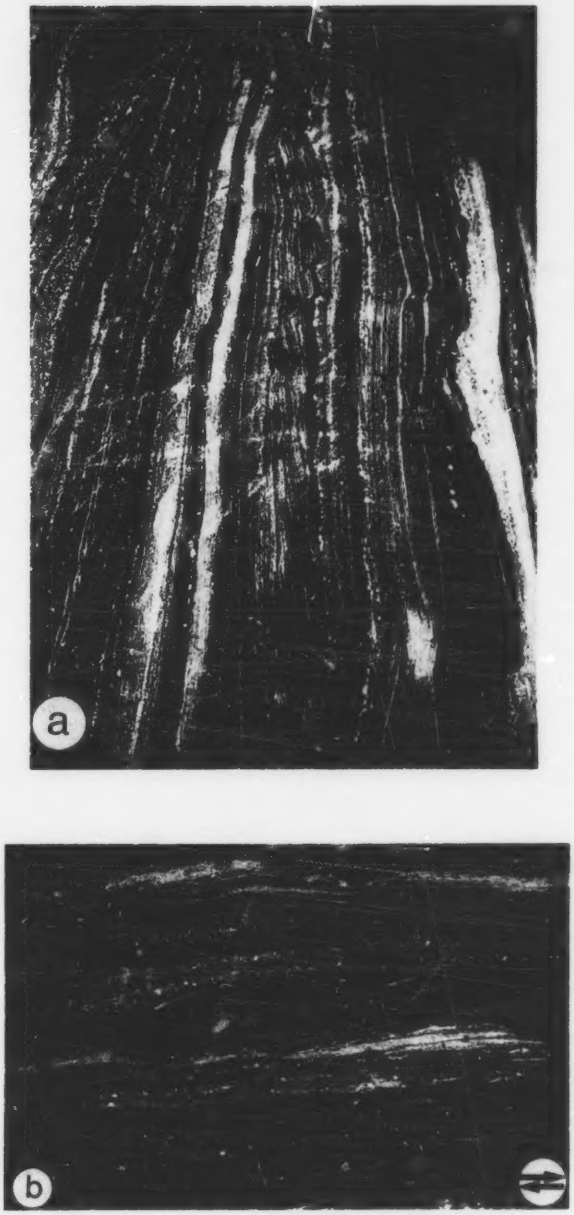

Figure 53. Natural back-rotated layer segments. Type IIb asymmetrical pull-aparts. (**a**) Back-rotated segments of layers in a banded mylonite, observed in the XZ plane of the finite strain ellipsoid. The segments are delimited by a set of asymmetrical extensional shear bands (section Asymmetrical extensional shear bands) which have preferentially developed in a more amphibolitic layer. Dextral shear-sense. The extensional shear bands and the layer segments rotated backwards as the layer extended. (**b**) Detail of A. The sense of shear along the shear plane is shown. Great Slave Lake Shear Zone, N.W.T., looking down. Taken from Hanmer and Lucas (1985). (GSC 204775-J and GSC 04129-B)

Figure 54. Natural back-rotated swells. Type IIa asymmetrical pull-aparts. (**a**) Back-rotated swells in a light coloured heterogeneously extended layer in a mylonite, observed in the XZ plane of the finite strain ellipsoid. Note the absence of discrete extensional shear bands between the back-rotated swells. Dextral shear-sense. (**b**) Detail of a. The sense of shear along shear plane is shown. Compare this structure with that illustrated in Fig. 53. Great Slave Lake Shear Zone, N.W.T., looking down. Taken from Hanmer (1986b). (GSC 204775-I and GSC 204128-W)

sub-set, the back-rotation of the fish or swell is simply a consequence of the slip on, and rotation of the asymmetrical extensional shear bands which bound them (Fig. 53). However, in the latter sub-set, it is not intuitively obvious what drives the structure backwards, against the shear-sense of the bulk flow (Fig. 54).

Laboratory simulation and tentative models

Back-rotated pinch-and-swell structure has been successfully simulated in laboratory experiment (Fig. 55; Hanmer, 1986b). Internally anisotropic blocky boudins and pinch-and-swell structure were deformed in bulk simple shear. The swell structures back-rotated, whereas the blocky boudins did not. By comparing the response of the blocky boudins with that of the pinch-and-swell structure in these experiments, Hanmer (1986b) proposed that the internal anisotropy was the major factor controlling the back-rotation of the swells. Let us examine Hanmer's reasoning, bearing in mind that "the fact that a particular rheological model can be used to produce a particular geometry may merely be a demonstration of the flexibility of the modelling process rather than its physical aptness" (Lister and Williams, 1983, p. 26).

Two factors influence the distribution of flow within the inserts: (i) a *geometrical stress-concentrator* effect due to the presence of the *sharp corners* and a material stress-concentrator effect due to the viscosity contrast between the insert and the matrix (Stephanson and Berner, 1971; Stromgard, 1973; Selkman, 1978; Lloyd & Ferguson, 1981); and (ii) the *canalizing effect of a rheological anisotropy* which maximizes slip along the anisotropy plane (Lister and Williams, 1983).

The response of the blocky boudins suggests that the first set of factors predominate over the second in their case. Angular corner volumes are sites of anomalously high mean stress (Selkman, 1978), while the inter-boudin gaps are sites

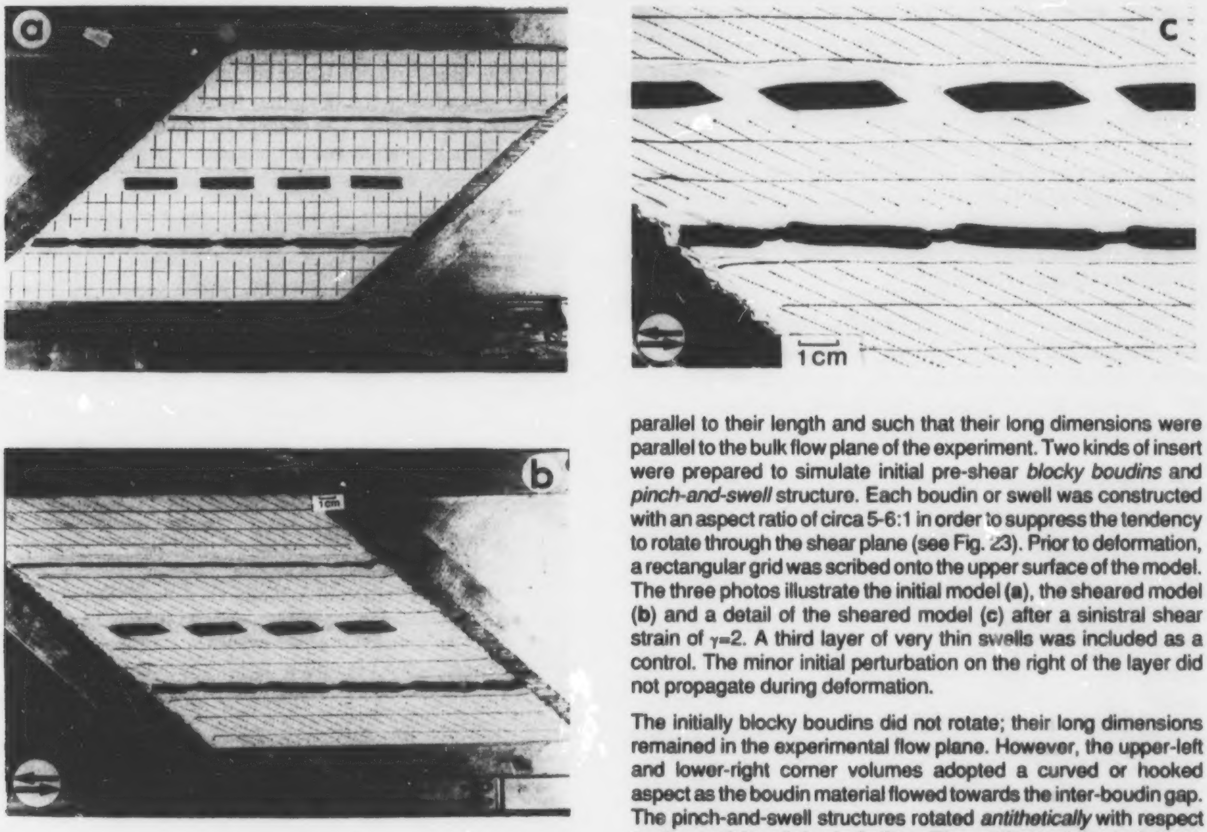

Figure 55. Asymmetrical pull-aparts in experiment. The back-rotation of segments of planar anisotropy has been simulated in laboratory experiment. Sections of internally anisotropic inserts, set in a matrix of isotropic silicone putty, were subjected to bulk simple shear. The sense of shear along the flow plane is shown. The inserts, made of finely laminated plasticine and silicone putty, were prepared and inlaid such that their internal anisotropy was parallel to their length and such that their long dimensions were parallel to the bulk flow plane of the experiment. Two kinds of insert were prepared to simulate initial pre-shear *blocky boudins* and *pinch-and-swell* structure. Each boudin or swell was constructed with an aspect ratio of circa 5-6:1 in order to suppress the tendency to rotate through the shear plane (see Fig. 23). Prior to deformation, a rectangular grid was scribed onto the upper surface of the model. The three photos illustrate the initial model (**a**), the sheared model (**b**) and a detail of the sheared model (**c**) after a sinistral shear strain of $\gamma=2$. A third layer of very thin swells was included as a control. The minor initial perturbation on the right of the layer did not propagate during deformation.

The initially blocky boudins did not rotate; their long dimensions remained in the experimental flow plane. However, the upper-left and lower-right corner volumes adopted a curved or hooked aspect as the boudin material flowed towards the inter-boudin gap. The pinch-and-swell structures rotated *antithetically* with respect to the vorticity of the bulk flow. The outlines of the individual, initially symmetrical swells show a mild left-handed skewness, reflecting sinistral slip along the internal anisotropy. Given that the bulk deformation corresponds to ideal simple shear, the rotation of the swells cannot simply be due to shortening along the shear plane, i.e. they are not the limbs of folds. Note the absence of any discrete shears in the pinches. Taken from Hanmer (1986b). (GSC 204105-J,K,L) of low mean stress. The boudin corner volumes respond by ductile flow towards the region of low mean stress (Ramberg, 1955). In the case of layer-parallel shearing, the existence of a local noncoaxial flow along the boudin long-side will result in an asymmetrical flow distribution within the boudin. Maximum strain rates will develop in those corner volumes lying within the extensional quadrants of the flow (Selkman, 1978). Hence, the initially symmetrical blocky boudins develop an asymmetry by flow from these corner volumes towards the inter-boudin gaps. From this asymmetry the disposition of the extensional and shortening quadrants of the flow can be determined. Since the curvature of the 'hook'-shaped corner volumes records the rotation of the finite strain ellipsoid with respect to the instantaneous stretching axes, the shear-sense of the flow can be deduced from such asymmetrical boudins (Fig. 56).

On the other hand, the absence of well developed corners in the pinch-and-swell structure suggests that the canalizing role of the internal anisotropy predominates over the competence contrast in influencing the flow within the competent material. In the absence of geometrical stress concentrators, the distribution of strain rate within an individual swell is more homogeneous than in the case of angular boudins. Therefore, the response to bulk shear is distributed throughout a given swell and the influence of the internal anisotropy on the flow pattern within the swell is enhanced relative to that of viscosity contrast. In fact, the enhancement is such that the presence of a viscosity contrast has no detectable influence and the structure can be considered as a segment of planar anisotropy. Hence, the discussion can now be extended to include foliation fish.

The mechanical effect of a rheological anisotropy is to canalize and maximize slip along the anisotropy plane. Consider a train of linked swells in bulk progressive simple shear. *What would be the consequence if the orientation of the internal anisotropy deviated slightly, but randomly, from that of the bulk flow plane, while the long dimension of the swell lay in the bulk flow plane?* There are three limiting cases, the first two of which are trivial. (i) Where the internal anisotropy lies in the bulk flow plane, slip on the anisotropy results in oblique extension of the swell, but no rotation of the internal anisotropy, if the strain rates within the swell and the matrix remain identical (see below). (ii) Where the internal anisotropy lies within the shortening quadrants of the bulk flow, extensional slip on the internal anisotropy produces an antithetic rotation of the internal anisotropy into the bulk flow plane (Freund, 1974; Platt and Vissers, 1980), so correcting the deviation and suppressing the perturbation. (iii) Where the internal anisotropy lies in the extensional quadrants of the bulk flow, the local flow along the oblique anisotropy is a general noncoaxial flow, because the local slip plane makes an angle of more than 45° with the minimum instantaneous stretching axis of the bulk flow, inducing shortening across the local flow plane (Fig. 57). If there is material continuity or good cohesion between the volume of oblique anisotropy and the surrounding matrix, the general noncoaxial flow will extend a short distance into the matrix. The long dimension of the volume of oblique anisotropy will thus lie within the field of back-rotation generated by the flow in its own matrix envelope. Back-rotation of the volume of oblique anisotropy further accentuates the deviation from simple shear within and about the volume. The process is, however, self-regulating since back-rotation and the increasing angle between the

Figure 56. Natural shear-modified blocky boudin. Initially blocky boudin in ultramylonite, observed in the XZ plane of the finite strain ellipsoid. The dextral sense of shear along the shear plane is shown. Compare with Figure 55. Note how the long dimension of the boudin remains aligned in the shear plane of the bulk deformation. Great Slave Lake Shear Zone, N.W.T., looking down. Taken from Hanmer (1986b). (GSC 204129-K)

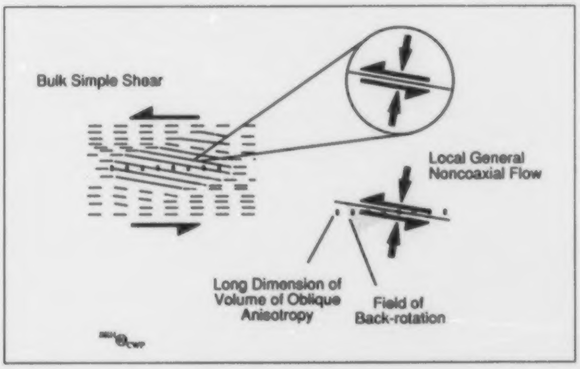
Bulk Simple Shear
Local General Noncoaxial Flow
Long Dimension of Volume of Oblique Anisotropy
Field of Back-rotation

Figure 57. Back-rotation of foliation segments. Model for the back-rotation of foliation segments proposed by Hanmer (1986b). Because of its canalizing effect, where a segment of oblique anisotropy lies in the extensional quadrants of the bulk flow, the flow within the volume it occupies is a general noncoaxial shear, even when the bulk flow is simple shear. The enlargement shows the orientation of the canalized flow within the volume of oblique anisotropy. The canalized flow plane is oblique to the bulk flow plane and makes an angle greater than 45° with the minimum instantaneous stretching axis of the bulk flow; hence the local flow is a general noncoaxial flow. If there is material continuity or good cohesion between the volume of oblique anisotropy and the surrounding matrix, the general noncoaxial flow will extend a short distance into the matrix. The long dimension of the volume lies within the field of back-rotation generated by the flow in its own matrix envelope (lower right). Field observation suggests empirically that back-rotation is balanced by rotational hardening after antithetic rotation of the order of 10-15°. Modified after Hanmer (1986b).

oblique anisotropy and the minimum instantaneous stretching axis of the bulk flow leads to a hardening of the oblique anisotropy with respect to slip. When slip on the oblique anisotropy becomes difficult, the deviation from simple shear in the enveloping matrix will attenuate and the volume of oblique anisotropy will tend to rotate synthetically in response to continuing bulk simple shear, so softening the oblique anisotropy with respect to slip (Fig. 57; Hanmer, 1986b).

However, it should not surprise the reader to find that there are alternative possibilities. Consider a relatively stiff domain in a noncoaxial flow. It can respond by a rotation of the entire stiff volume in the same direction as the bulk shear-sense, or shear induced vorticity may be repartitioned into spin of the same sense. A similar, but opposite effect could result from the presence of a relatively soft volume of material, for example caused by the presence of a foliation. If slip on the internal foliation results in a higher strain rate in the weak volume than that of the bulk flow, the entire volume must rotate antithetically in order to maintain compatibility; locally enhanced shear induced vorticity is countered by spin in the opposite direction. Again, this 'back-rotation' could be reversed by hardening after a certain amount of rotation.

While it is tempting to attempt to apply the models outlined here to explain natural occurrences of back-rotated foliation fish, etc., we must remind ourselves that they are just models and as such they require further testing. For example, can one *demonstrate* synthetic slip along the oblique anisotropy segments in natural examples? So far, we have not been able to do so.

Mica fish

Mica fish (Eisbacher, 1970; Lister and Snoke, 1984) have certain geometrical features in common with the foliation fish described here (Fig. 58). However, they are also frequently associated with long, straight, narrow trails of fine white mica which extend from the apices of the mica fish, along the shear plane, for distances an order of magnitude greater than the size of the mica fish. They commonly occur in mylonites where they are oriented in the extensional quadrants of the flow, making an angle of about 10-15° with the shear plane. There is at present no satisfactory explanation of how mica fish form, nor why they occur with their particular angular

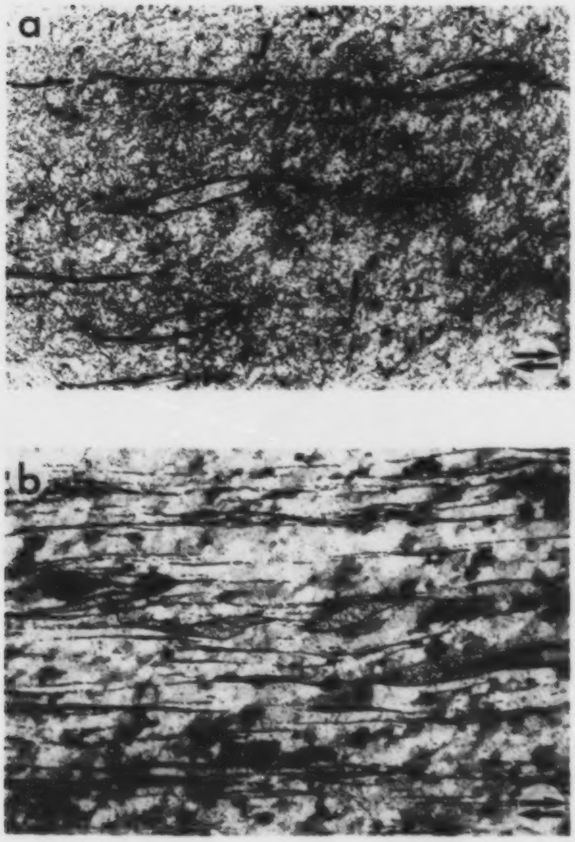

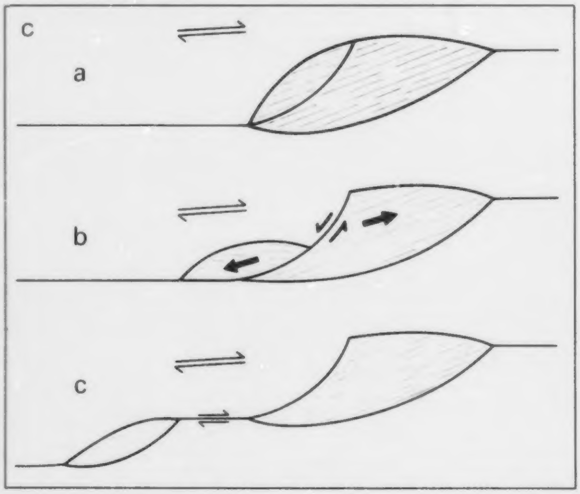

Figure 58. Mica fish. (a and b). White mica fish in quartzo-feldspathic mylonites oriented with their long dimensions systematically counterclockwise with respect to the mylonitic foliation, itself parallel to the shear plane of the deformation. Observed in the XZ plane of the finite strain ellipsoid. The sense of shear along the shear plane is indicated. The 001 cleavage planes of the mica fish are always oriented subparallel to the long dimensions of the fish. Note that the trails of fine mica parallel to the shear plane are often attached to the apices of the mica fish. Photos courtesy of Larry Lane. Columbia River Fault, Revelstoke, British Columbia, looking north (see Lane et al., 1989).

(c) 'Calving' of daughter mica fish from a parent grain as proposed by Lister and Snoke (1984). Note that this sequence implies a general noncoaxial flow. The horizontal lines drawn in a-c from the apices of the fish are sometimes decorated with fine mica grains. We note that the reorientation of the daughter grain in the step from b to c in this model is not self-evident. Nor is it obvious from this model why the fish do not rotate forwards with progressive deformation and thus deflect the proximal parts of the fine mica trails. Taken from Lister and Snoke (1984).

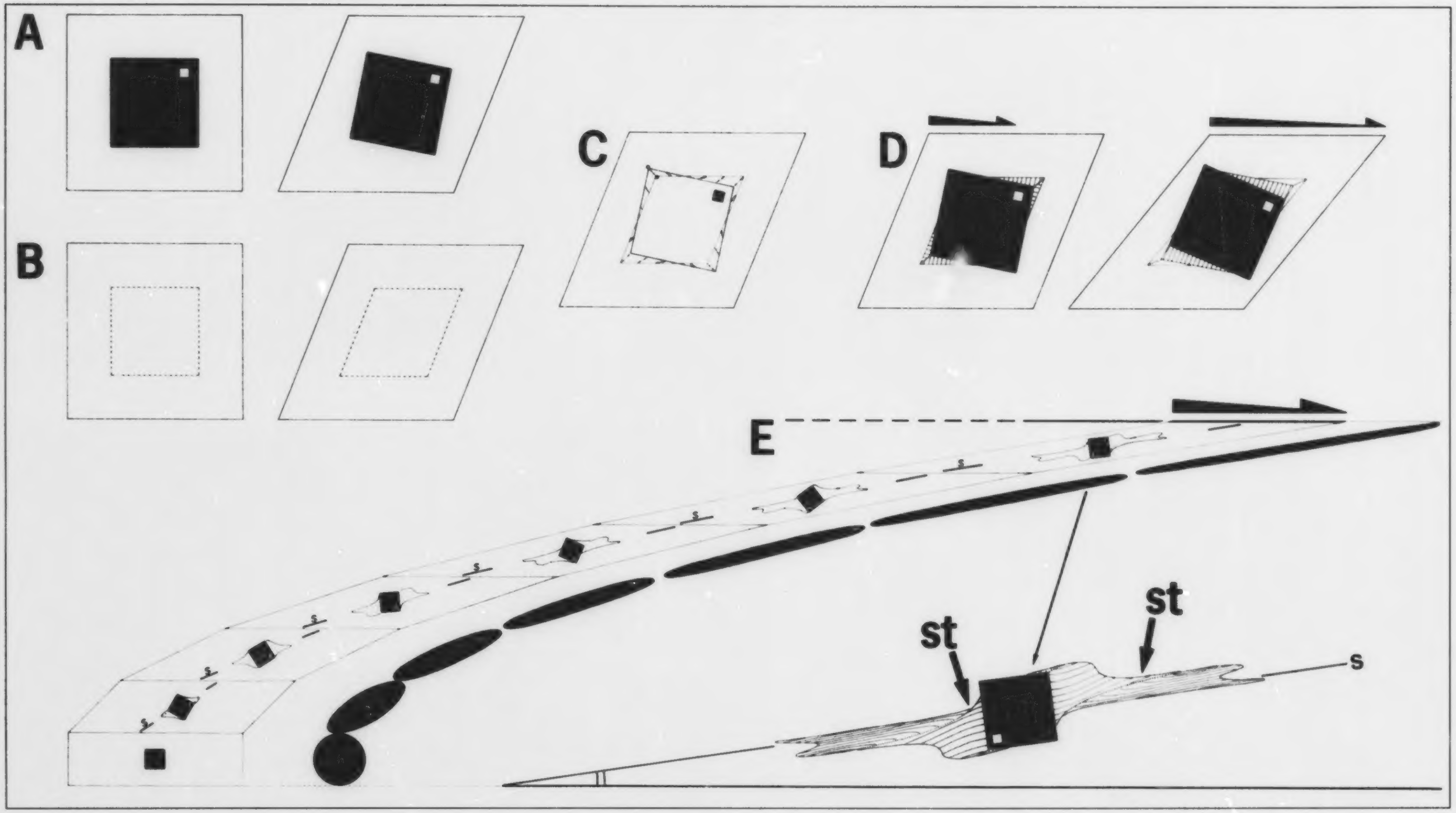
A
B
C
D
E
s
st
st
s

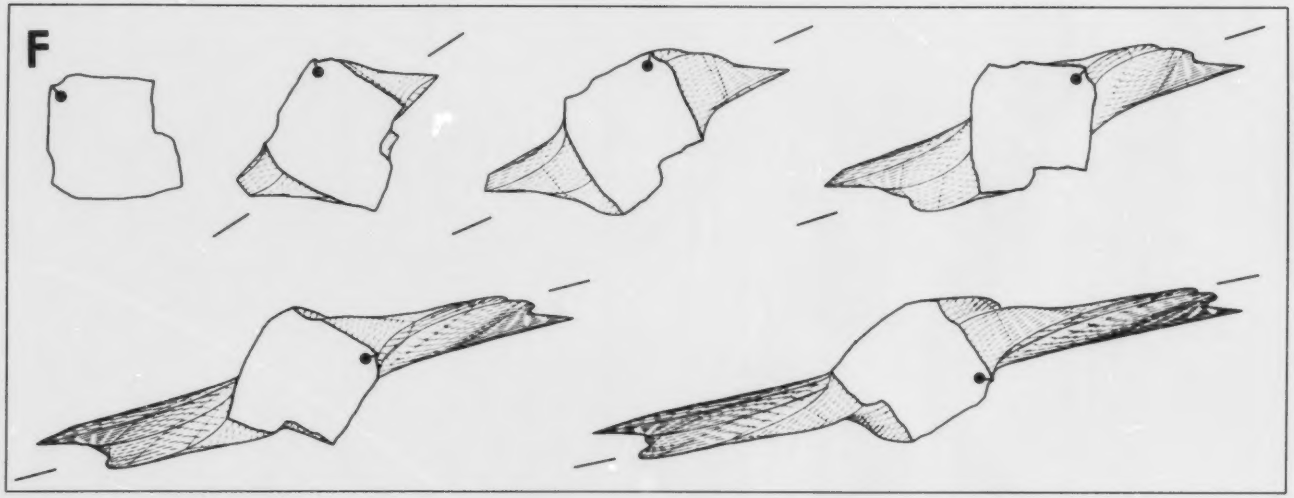

Figure 59. Face-controlled deformable fibres. Face-controlled, deformable fibres formed and deformed in progressive dextral simple shear. In the example illustrated here the fringe material is assumed to be as weak as the matrix. Etchecopar and Malavielle (1987) model an increment of fibre formation as an increment of deformation and an increment of growth. As an equant inclusion, a pyrite cube rotates at a constant rate in the same sense as the the imposed bulk shear (Fig. 23); the small square tracks the rotation (A to D to E). At the same time, material lines in the enclosing matrix undergo changes in length and rotations which reflect the simple shear flow type (B). In the model, this is represented by deforming the outline of the pyrite, ignoring the rheological contrast across the pyrite/matrix interface. Combining (A) and (B), the volumes occupied by the rotated inclusion and the model deformed pyrite/matrix interface do not match (C).

While pressure solution may alleviate the space problem in the shortening quadrants of the bulk flow, there is a tendency for gaps to open between the pyrite and its matrix adjacent to faces making significant angles with the maximum instantaneous stretching axis of the flow. Fibrous material grows at these low-pressure sites such that the fibres are oriented perpendicular to the pyrite crystal face (D). During the next model increment, the pyrite turns, while the matrix and the pressure fringe deform together. The fringes rotate more slowly than the pyrite (because of their shape) and tend to pull away from the inclusion (D; see Fig. 23). The next increment of new fringe material grows with the fibres oriented perpendicular to the pyrite crystal face.

The *average fibre orientation from segment to segment* shows a right-handed curvature (proximal to distal curve to the right; E). However, the sense of *curvature within segments* is variable, depending upon whether the normal to the crystal face against which the fibres were growing was rotating toward or away from the direction of maximum finite extension (S in part E; compare D with E and F). This reflects the deformable nature of the fibres and the simple shear flow type in this model; the fibres are deflected by progressive deformation from their relatively rapidly changing face-controlled growth orientation towards the more slowly rotating flattening (X/Y) plane of the finite strain ellipsoid (see Fig. 23).

After several increments of rotation, distortion and growth, the fibre curvature is attenuated as the fibres themselves deform and attempt to track the XY plane of the finite strain ellipsoid. Strong curvature is only preserved at the less deformed proximal end of the pressure fringe (E). Since contemporaneous fibre segments which grow on two adjacent inclusion faces are oriented perpendicular to each other, a *suture* (st) forms within the pressure fringe which marks the trace of the rotating corner of the pyrite cube (E). Such sutures form at any significant irregularity on the inclusion surface and may give rise to complex suture patterns (F). In contrast to that of the fibres, *the sense of curvature of the sutures is constant for a given sense of shear.*

In the mature pressure fringe, the overall geometry of the fringe outline tends towards a bilateral symmetry reflecting the orientation of the finite strain ellipsoid (F). Internally, the dextral shear-sense of the flow can either be read by matching fibre segments to the inclusion faces against which they originally grew, or from the right-handed curvature (proximal to distal curve to the right) shown by the sutures. (A-E) taken from Etchecopar and Malavieille (1987). (F) taken from Malavieille et al. (1982).

relationship to the mylonitic foliation. We suggest that the analysis of back-rotated anisotropy segments summarized above may provide a potentially fruitful avenue in the search for a kinematic explanation for the shear-sense which Lister and Snoke (1984) originally proposed for the structure. Note that Lister and Snoke consider mica fish as porphyroclasts, whereas it is possible that the micas could grow synkinematically.

We are unable to offer an explanation for the mica trails. Clearly, since they are not ubiquitous, they do not constitute an essential feature of mica fish. Lister and Snoke (1984) suggested that the mica grains comprising the trails are 'fragments', implying that they represent debris torn away from the mica fish (Fig. 58). Their length should therefore be related to the amount of slip accommodated on a given slip surface within the matrix enclosing the mica fish. We hesitate to subscribe to the notion of fragments, since it is quite possible that the trails include a component of material carried along a direction of easy transport by advective or diffusive mass transfer.

In summary, mica fish have been shown empirically to show a systematic angular relationship to shear-sense in cases where the shear-sense of the flow has been independently established. While they are useful tools, further efforts are required if we are to understand them.

PRESSURE SHADOWS AND FRINGES

Pressure fringes (Fig. 59, 60) are elongate volumes of quartz or calcite precipitated adjacent to stiff crystals or aggregates in fine grained rocks (e.g. Fairbairn, 1950; Zwart and Oele, 1966; Choukroune, 1971; Durney and Ramsay, 1973; Beutner and Diegel, 1985; Etchecopar and Malavieille, 1987). In terms of their general shape and spatial relationship to inclusions, *pressure shadows* resemble pressure fringes, but they are polycrystalline aggregates without internal shape fabrics. Put loosely, *fringes have an internal fibrous structure, while shadows do not* (Spry, 1969, p. 240-247). While Spry's definition of a pressure fringe is certainly more complex than this, very few structures correspond exactly to Spry's formulation. Pressure fringes have recently been comprehensively reviewed (Ramsay and Huber 1983; Etchecopar and Malavieille, 1987). Despite their more common occurrence, pressure shadows have not received the same detailed consideration.

All pressure fringes and most pressure shadows are volumes of material deposited at the contact between the stiff inclusion and its less competent matrix by precipitation from solution. Material may be transported to the site of precipitation by diffusive and/or advective mass transfer. The nature of the inclusion may range from a cubic crystal of pyrite to a block of amphibolite, while the precipitated material can be anything from quartz or calcite to mica or feldspar. Some workers have extended the term 'pressure shadow' to include features derived by the deformation of core-and-mantle microstructure (Takagi and Ito 1988), essentially identical to the initial stages of formation of sigma-shaped (σ) winged porphyroclasts (Fig. 44). Unfortunately, we find that this practise leads to some confusion. We suggest that the terms 'shadow' and 'fringe' should only be employed in reference to material *not* derived by recrystallisation from the associated stiff inclusion.

What determines the site of precipitation at the inclusion/matrix interface? When subjected to progressive deformation, the soft matrix tends to flow away from those inclusion faces making an high angle with the maximum instantaneous stretching axis of the flow, simply because the matrix extends faster than does the stiff inclusion. The result is a zone of anomalously low pressure. Whether by fluid advection or by fluid-enhanced diffusion, material migrates along the pressure, or more correctly the chemical potential gradient, towards the low pressure zones (e.g. Durney and Ramsay, 1973; Rutter, 1976, 1983). The distinction between pressure fringes and mass-transfer associated pressure shadows is a reflection of the processes occurring at the reaction site in the low pressure zone.

Pressure fringes

The general outline of a pressure fringe can be smooth to irregular. The disposition of the long dimension of the fringe with respect to the general orientation of the matrix foliation is variable. Some examples are oblique, while others are parallel; the longer the fringe, the greater the tendency to a parallel disposition. The internal structure of the fringe is often segmented. The material within each segment is fibrous and the fibre orientation may change abruptly across the segment boundaries. Durney and Ramsay (1973) distinguished two end-member types of fringe; (i) *crinoid-type*, where fibres grow *syntaxially* with respect to the inclusion, and (ii) *pyrite-type* where the fibres grow *antitaxially*. The latter type is by far the more common and will be dealt with here; we refer the interested reader to the excellent illustrations of the former in Ramsay and Huber (1983). Two types of phyllosilicate fringe have been described. Mugge (1930) described fan-like phyllosilicate fringes; however, we are not aware of any publication using such structures as shear-sense indicators. Williams (1972) described beard-like mica fringes which may be considered as a simple phyllosilicate equivalent of the geometrically more complex quartz or calcite fringes. In this contribution, we shall concentrate on quartz and calcite fringes.

Pressure fringe fibres are classified into two types, according to the nature of the phenomena controlling their orientation at the growth site; (i) face-controlled, where the fibres grow perpendicular to the growth surface, and (ii) displacement-controlled, where the fibres grow parallel to the direction of displacement of the walls of the void filled by precipitation of the fibres (Fig. 61; Durney and Ramsay, 1973; Ramsay and Huber, 1983).

Displacement-controlled fibres

The internal geometries of displacement-controlled fringes are relatively simple. Even in noncoaxial flow, if the flow type remains invariant, the orientation of the boundaries of new fibre segments is constant throughout the progressive deformation (Fig. 60). The inclusion need not be bound by euhedral crystal faces, but could consist of framboidal pyrite, or any kind of aggregate. However, even adjacent to euhedral pyrite crystals, the fibres can lie oblique to the pyrite/matrix interface (Choukroune 1971; Ramsay and Huber 1983; Etchecopar and Malavieille 1987). During progressive simple shear, flow in the matrix tends to draw the previous growth increment(s) of fringe material away from the inclusion; the inclusion undergoes a rigid-body rotation while the fringe undergoes a rotation and possibly a shape-change. New fibre segments are formed at the inclusion/matrix interface, oriented at $\alpha=45°$, parallel to the maximum instantaneous stretching axis. After several increments of rotation and growth the average fibre orientation from segment to segment describes a proximal to distal curvature, reflecting the rotation of the finite strain ellipsoid with respect to the directions of the instantaneous stretching axes and indicating the shear-sense of the flow (Fig. 61B).

Face-controlled fibres

The internal geometries of face controlled fringes are potentially more complex than those of displacement controlled ones. The classical examples of face-controlled fibres are associated with euhedral crystals of pyrite in fine grained meta-pelites (Fig. 59, 61). Elongate crystals (fibres) of quartz or calcite grow adjacent to the pyrite. As an equant inclusion, a pyrite cube rotates at a constant rate in the same sense as the imposed bulk shear. At the same time, material lines in the enclosing matrix undergo length changes and rotations which reflect the simple shear nature of the flow. There is a tendency for the matrix material to flow away from the pyrite in the extensional quadrants of the deformation (Fig. 59). Fibres of new material grow in optical continuity with the matrix grains on which they nucleate and are oriented perpendicular to the pyrite crystal face. During subsequent deformation increments, the pressure fringe material is carried along or deforms with the flowing matrix. According to theoretical models (Fig. 59), the pyrite rotates while the pressure fringe pulls away and uncouples from the inclusion. The new increment of fringe material grows in the resultant gap, with the fibres oriented perpendicular to the pyrite crystal face. Meanwhile, the fibres of the previous growth increment(s) undergo a further change in length and/or a rotation. In simple shear, because of the difference in aspect ratio (R), the elongate fringe rotates more slowly than the equant inclusion (Fig. 59).

Since contemporaneous fibre segments which grow on two adjacent inclusion faces are oriented perpendicular to each other, a suture forms within the pressure fringe which marks the trace of the rotating corner of the pyrite cube (Fig. 59; see Ramsay and Huber (1983) and Etchecopar and Malavieille (1987) for detailed description and analysis). In contrast to the fibre orientation, the sense of curvature of sutures

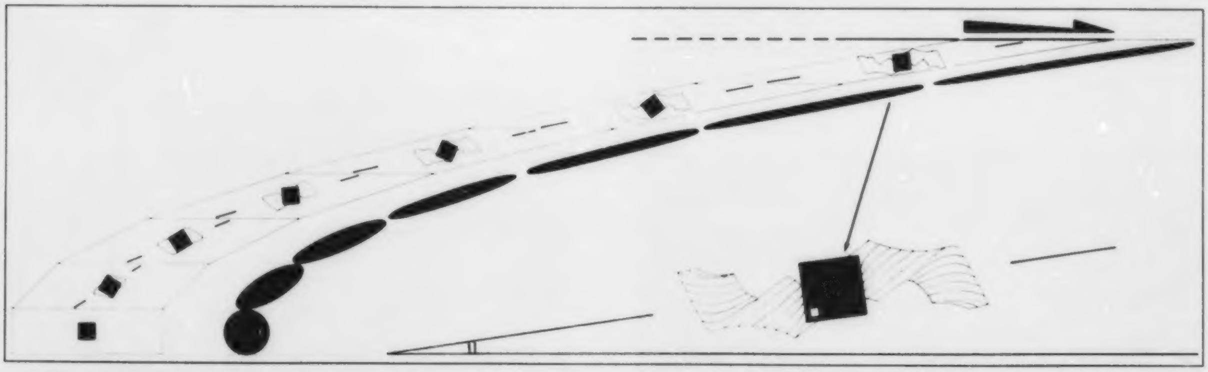

Figure 60. Displacement-controlled rigid fibres formed in dextral simple shear. In the example illustrated here the fringe material is assumed to be as stiff as the inclusion. Etchecopar and Malavieille (1987) model an increment of fibre formation as an increment of deformation and an increment of growth. In their model, the principles governing formation of the site of growth of the pressure fringe material are as outlined in Figure 59. During the increment of deformation, flow in the matrix draws the pressure fringe away from the inclusion. Both the inclusion and the fringe undergo a clockwise rotation. In the model, because of the difference in their aspect ratios, the inclusion and the fringe rotate at different rates; since the bulk model flow is simple shear, the equant inclusion rotates faster than the pressure fringe, within the range $45° < \alpha < 90°$ (Fig.23).

New fibre segments are formed at the inclusion/matrix interface, oriented at $\alpha=45°$, parallel to the maximum instantaneous stretching axis of the flow. After several increments of rotation and growth the average fibre orientation from segment to segment describes a right-handed curvature (proximal to distal curvature to the right), reflecting the rotation of the finite strain ellipsoid with respect to the instantaneous stretching axes. In a mature pressure fringe, the overall geometry of the fringe outline tends toward an asymmetrical 'hook' shape whose overall right-handed curvature (proximal to distal curve to the right) marks the dextral sense of rotation of the structure.

The fibres in the distal segments are more curved than in the more proximal segments. This reflects a deceleration of the rotation rate of the pressure fringe with increasing deformation. At a constant bulk strain rate in simple shear, two factors lead to a decrease in the rotation rate of an inclusion (Fig. 23): (i) a decrease in the obliquity with the shear plane and (ii) an increase in the aspect ratio. Both of the factors apply to the case examined here and contribute to the decreasing curvature of the fibres.

Illustration taken from Etchecopar and Malavielle (1987).

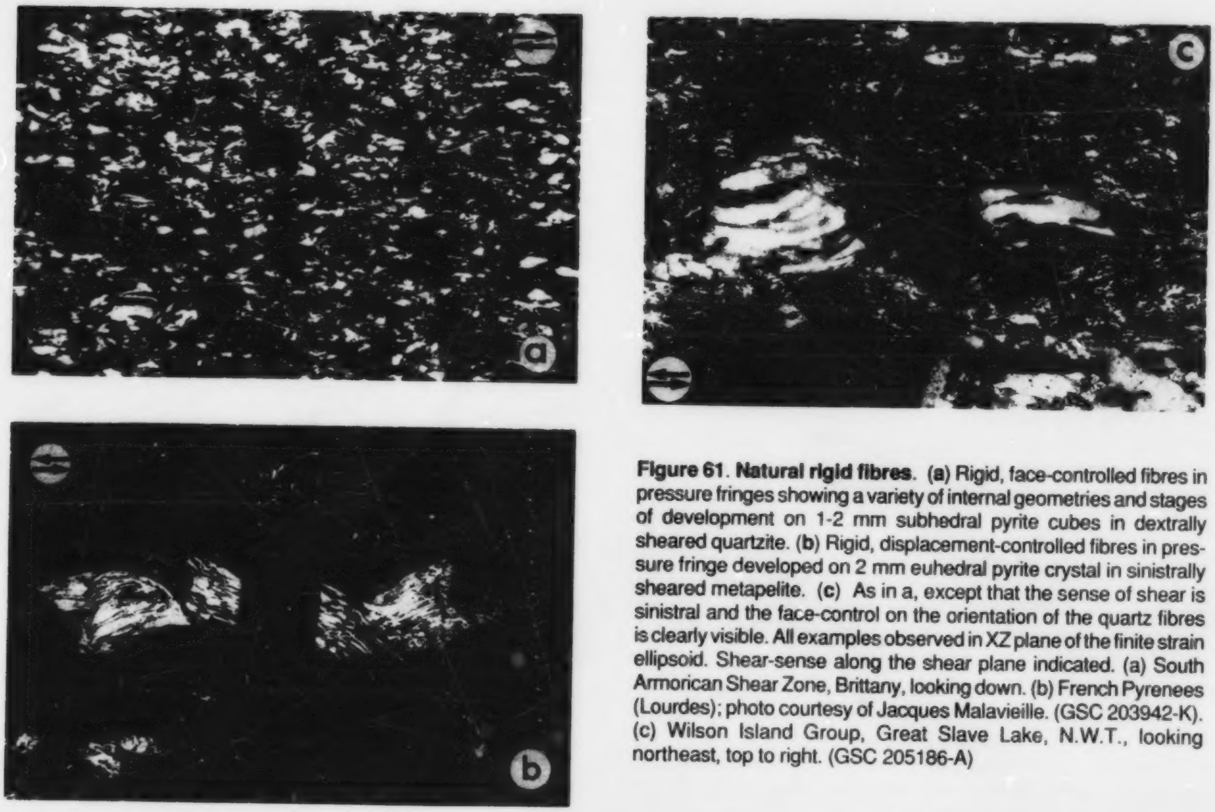

Figure 61. Natural rigid fibres. (**a**) Rigid, face-controlled fibres in pressure fringes showing a variety of internal geometries and stages of development on 1-2 mm subhedral pyrite cubes in dextrally sheared quartzite. (**b**) Rigid, displacement-controlled fibres in pressure fringe developed on 2 mm euhedral pyrite crystal in sinistrally sheared metapelite. (**c**) As in a, except that the sense of shear is sinistral and the face-control on the orientation of the quartz fibres is clearly visible. All examples observed in XZ plane of the finite strain ellipsoid. Shear-sense along the shear plane indicated. (a) South Armorican Shear Zone, Brittany, looking down. (b) French Pyrenees (Lourdes); photo courtesy of Jacques Malavieille. (GSC 203942-K). (c) Wilson Island Group, Great Slave Lake, N.W.T., looking northeast, top to right. (GSC 205186-A)

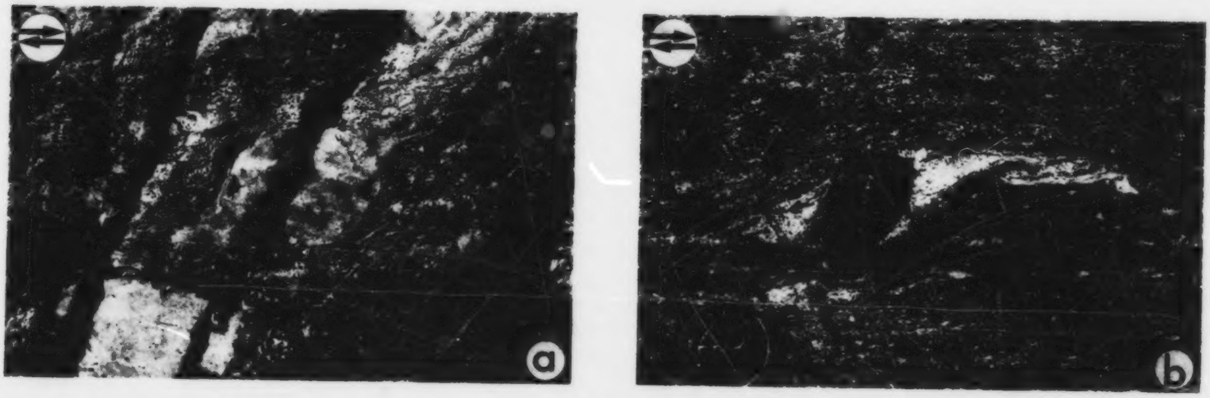

Figure 62. Simple pressure shadows. Dextral pressure shadows developed in mylonites, observed in the XZ plane of the finite strain ellipsoid. Shear-sense along the shear plane is shown. (**a**) Non-fibrous quartz pressure shadows developed at the boundary of a feldspar porphyroclast. The sharp outlines of the discrete pressure shadows suggest that they are void-fill precipitates, rather than metasomatic in origin. (**b**) Non-fibrous plagioclase pressure shadows developed at the boundary of a garnet porphyroclast in a mylonite, observed in the XZ plane of the finite strain ellipsoid. The indistinct outlines of the pressure shadows suggests that they might be metasomatic in origin, rather than void-fill precipitates. Both (a) and (b) formed in the extensional quadrants of the flow. New material was added to the shadows at the interface with the inclusion. The mildly developed 'S'-shaped sigmoid form of the shadows is due to the deformation and rotation of the more distal parts of the shadows which in turn reflects the clockwise rotation of the finite strain ellipsoid with respect to the instantaneous stretching axes of the flow and the flow plane. Both examples are from Great Slave Lake Shear Zone, N.W.T., looking down. (GSC 204775-Q and GSC 204786-T)

is constant for a given sense of shear. Internally, the shear-sense of the bulk flow can either be read by matching fibre segments to the inclusion faces against which they originally grew, or from the proximal to distal curvature of the suture.

Fibre stiffness

Ramsay and Huber (1983) examined the relative rheology of fibres in fringes. *Deformable fibres* undergo distortion with the matrix and the overall shape of the fringe tends to resemble that of the strain ellipse in the section of observation (Fig. 59). In noncoaxial flow, assuming displacement-controlled growth, the older sections of fibre would attempt to track the XY plane of the finite strain ellipsoid and rotate towards the flow plane. Thus the proximal to distal curvature of the fibres within the fringe records the sign of the shear-induced vorticity of the flow, and can be used to determine the sense of shear. However, the complexity of the internal fibre geometry in the older growth increments is attenuated with progressive deformation as the internal angular discordances are modified by change in length and rotation of the fibres. Note that the rotation of the inclusion itself is not necessarily a factor in the determination of the shear-sense of the flow. If we assume face controlled growth (Fig. 59), the resulting internal structure of the pressure fringe is more complex.

Rigid fibres form under similar conditions of flow and growth to those described for deformable fibres. However, they record the rotational component of the deformation as a rigid-body rotation (Fig. 60, 61). Since the pressure fringe itself is rigid, the growth site could potentially switch to the distal ends of the fringe, where secondary fringes recording the displacement direction may form. Such fringes may be spectacularly developed (Choukroune, 1971, Fig. 3). Since the fibres are rigid, the complexity of the internal fibre geometry in the older growth increments does not attenuate with progressive deformation, but is preserved (Fig. 61).

A paradox?

At this point we wish to point out an apparent internal contradiction within both the displacement-controlled and face-controlled fibre models. Most workers accept, implicitly or explicitly, that the *axis of rotation* of both the inclusion and the components of the fringe lies within the pyrite (Etchecopar and Malavieille, 1987). This implies that the fringe does not uncouple from the inclusion. Yet, it is a simple observation that the proximal parts of pressure fringes are not entrained by the rotation of the adjacent inclusion, in the manner of delta-shaped (δ) winged inclusions (see section *Winged porphyroclasts*). Furthermore, we point out that whereas the

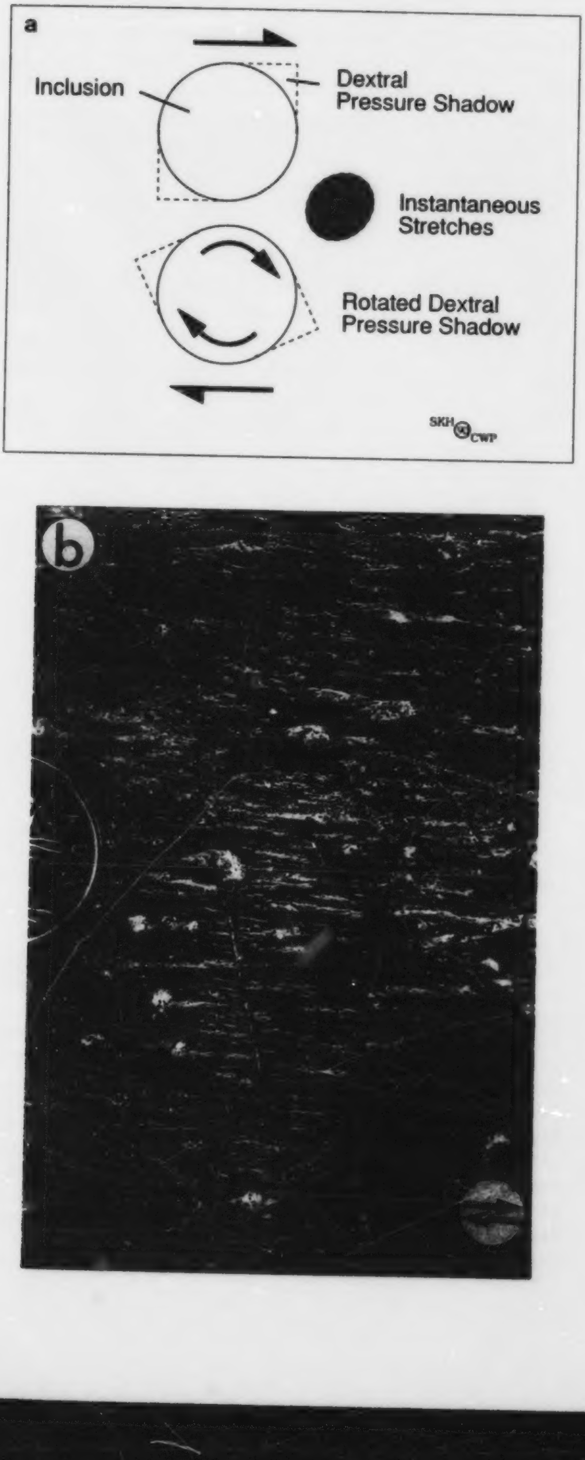

Figure 63. Rotated pressure shadows. **(a)** Pressure shadow form adjacent to those faces of stiff inclusions which make an high angle with the maximum instantaneous stretching axis of the flow in the matrix. However, if the entire structure were to rotate, the pressure shadow could be readily misinterpreted as having formed in sinistral shear.

(b) Quartz pressure shadows on feldspar porphyroclasts in mylonite, observed in the XZ plane of the finite strain ellipsoid. Although the long dimension of the pressure shadows lies anticlockwise with respect to the mylonite foliation, the pressure shadows make contact with the lower right and upper left parts of the perimeters of the porphyroclasts. Are these pressure shadows formed during noncoaxial progressive deformation with a sinistral sense of shear, or are they deformed and rotated pressure shadows whose proximal parts have been dragged into the shortening quadrants of the flow in a progressive deformation of dextral shear-sense? In this particular case, abundant independent evidence allows us to opt for the latter! (see Hanmer, 1988a). Great Slave Lake Shear Zone, N.W.T., looking down. (GSC 204776-A) internal structure of face-controlled fringes is taken by all workers to reflect the relative rotation of the pyrite with respect to the long dimension of the fringe, there is nothing inherent about the structure of displacement-controlled fringes which requires that the inclusion must have rotated with respect to the long dimension of the fringe. However, where displacement-controlled fibres grow adjacent to an euhedral pyrite crystal (Etchecopar and Malavieille, 1987, Fig. 9 and 10), re-entrants form in the outline of the fringe which match symmetrically on either side of the inclusion (Fig. 60). They are caused by variation in the surface area of contact at the fringe/pyrite interface due to the relative rotation of the inclusion, coupled with the pulling away of the fringe.

In both the displacement-controlled and the face-controlled fibre models in simple shear, the problem remains: (i) *if uncoupling does not occur, how can pyrites and fibre fringes rotate at different rates without entrainment of the fringes adjacent to the pyrites? and (ii) if uncoupling does occur, why do the two halves of pressure fringes rotate about an axis centred on the inclusion?* A potentially fruitful avenue of research might be to investigate general noncoaxial flow models where the fringe does not rotate, except in its most immature stages of development.

Fibre growth

What are the processes occurring at the proximal growth site in a pressure fringe? Most authors accept, either implicitly or explicitly, a process of *plucking* of the matrix and existing fringe material away from the inclusion, lack of material continuity/cohesion at the inclusion/matrix interface and the filling of a potential void (Ramsay and Huber, 1983; Beutner and Diegel, 1985; Etchecopar and Malavieille, 1987). However, as we have seen, there is an apparent contradiction between the uncoupling, void-fill growth model and the rotational behaviour of both the fringe and the inclusion. This poses a fundamental problem since, if the fringe does not uncouple from the inclusion, how can the fibrous material precipitate at the proximal deposition site as proposed? Indeed, how can oriented fibres develop at all? In a general discussion of fibrous structures, Durney and Ramsay (1973) argued that in the case of *displacement-controlled fibres* growth must have taken place in the *solid-state, without uncoupling*. They proposed that the fibres grow in the direction of least resistance to growth-induced local volume increase. However, such a growth model would still not account for (i) the paired re-entrants in the fringe outline in displacement-controlled fibres, (ii) synchronous growth and rotation in face-controlled fibres, both of which require decoupling, or (iii) the absence of entrainment of the proximal parts of fringes adjacent to the rotating pyrite.

Pressure shadows

In terms of their general shape and spatial relationship to inclusions, pressure shadows resemble pressure fringes. However, pressure shadows are polycrystalline aggregates without an internal shape fabric. There are at least four possible modes of formation:

(i) Precipitation of a non-fibrous fill in a void at the inclusion/matrix interface in the same manner as discussed above for fringes (Fig. 62A).

(ii) Metasomatic replacement or metamorphic differentiation of matrix material adjacent to the inclusion (Fig. 62B). These processes both involve changes in mineral and/or chemical composition of the matrix material in a pressure shadow. Examination of the details of these processes is beyond the scope of this contribution; the interested reader is referred to the literature (e.g. Robin, 1979; Wintsch, 1986; van der Molen, 1985). For our purpose, it suffices to recognize that material moves into and out of the pressure shadow by mass transfer associated with diffusion and/or advection. However, whereas the reaction site is fixed with respect to the orientation of the instantaneous stretching axes, the early formed parts of the shadow flow with the matrix, away from the inclusion. If the strain rate is slow enough, the weak matrix can flow into the low pressure zone between the inclusion and the existing shadow material. Continued reaction, leading to compositional change in the newly arrived matrix material, would result in proximal addition to the developing pressure shadow. Pressure shadows formed in this way may be difficult to distinguish from these formed by precipitation of non-fibrous void fill. However, one would expect to find rather diffuse contacts between shadow and matrix in the former case and sharp contacts in the latter.

(iii) Mantle flow in a core-and-mantle microstructure; a situation which we have already discussed under the heading of winged objects (see section *Winged porphyroclasts*). We strongly recommend that the geologist interpret such structures as winged inclusions rather than pressure

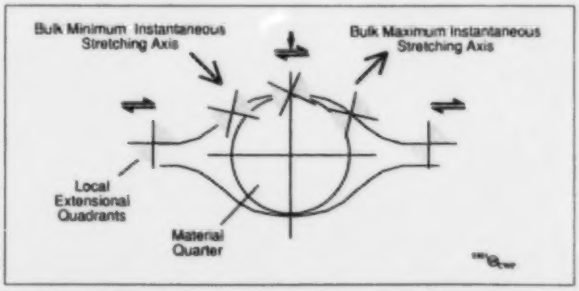
Bulk Minimum Instantaneous Stretching Axis
Bulk Maximum Instantaneous Stretching Axis
Local Extensional Quadrants
Material Quarter

Figure 64. Material quarters and noncoaxial flow. The presence of a stiff inclusion perturbs the flow in the adjacent matrix, which can be considered in terms of four material quarters. In this illustration, the inclusion is set in a foliated matrix undergoing progressive simple shear along the foliation plane, as indicated. Note the local component of shortening, normal to the flow plane, induced by the perturbation. In two quarters (upper-left and lower-right), the matrix foliation lies in the extensional quadrants of the local flow. In these quarters, *foliation-normal shortening* may lead to concentration of less soluble phases such as micas. In the other two quarters, the foliation lies in the shortening quadrants of the local flow and may respond to *foliation-parallel shortening* by folding.

shadows and we only mention them in this section because they have already been considered as pressure shadows in the literature. The structure can usually be distinguished from pressure shadows, as discussed above, by the fact that central object and tails are of the same mineral composition and the progressive microstructural transition between the wings and the central inclusion.

(iv) Recrystallization of a pressure fringe.

Sigmoid pressure shadows whose proximal parts lie in the extensional quadrants of the flow, but whose distal parts are subparallel to the shear plane, are common (Fig. 62). The outlines of such pressure shadows are very similar to those of pressure fringes composed of deformable fibres, discussed above (Fig. 60). In that discussion we saw that the pressure fringe material deforms with the matrix and attempts to record the orientation of the finite strain ellipsoid. In the same way, the proximal to distal curvature of sigmoid pressure shadows records the progressive rotation of the finite strain ellipsoid with respect to the instantaneous stretching axes, from which one can deduce the sign of the shear-sense of the flow.

Rotated pressure shadows

White and Wilson (1978) have suggested that, if a mature pressure shadow develops a good cohesive contact with the inclusion, it could itself be entrained by the rotation of the

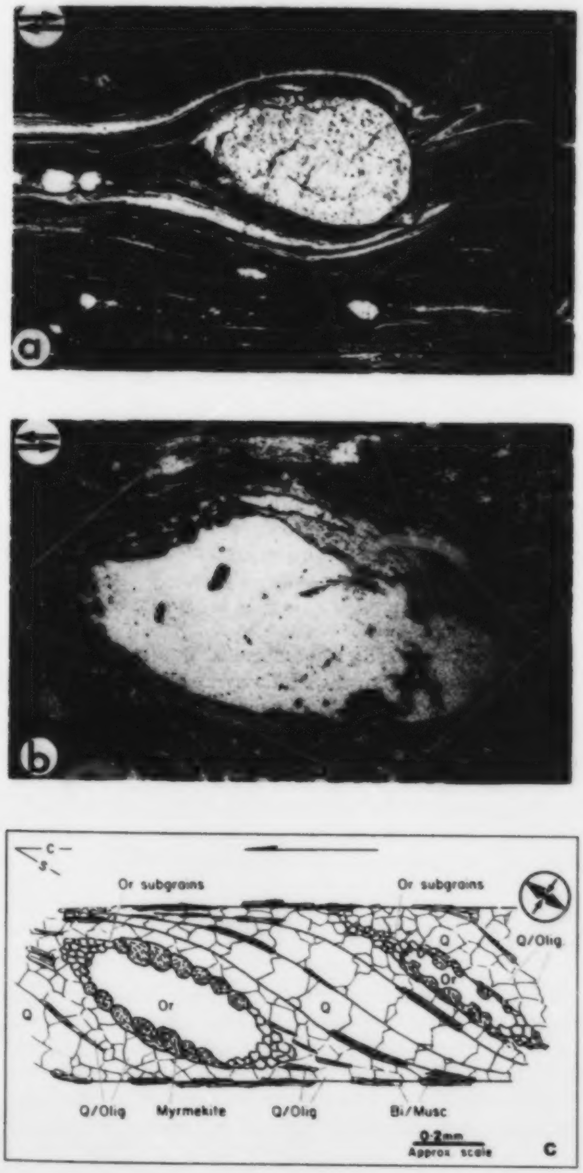

Figure 65. Quarter structures. Different types of structures develop in the quarters (Fig. 64) in the matrix adjacent to stiff inclusions, according to the angular relations between the local perturbed flow and the foliation/layering in the matrix. In a bulk coaxial flow, the foliation/layering of the matrix in all four quarters would be subjected to layer normal shortening. However, in bulk noncoaxial flow, the perturbed local flow is asymmetrically disposed about the stiff inclusion in a manner which directly reflects the sign of the vorticity of the bulk flow in the matrix (see Fig. 64). The examples shown here are observed in the XZ plane of the finite strain ellipsoid. The sense of shear along the shear plane, and in C the extensional and shortening quadrants of the flow, are shown.

(**a**) A *quarter fold* developed adjacent to a 1 mm feldspar porphyroclast in an ultramylonite where the foliation/layering was subjected to layer-parallel shortening. (GSC 204776-U). (**b**) *Quarter mats* of muscovite developed adjacent to a 1.5 mm feldspar porphyroclast in a mylonite where the foliation was subjected to layer-normal shortening. The mats form by removal of the quartz component of the normal matrix by mass transfer, resulting in a concentration of the less soluble mica which has subsequently recrystallized. (GSC 204775-Y). (**c**) Disposition of kinematically controlled myrmekite developed within K-feldspar porphyroclasts (Or), adjacent to inclusion faces making an high angle with the minimum instantaneous stretching axis of the bulk flow, from whose angular relationship to the shear plane of the deformation one deduces a sinistral sense of shear. Discussed in text. (a) and (b) from Great Slave Lake Shear Zone, N.W.T., looking down. (c) is taken from Simpson (1985).

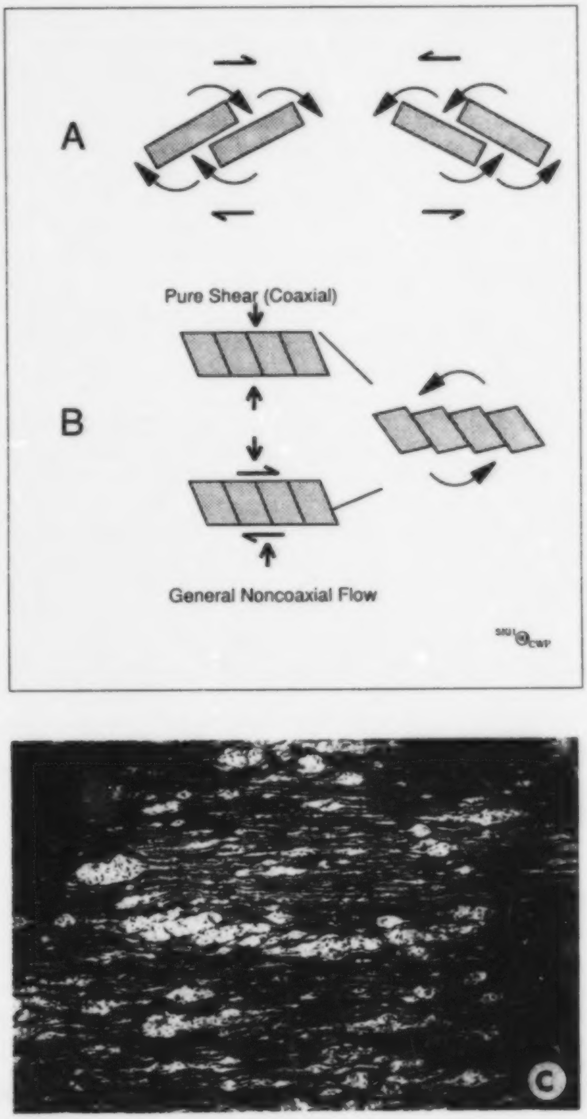

Figure 66. 'Tullage' or tiling. (**A**) Rotating inclusions in dextral shear may block at right-stepping overlaps; in sinistral shear they may block at left-stepping overlaps (Blumenfeld, 1983). Note that in the illustration it is assumed that the distance between the centres of rotation of neighboring inclusions remains constant during the progressive deformation. However, the geometries illustrated in (A) could equally have resulted from the clockwise or anticlockwise rotation of sets of 'domino structures' (**B**); for example a feldspar grain transected by a set of slip surfaces oriented an high angle to the bulk shear plane and subjected to general shearing flow. In our example, we allow the distance between the centres of rotation of the individual 'dominoes' to increase with progressive deformation. Our 'dominoes' are defined by slip surfaces making an oblique angle (70°) to the layer. In either pure shear, or a general noncoaxial flow, the rotation of the dominoes is a function of the angle they make with maximum instantaneous stretching axis of the coaxial component of the flow (i.e. the bulk flow plane). (**C**) How would the reader propose to discriminate between models A and B in order to interpret this natural example of tiling? We suggest that such structures are not reliable shear-sense indicators. (A) is adapted from Blumenfeld (1983). (C) Monte Rosa Nappe, Italy. (GSC 204776-N)

inclusion (Fig. 63). At least the proximal part of the pressure shadow could rotate out of the low pressure region and into an higher pressure region, adjacent to a face of the inclusion making a high angle with the minimum instantaneous stretching axis. If solution, transport and precipitation in the mass transfer process were all operating with a high degree of efficiency, the entrained pressure shadow material would be removed into solution, perhaps to eventually reprecipitate elsewhere in a low pressure region. However, where the solution process is relatively inefficient, perhaps due to decrease in water activity with retrogression (Yardley, 1981), or to a decrease in temperature, or simply to an increase in the strain rate, the rotated pressure shadow configuration may be preserved. The rotated nature of pressure shadows is readily observed where they are long, narrow and deformable; to some degree, their geometry resembles that of δ porphyroclasts (Fig. 63B). This is less obvious in the case of short, stubby and stiff pressure shadows, which may rotate as an integral part of the inclusion (Fig. 63A). They are easily confused with non-rotated pressure shadows; such an interpretation would give the incorrect sense of shear .

QUARTER STRUCTURES

Asymmetrical folds and concentrations of relatively insoluble material, such as micas, are often observed adjacent to stiff inclusions, especially at the microscopic scale (Simpson and Schmid, 1983; Vernon, 1987). Where the matrix foliation is deflected around a stiff inclusion, folds form in two diametrically opposed material quarters of the matrix adjacent to the inclusion, whereas the insoluble concentrates form in the other two quarters. We call these features *quarter structures*.

Consider a soft matrix, subjected to noncoaxial flow, whose foliation or layering is symmetrically wrapped about a stiff inclusion. Away from the inclusion, the deformation is oriented such that the bulk flow plane is parallel to the average foliation direction. The presence of the inclusion perturbs the flow so as to create four quarters in the immediately adjacent matrix, wherein the instantaneous stretching axes lie at different orientations with respect to those of the bulk flow. We refer to these as *material quarters* (Fig. 64), which should not be confused with the shortening and extensional *quadrants* of the flow. In two of the quarters, the matrix foliation may lie in the extensional quadrants of the local flow, whereas in the other two quarters it may lie in the shortening quadrants (Fig. 64; cf. Bell, 1981). In a bulk coaxial flow, the foliation/layering of the matrix in all four quarters would be subjected to layer normal shortening. However, in bulk noncoaxial flow, the perturbed local flow is asymmetrically disposed about the stiff inclusion in a manner which directly reflects the shear-sense of the bulk flow in the matrix (Fig. 64).

Where subjected to local *foliation-parallel shortening*, the matrix may respond by the formation of micro-folds, asymmetrically disposed about the inclusion (Fig. 65A). As the fold amplifies and tightens with progressive deformation, so its axial plane will attempt to track the rotation of the finite strain ellipsoid with respect to the instantaneous stretching axes of the flow. In those quarters where the foliation is subjected to local *foliation-normal shortening*, deformation may be accommodated by local volume loss of soluble material leading to the formation of polycrystalline aggregates or *mats* of less soluble phyllosilicates, asymmetrically disposed about the inclusion (Fig. 65B). Both the external outline and the internal shape fabric of the mat will be aligned at an high angle to the minimum instantaneous stretching axis of the bulk flow. We propose the terms *quarter folds* and *quarter mats* for these asymmetrically disposed structures developed in the matrix adjacent to porphyroclasts.

Alternatively, metamorphic reactions may occur *within* some species of porphyroclast in those quarters where the porphyroclast surface is oriented at an high angle to the bulk minimum instantaneous stretching axis. K-feldspar, for example, may develop an asymmetrically disposed myrmekite microstructure (Fig. 65C). Compression in these quarters reduces the concentration of space lattice vacancies within the K-feldspar. This induces diffusion of vacancies towards the compressed volume resulting in a charge imbalance which is neutralized by the rapid diffusion of small Na cations (Simpson, 1985). However, since myrmekite is a common post-tectonic feature of many mylonites (Hanmer, 1982a), it is necessary to demonstrate that the microstructure used in shear-sense determination is truly syntectonic in origin.

The disposition of kinematically distinctive quarters, as described here, is a direct reflection of the orientation of the instantaneous stretching axes of the flow, from which the shear-sense of the bulk flow may be determined. The effect of a general noncoaxial flow, rather than simple shear, is to add a component of extension to all four quarters; hence distinctive asymmetrical quarter structures are unlikely to form in flows where $W_k << 1$.

TILING AND DOMINO-STRUCTURES

Mutually interfering inclusions may block each other's rotational behaviour. Rotating inclusions in dextral shear may block at right-stepping overlaps; in sinistral shear they may block at left-stepping overlaps (Fig. 66A). Such structures have been coined *tuilage* or *tiling* structures by Blumenfeld (1983; Blumenfeld and Bouchez, 1988). However, this simple interpretation is not a unique explanation of the observed geometry (Fig. 66B, C). Consider a set of *domino* type slip surfaces within an inclusion, subjected to general noncoaxial flow. A given geometry might result from forward directed rotation of the slip surfaces in a bulk flow of a given shear-sense (Fig. 66A). However, if the slip surfaces rotated antithetically, the same geometry could equally well be produced by bulk noncoaxial flow of the opposite sense (Fig 66B). Note also that, with a suitably oriented initial configuration, identical geometries can result from both noncoaxial and coaxial progressive deformations (Fig. 66B). Thus tiling structure is not a reliable shear-sense indicator. By the same reasoning, we strongly advise against attempting to determine the shear-sense of the bulk flow from the slip and rotation of any domino-like structures (cf. Simpson and Schmid, 1983; Brunel, 1986; Takagi, 1986).

VEINS AND FOLDS

In this section we examine the kinematic significance of an eclectic assemblage of structures: (i) sigmoid synkinematic veins, (ii) oblique and curved fibres in synkinematic veins, (iii) deformed competent and incompetent veins, and (iv) asymmetrical folds. Some have long been tacitly assumed to be shear-sense indicators *par excellence*. Others, although widespread, have only recently been proposed as kinematically useful.

VEINS AND VEIN ARRAYS

Fibrous veins

Dilational veins have long been used to determine the orientation of the finite strain ellipsoid and its progressive rotation with respect to the instantaneous stretching axes of the flow (e.g. Choukroune and Seguret, 1968; Ramsay and Graham, 1970; Wilcox et al., 1973; Beach, 1975; Gamond, 1983). In en-echelon arrays of sigmoid veins (*tension gashes*), the reasonable assumption is that the propagating tips open perpendicular to the maximum instantaneous stretching axis (Fig. 67). The mid-sections of each vein, representing a greater finite strain than the tips, have rotated in the same sense as the bulk shear. Hence the sigmoid shape of the veins is an excellent shear-sense indicator (Ramsay and Graham, 1970). Note that, unlike the situation illustrated in Figure 67, in general noncoaxial flows the veins will not initiate at 45° with respect to the shear plane.

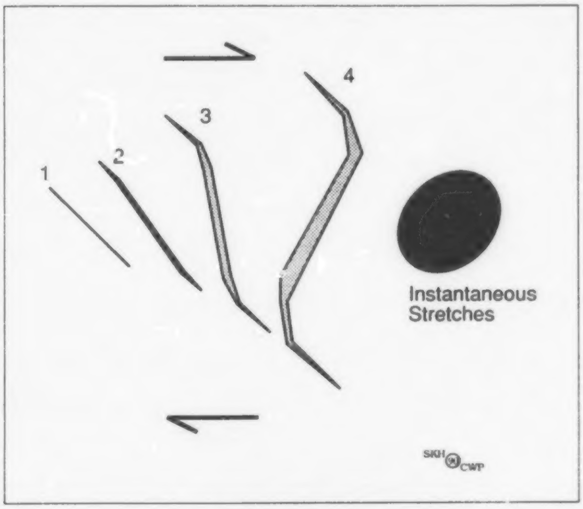

Figure 67. Sigmoid tension gashes. The sigmoid form of en-echelon tension gashes reflects the fact that the younger, narrower tips form as fractures initially oriented perpendicular to the maximum instantaneous stretching axis of the flow, while the older dilated central portion rotates with the same sense as the vorticity of the flow during progressive deformation.

Where veins are straight, either arranged in en-echelon arrays or otherwise disposed, a fibrous quartz or calcite fill may mark their progressive dilation (Fig. 68). The fibres of the fill may be straight, orthogonally or obliquely oriented with respect to the vein, or curved. If the relationship between fibre orientation and wall rock displacement during vein formation were simple, it would be fairly easy to use arrays of fibrous veins to reconstruct the orientation of the finite strain ellipsoid through time and to determine the sense of vorticity of the flow. However, there are two main schools of thought concerning the kinematic significance of fibrous vein-fill. For some workers, the orientation of new fibre growth is *displacement-controlled* (see section *Displacement controlled fibres*). Ramsay (1980b) described a process of vein growth by sequential cracking and sealing whereby quartz or calcite fibres, oriented at a high angle to the vein wall, are associated with fibre-parallel trails of inclusions or zones of inclusion bands (Fig. 69). He interpreted the trails and the bands of inclusions as reflecting the chemical influence of the wall rock minerals at the vein/wall rock interface

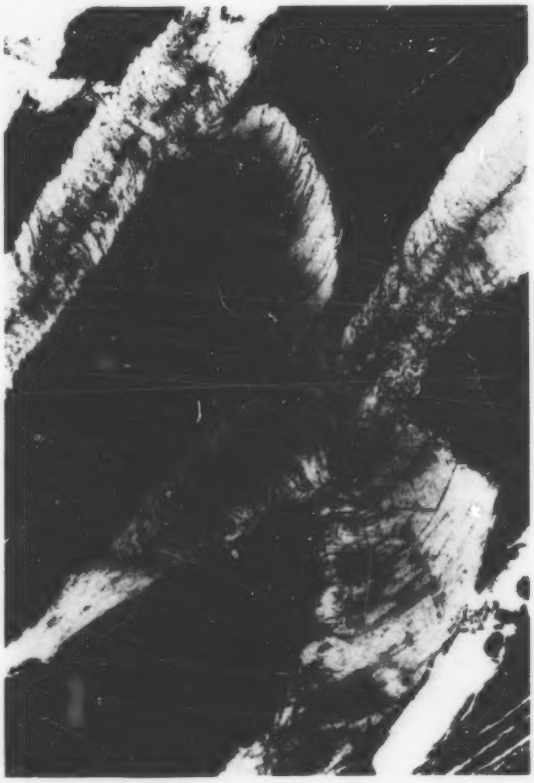

Figure 68. Quartz veins with fibrous fill. Two sets of quartz veins with fibrous vein-fill. Note the curved nature of the fibres.

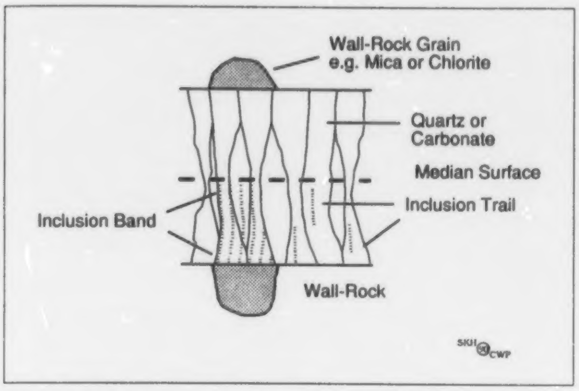

Figure 69. Displacement-controlled fibres in dilational veins. In the opinion of some workers, fibrous crystals in quartz or calcite vein-fill are displacement-controlled and will track the opening vector of the dilating vein during its formation. In the example illustrated here, new fibre growth occurs at the vein wall, sealing successive fractures between the wall rock and the older vein-fill. The fibres are not in optical continuity with wall rock grains. The median line is a train of relic fragments of wall rock, marking the initial fracture. Inclusion trails and inclusion bands reflect chemical control of the wall rock mineralogy on the composition of the immediately adjacent vein-fill. According to the '*crack-seal* ' model, both the quartz/carbonate fibres and the inclusion trails/bands track the opening vector through the dilation history of the developing vein: in this case, orthogonal to the vein wall. Redrawn from Ramsay (1980b).

during vein dilation. He also implicitly interpreted the quartz and calcite fibres as displacement controlled. Accordingly, the orientation of the opening vector of the dilating vein can be read from the orientation of optically strain-free fibres and the associated inclusion trails and zones of inclusion bands (Fig. 69; Durney and Ramsay, 1973; Wickham, 1973; Philip and Etchecopar, 1978; Casey et al., 1983; Ramsay and Huber, 1983).

However, by comparing fibre orientations with inclusion trails within the veins, or with offset markers in the vein wall, other workers have found that quartz or calcite *fibres do not necessarily track the opening vector of the vein* (Cox and Etheridge, 1983; Cox, 1987; van der Pluijm, 1984; Williams and Urai, 1989). Cox (1987) observed that the quartz and calcite fibres are not necessarily parallel to inclusion trails and the boundaries of zones of inclusion bands (Fig. 70). He proposed that fibres grow perpendicular to the vein wall, irrespective of the opening vector of the vein: in other words, they are *face-controlled* (see section Face-controlled fibres). Only the inclusion trails, which must be directly related to mineral grains in the wall rock, would track the opening history of the dilating vein (Fig. 70). Furthermore, Williams and Urai (1989) have shown that some natural examples of curved, optically strain-free fibrous crystals are in fact recrystallized, deformed fibres which were initially straight and orthogonal to the vein wall. As stated by these authors, without independent evidence to prove the relationship of crystal growth to the vein opening vector (e.g. Passchier and Urai, 1988), *the orientation of curved or oblique vein fibres should not be used to infer the kinematics of vein formation.*

Deformed veins

Rheologically, deformed veins fall into three categories: more competent, less competent, and of equal competence with respect to their wall rocks. The response of the veins to the imposed bulk deformation is a partial function of the rheological contrast with the wall rock. Where there is no competence contrast, individual veins are passive markers

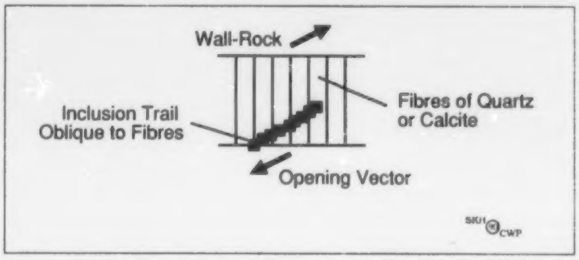

Figure 70. Face-controlled fibres in dilational veins. In some fibrous veins, inclusion trails are not parallel to the long dimensions of quartz or calcite fibres. Clearly, they cannot both track the opening of the vein. This illustration is redrawn from Cox (1987) who proposed that the inclusion trails are displacement controlled, whereas the fibres are face-controlled.

Figure 71. Folded boudins. Amphibolite layers in granitic gneiss were heterogeneously extended (boudined) prior to subsequent folding. Note how the boudins are clearly visible in the hinge zone of the fold, not just in the limbs. Central Gneiss Belt, Grenville Province, Ontario. (GSC 204105)

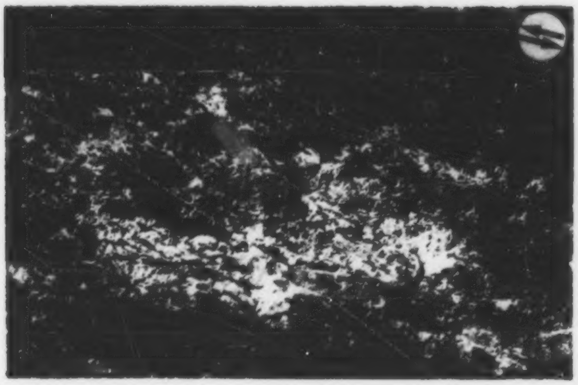

Figure 72. Oblique internal foliation in concordant veins. A natural example of a vein, lying concordant with respect to the mylonitic foliation of the wall rocks. It carries an internal foliation which is oblique to both the vein wall and the shear plane in the mylonite. Often, the internal oblique fabric is sufficiently weak to preserve some of the igneous aspects of the vein. The obliquity of the weaker fabric with respect to the mylonitic fabric may be considered to indicate the approximate relative orientations of the principal finite strains associated with the mylonite and the the internal foliation. If it is *assumed* that these finite strains are two components of a progressive deformation, then the angle between the two foliations indicates the sense of rotation of the principal finite strains with respect to the flow plane, thereby allowing deduction of the shear-sense of the flow. Accordingly, our example is sinistral. Central Metasedimentary Belt boundary thrust zone, Grenville Province, Ontario, looking northeast. (GSC 204776-L)

and cannot be used to determine shear-sense. Competent veins will fold or boudin according to their orientation with respect to the instantaneous stretching axes of the flow. However, if the competence contrast is extreme, strain refraction will simplify the local angular relationships; shortening will tend to be either vein-parallel or vein-normal (Fig. 27). A similar kinematic picture applies to the case of incompetent veins. However, the shapes of folds in shortened veins will be quite distinctive, while extension of veins will occur homogeneously, without boudinage (Talbot, 1982).

Folded and boudined veins have long been used as indicators of the orientations of the principal directions of the finite strain ellipsoid (e.g. Talbot, 1970, 1982; see Fig. 17). A number of authors (e.g. Talbot, 1970; Hutton, 1982; Passchier, 1990a, b) have shown that if a population of differently oriented veins is subjected to progressive noncoaxial deformation, the spatial distribution of veins which have been folded, boudined, or initially folded prior to subsequent boudinage (*boudined folds*), is a function of finite strain, dilatancy rate and vorticity. Although, in theory, absolute values for these parameters could be established from the distribution of deformed veins (Passchier, 1990), this is rarely possible in practice. However, the distribution of orientations of initially folded and subsequently boudined veins can be used to determine the angular disposition of fields of extension and shortening, from which the sense of shear can then be deduced (Fig. 16).

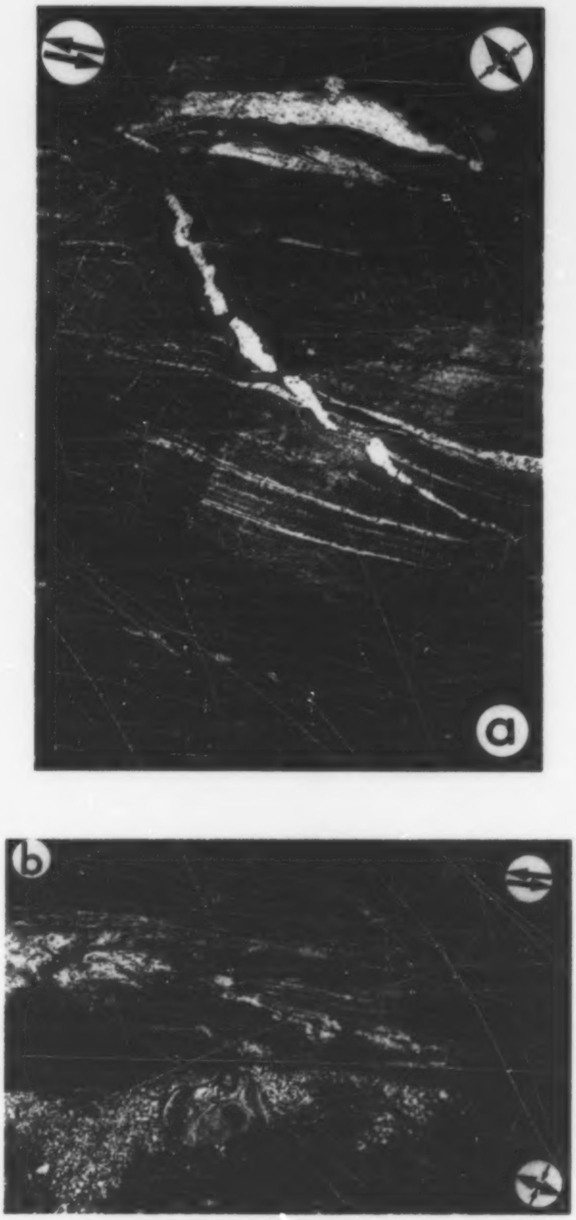

Figure 73. Oblique boudin trains. Natural examples of oblique boudin trains derived by the heterogeneous extension of oblique veins, observed in the XZ plane of the finite strain ellipsoid in mylonites of ductile thrust zones of the Grenville Province, Ontario. The sense of shear and the extensional and shortening quadrants of the flow are shown. Strictly speaking only the latter can be deduced from such structures; the shear-sense indicated here was deduced independently. In all three examples, the vein, having lost its rheological integrity as a continuous, competent sheet, has extended in its own plane along the approximate direction of the maximum instantaneous stretching axis of the flow. (**a**) Central Metasedimentary Belt, looking northeast. (**b**) Matrix beginning to flow around the extending vein. Parry Sound Thrust Zone, looking northeast. (GSC 204775-O and GSC 2904776-S).

We wish to draw attention here to the importance of *folded boudins* (Fig. 71). In general noncoaxial flows $(0<W_k<1)$, veins which initially lie in the shortening quadrants of the flow and are folded, will rotate with progressive deformation into the extensional quadrants, where they may subsequently boudin. However, veins which were initially boudined will not subsequently fold because they do not rotate into the shortening quadrants of the flow (Fig. 16). Although folded boudins can easily form in polyphase deformation, they can only form in progressive deformation in the special case of *spinning simple shear* $(W_k>1)$, or in a noncoaxial flow associated with *change in area* of the surface of observation (Passchier, 1990a, b). Therefore, the occurrence of folded boudined veins in shear zone rocks should alert the geologist to attempt a special study of their orientation and geometry, since the special circumstances of their formation imply that they may yield important information on vorticity or volume change (Von Brun and Talbot, 1986) associated with the local deformation history (see Passchier, 1990a, b).

Natural examples of deformed veins have been used by some workers to determine shear-sense (e.g. Davidson, 1984; Hanmer, 1984a). Two kinds of vein geometry have been used by these authors: obliquely foliated concordant veins (Fig. 72) and oblique boudin trains (Fig. 73). Both occur as intrusive sheets, cutting highly strained mylonites whose foliation lies parallel to the regional shear plane. The first kind comprise *concordant granitic or pegmatitic veins* which carry a systematically *oblique, internal foliation*. The second type comprises trains of boudins, derived by the heterogeneous extension of *oblique veins* such that the train of boudin centres is itself systematically oblique to the mylonitic foliation of the wall rock. In both cases, the coarse grain size, the relatively poorly developed foliation and the association with other crosscutting veins indicates that the veins were emplaced late-syntectonically with respect to the mylonitisation. However, this apparent simplicity is in fact very complicated. Without due care and attention, plus a degree of serendipity, such veins as illustrated here can be kinematically ambiguous, as we shall now see.

Rheological interfaces and induced noncoaxial flow

In any progressive deformation, planar elements such as veins rotate towards the flow plane. Where there is a competence contrast across the interface, a component of *induced noncoaxial flow*, directly reflecting the shear-sense of the bulk flow, may be resolved along the vein wall, if the vein is oblique to the instantaneous stretching axes of a bulk noncoaxial flow. In addition, a component of noncoaxial flow associated with the rotation of the vein itself may be induced along the contact (Fig 74). This *locally induced noncoaxial flow* is of opposite sense to that of the rotation of the vein. The reader will remember that the relationship between the rotation sense and rotation rate, and the orientation of any material line is a function of the flow type (Fig. 16). Also, the sense of rotation of a layer in a noncoaxial progressive deformation is a partial function of its orientation with respect to the flow plane. Therefore, the ratio of the shear strain rates of these two components of noncoaxial flow depends in part on the orientation of the vein, and in part on the nature of the bulk flow.

Incompetent veins

Incompetent veins respond to the bulk imposed flow by developing an internal fabric (Berger, 1971; Talbot, 1982). The orientation and geometry of the internal fabric is in part a reflection of the bulk deformation. However, it is also, in part, a reflection of the locally induced noncoaxial flow within the vein as the vein rotates in response to the bulk flow (Fig. 74). If the resultant flow within the vein is noncoaxial, then the internally developed fabric will lie oblique to the vein/wall rock interface, given that the local flow plane is parallel to the vein walls. With progressive deformation, the internal foliation rotates towards the vein wall. The sign of the angle between the internal foliation and the vein wall, and the direction of rotation of the internal foliation with progressive deformation, are direct reflections of the shear-sense of the flow within the vein (Berger, 1971; Talbot, 1982). Commonly the most intense shear strain develops at the vein boundary. As in any shear zone (Fig. 30), the internal foliation

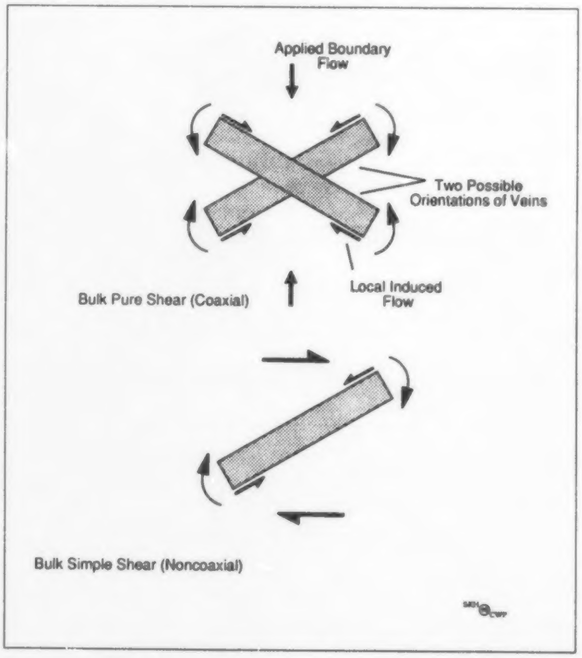
Applied Boundary Flow
Two Possible Orientations of Veins
Local Induced Flow
Bulk Pure Shear (Coaxial)
Bulk Simple Shear (Noncoaxial)

Figure 74. Local Induced flow. In any progressive deformation, planar elements, such as veins, rotate towards the direction of zero angular velocity of the flow (see Fig. 23). Where there is a competence contrast across the interface, a locally induced noncoaxial flow is set up along the vein wall, of opposite sense to that of the rotation of the vein itself, is induced along the vein wall. Whether the locally induced flow occurs within the vein or within the wall rock depends upon the relative competencies of the two materials. The upper illustration is for bulk coaxial flow. In bulk noncoaxial flow (lower illustration), the locally induced flow may be of opposite shear-sense to that of the bulk flow.

develops a sigmoid configuration along the strain gradient, reflecting the progressive rotation of the of material lines (shear-induced vorticity) with respect to the instantaneous stretching axes of the local flow within the vein.

We must emphasize here that *local observation of oblique internal foliation in a vein only yields information concerning the local noncoaxial history*. In general noncoaxial flows, because of the relatively rapid rotation rates (Fig. 23), it is particularly likely that the locally induced component of noncoaxial flow will dominate over that induced by the bulk flow. Only in the special case where it can be shown that the vein was initially concordant to the bulk shear plane of the deformation can the bulk shear-sense be directly determined from the orientation of the oblique internal foliation (Fig. 72). For all other cases, the sense of shear within the veins may be opposite to the bulk shear-sense. Only with knowledge of the initial orientation of the vein and the flow type can the geologist determine the bulk shear-sense from such veins (Fig. 74).

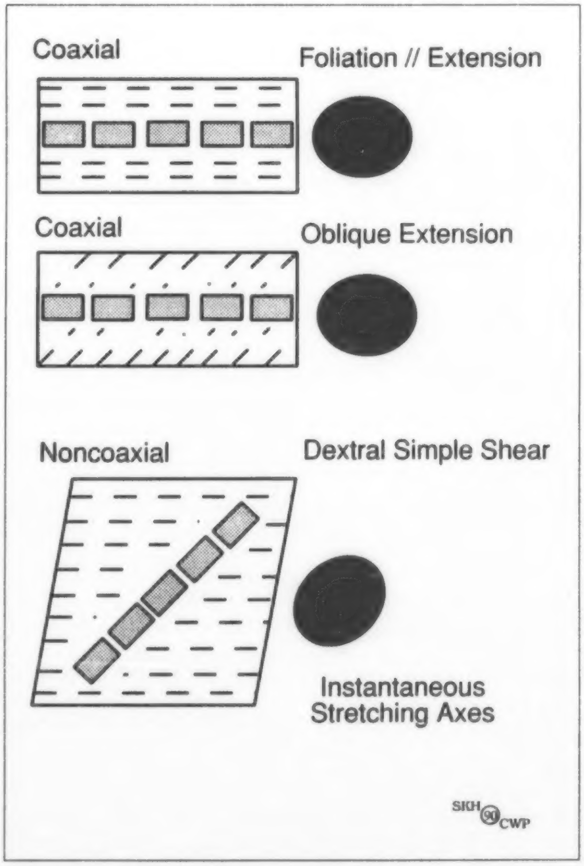

Figure 75. In-plane separation of boudins. As a competent vein is heterogeneously extended, it loses its rheological integrity. The continued separation of the boudins will depend upon the angle between the line of centres of the boudins and the maximum instantaneous stretching axis of the bulk flow. If the angle is small, then the extension will continue to be *in-plane*.

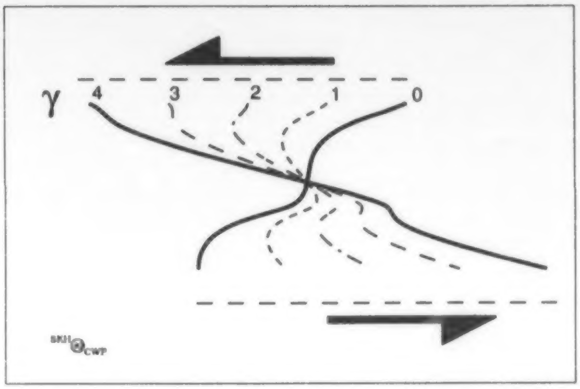

Figure 76. Fold asymmetry. With progressive deformation, folds produced in noncoaxial flow by the shortening of layers oblique to the flow plane, will change their asymmetry as a normal consequence of the deformation. In the example here, a train of 'S' folds evolves to a 'Z' asymmetry at modest values of shear strain. While it would require improbably extensive homogeneous deformation to 'switch' the asymmetry of folds over a regionally extensive area, the structural sequence illustrated here should caution the geologist against hasty attribution of kinematic significance to local observations of fold asymmetry. Adapted from Ramsay et al. (1983).

Competent veins

Consider a competent vein oriented in the extensional quadrants of the flow in a deforming matrix. As long as the vein maintains its integrity as a competent sheet, and if strain refraction is important (see section *Strain and flow refraction*), the vein will initially extend heterogeneously in its own plane (*in-plane*), irrespective of the flow type. As the vein divides into segments, either by boudinage, or by ductile necking and strain softening, it loses its rheological integrity as a competent sheet. The continued separation of the boudins will now depend upon the angle between the line of centres of the boudins and the direction of maximum infinitesimal extension in the matrix. If the angle is small, then the boudins will continue to separate approximately in-plane (Fig. 75). If the angle is large, in-plane separation is no longer possible because the boudins and the line of their centres will rotate at different rates, on account of their different aspect ratios (see Fig. 23, 52). In other words, in order to identify the approximate orientation of the maximum instantaneous stretching axis of the bulk flow from oblique boudin trains, the geologist must be able to identify *the stage at which the vein loses its integrity as a continuous, competent sheet and begins to reflect flow in the matrix*. Clearly, these are very specific requirements. We must emphasise that this structure only yields data on the approximate orientation of the bulk instantaneous stretching axes (Fig. 75), but that data itself can be used to support, or to test, shear-sense determinations based upon other criteria.

FOLD ASYMMETRY

Of all shear-sense indicators, the asymmetry of shear associated folds is perhaps the most venerable. Usually, in strongly deformed rocks, the geologist is only able to observe the final shape of the folds and cannot demonstrate the folding history. The determination of the kinematic significance of asymmetrical folds is based upon a series of often injudicious assumptions that the geologist rarely seeks to justify:

(1) The folds are "*drag-folds*", or the shape of the initially symmetrical folds was modified by later noncoaxial progressive deformation (Ramberg, 1963).

(2) The *scale* of the observed folds is appropriate to directly reflect the vorticity of the imposed bulk flow. This assumption is rarely justifiable. According to the 'Pumpellyan' principal of fold symmetry, the asymmetry of minor folds on a major fold switches from 'S' to 'Z'

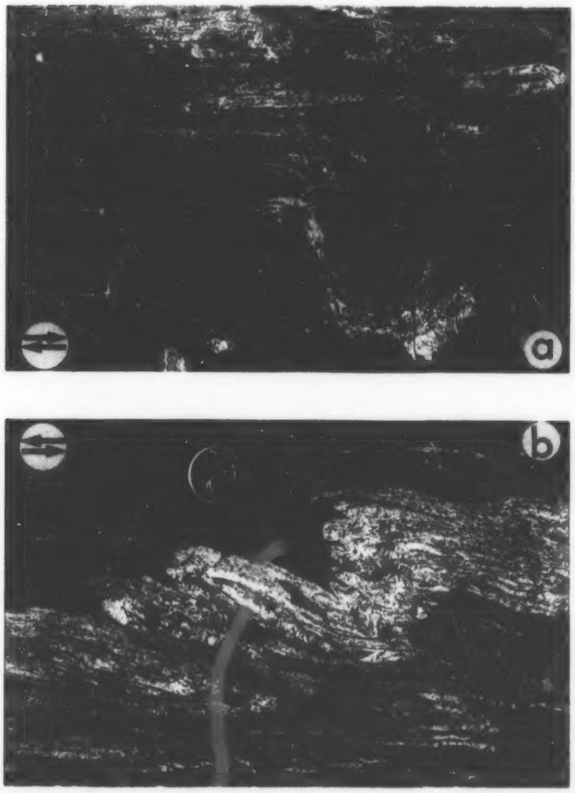

Figure 77. Rotation of fold axial planes. Fold trains in mylonites with profiles of various degrees of tightness, observed in the XZ plane of the finite strain ellipsoid. The sense of shear along the shear plane is shown. The rotation of fold axial planes with progressive tightening of the folds reflects the rotation of the principal directions of finite strain with respect to the instantaneous stretching axes of the flow. (**a**) The axial plane of the tighter fold (left) has rotated clockwise compared to the axial plane of the more open fold (right), indicating dextral shear. (**b**) The axial plane of the near-isoclinal fold (lower field) has rotated anticlockwise compared to the axial planes of the train of more open folds developed in the white layer, indicating sinistral shear. This is confirmed by the presence of a weakly developed set of asymmetric extensional shear bands in the lower field. Both examples are from Great Slave Lake Shear Zone, N.W.T., looking down. (GSC 204775-G and GSC 204776-B)

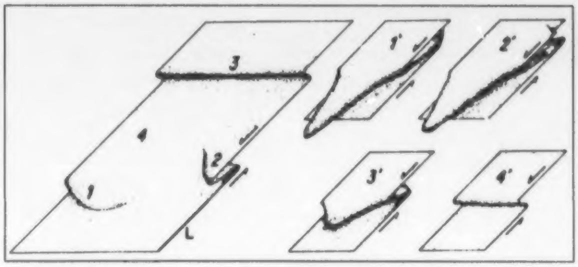

Figure 78. Sheath folds. If subjected to sufficiently high finite strain, a fold axis will tend to rotate towards the direction of maximum finite extension (L=X), while the fold axial plane will rotate towards the XY plane of the finite strain ellipsoid. Since real fold axes are not perfectly straight, and since the maximum extension direction varies slightly throughout any real flowing material, different segments of a given fold axis rotate in opposite directions towards X. The result is that the fold axis curves about the direction of finite extension. At high strains, the fold axis resembles an hair-pin bend whose long segments are subparallel to the finite extension direction; such structures are termed *sheath-folds*. Kinematic interpretation of the geometry of the fold profile is obviously dependent on the location of the profile in the fold structure. Taken from Quinquis et al. (1978).

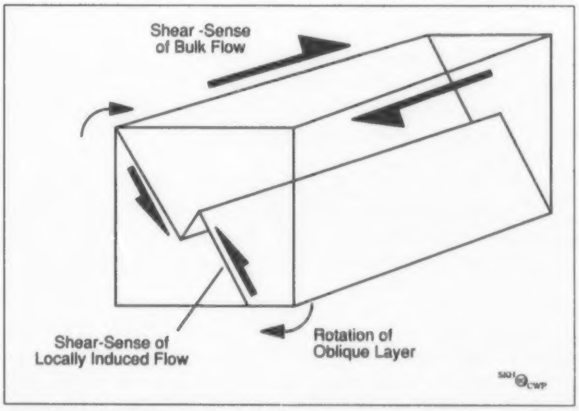

Figure 79. Fold axes parallel to the flow direction. There are numerous ways to produce fold axes which lie subparallel to the flow direction in noncoaxial flows. One way involves a locally induced noncoaxial flow associated with the rotation of a competent layer towards the XY plane of the finite strain ellipsoid (see Fig. 74). A competent layer initially makes an angle of less than 90° with the minimum instantaneous stretching axis of the bulk flow. With progressive deformation, the layer rotates towards the flow plane. This rotation is three dimensional and induces a local component of noncoaxial flow along the layer, such that the local flow direction is oriented at an high angle to the bulk flow direction. Folds which form in response to local flow will initiate with their fold axes sub-parallel to the bulk flow direction. Note the asymmetry of such folds is a function of the orientation of the competent layer with respect to the shear zone. Recall that the locally induced noncoaxial flow will tend to be all the more important if there is a strong component of shortening across the bulk shear plane. Compare this structure with Figures 27 and 78. Adapted from Brun and Merle (1988).

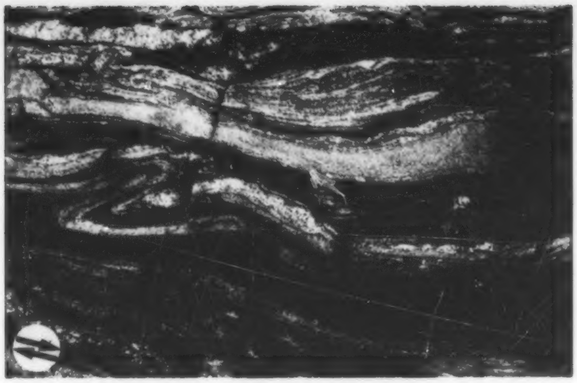

Figure 80. Asymmetrical amplification of a single fold. An example of a fold which has grown by amplification of a single local perturbation in shear-parallel layering (centre-left), observed in the XZ plane of the finite strain ellipsoid. The bulk sense of shear is shown. The initial perturbation was probably provoked by flow of the now folded layer into the isolated gap caused by the heterogeneous extension of the adjacent layer. The fold has amplified along a direction oriented within the extensional quadrant of the flow, reflecting the dextral shear-sense. Central Metasedimentary Belt boundary zone, Grenville Province, Québec, looking down. (GSC 204776-E)

across the major axial plane. Clearly, even if the shape of the major fold is directly related to the vorticity of imposed flow, the symmetry of its associated minor folds will vary from place to place.

(3) The symmetry of the observed fold has not changed as the fold developed. However, even relatively moderate values of shear strain may suffice to *reverse the sense of asymmetry* of folds related to noncoaxial flow (Ramsay et al., 1983; Fig 76).

Under what circumstances can observation of fold asymmetry be used to infer shear-sense? Where a readily identifiable set of contemporaneous folds shows a *regionally extensive consistent asymmetry*, it is reasonable to assume that the fold shape does reflect the sense of the regionally imposed shear. Where the geologist can observe evidence of the *progressive development of the fold shape* with deformation, the rotation of planar structures (axial planes, fold limbs) with respect to the instantaneous stretching axes of the flow (shear-induced vorticity) directly reflects the shear-sense of the flow (Fig. 77; Murphy, 1987).

Under what circumstances should fold asymmetry *not* be used to infer shear-sense? Many folds initially form with their axes oriented at an high angle to the direction of maximum finite extension, but may evolve into sheath folds (Fig. 78; Quinquis et al., 1978; Cobbold and Quinquis, 1980). Sheath-folds form at all scales from centimetres to kilometres in wavelength (Lacassin and Mattauer, 1985). It is therefore quite possible for a geologist working on a segment of a kilometric sheath fold to observe a consistent sense of fold asymmetry. Moreover, a competent layer, oriented obliquely with respect to the flow plane of a shear zone, might readily develop consistent asymmetrical folds with axes subparallel to the flow direction (Fig. 79). Setting aside for the moment the question of shear-sense, it is obvious that the unwary geologist could incorrectly infer the *shear direction* from such observations (see case study in Hanmer, 1981). Regarding the *sense of shear*, assuming that the questions of major versus minor fold scale and consistency of observed fold shape have been considered, the geologist must still be able to demonstrate the sense of rotation of the fold axis in the sheath fold example, in order to extrapolate from the field data to the regional shear-sense; this is rarely feasible. In the example of an oblique layer, the fold asymmetry is more likely to reflect the sense of the locally induced noncoaxial flow associated with the folding layer (Fig. 79), rather than the shear-sense of the bulk deformation, especially if deformed in general noncoaxial flow.

Some authors have suggested that, where the total geometry of the fold can be observed, the asymmetry of sheath-folds *per se* can be taken to directly reflect the shear-sense of the bulk flow. This undoubtedly holds true where a given sheath-fold is the result of the *amplification of a single perturbation in shear-parallel layering* (Fig. 80). While many observed sheath-folds are single, isolated fold closures or pairs of closures, this geometry does not preclude their formation as

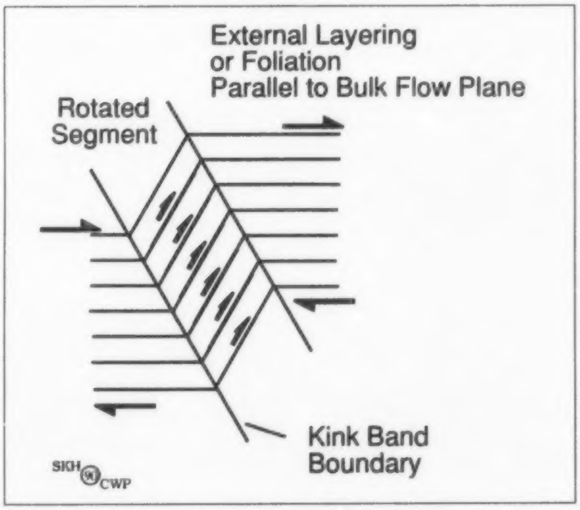

Figure 81. Fold mechanisms and bulk flow. According to the mechanism of *ideal kink folding* (Paterson and Weiss, 1962, 1965), the rotation of the short fold limb is driven by slip along the rotating foliation segment. Accordingly, the sense of slip on the rotating segment would be antithetic to the sense of rotation of the segment itself. If an asymmetrical set of kinks forms during bulk noncoaxial deformation, there must be compatibility between the slip on the foliation, both within and external to the kinks. This is readily appreciated if one considers the former as a set of 'ramps' and the latter as 'flats'. Hence, the sense of rotation of the kink fold limb is antithetic to the sense of the imposed bulk shear. This breaks down if the deformation is driven by shear stresses resolved onto the kink band boundaries (e.g. Dewey, 1965, 1969). However, it is unlikely that the geologist will be able to unequivocally discriminate between these two possibilities.

classical intrafolial folds, by the transposition and disruption of once continuous fold trains of minor folds on larger, major folds. In such a case, the questions raised above regarding scale and evolving fold shape with progressive deformation and the problems they imply for kinematic interpretation of fold asymmetry (Fig. 76), apply equally to sheath-folds.

When attempting to determine shear-sense from fold geometries, the implicit assumption is often made that the folding mechanism involved a component of *drag* (see discussion in Ramberg, 1963). Let us not forget that there are a number of ideal models of folding and that some of them may involve internal noncoaxial flows which must interact with the bulk flow. As an illustration, let us look at one particularly simple fold type. A kink fold comprises two kink band boundaries which separate an internal rotated segment of foliation or layering (short limb) from the external foliation or layering (long limb), which may or may not itself undergo a rotation of opposite sense to that of the short limb (Fig. 81). According to the mechanism of classical kink folding, the rotation of the short limb of a kink involves slip on the rotating segment, antithetic to the sense of rotation of the fold limb (e.g. Paterson and Weiss, 1962, 1965; Ramsay, 1967, p. 452). In a volume constant deformation, if slip occurs on the foliation or layering segments outside of the kink band boundaries and these external segments do not themselves rotate, then the sense of slip on the short limbs and that on the long limbs must be the same in order to maintain compatibility and material continuity. Put simply, contrary to the "drag-fold" model, Z-shaped kinks are favoured by bulk sinistral shear, while S-shaped kinks are favoured by dextral shear. This has been documented in both natural examples (Hanmer, 1982b) and laboratory simulation (Reches and Johnson, 1976).

In summary, while fold asymmetry can be kinematically significant, we suggest that it should be used more judiciously than the published literature would indicate has been the case until now.

REFERENCES

Anthony, M. and Wickham, J.
1978: Finite-element simulation of asymmetric folding; Tectonophysics, v. 47, p. 1-14.
Ave Lallemant, H.G.
1983: The kinematic insignificance of mineral lineations in a late Jurassic thrust and fold belt in eastern Oregon, U.S.A.; Tectonophysics, v. 100, p. 389-404.
Beach, A.
1975: The geometry of en-echelon vein array; Tectonophysics, v. 28, p. 245-263.
Behrmann, J.H.
1987: A precautionary note on shear bands as kinematic indicators; Journal of Structural Geology, v. 9, p. 659-666.
Bell, T.H.
1981: Foliation development - the contribution, geometry and significance of progressive, bulk, inhomogeneous shortening; Tectonophysics, v. 75, p. 273-296.
1985: Deformation partitioning and porphyroblast rotation in metamorphic rocks : a radical reinterpretation; Journal of Metamorphic Geology, v. 3, p. 109-118.
Bell, T.H. and Hammond, R.L.
1984: On the internal geometry of mylonite zones; Journal of Geology, v. 92, p. 667-686.
Bell, T.H., Rubenach, M.J., and Fleming, P.D.
1986: Porphyroblast nucleation, growth and dissolution in regional metamorphic rocks as a function of deformation partitioning during foliation development; Journal of Metamorphic Geology, v. 4, p. 37-67.
Berger, A.R.
1971: Dynamic analysis using dykes with oblique internal foliations; Geological Society of America Bulletin, v. 82, p. 781-786.
Berthé, D., Choukroune, P., and Jegouzo, P.
1979a: Orthogneiss, mylonite and non-coaxial deformation of granites: the example of the South Armoricain shear zone; Journal of Structural Geology, v. 1, p. 31-42.
Berthé, D., Choukroune, P., and Gapais, D.
1979b: Orientations préfèrentielles du quartz et orthogneissification progressive en régime cisaillant: l'exemple du cisaillement sud-armoricain; Bulletin de Minéralogie, v. 102, p. 265-272.
Beutner, E.C. and Diegel, F.A.
1985: Determination of fold kinematics from syntectonic fibres in pressure shadows, Martinsburg Slate, New Jersey; American Journal of Science, v. 285, p. 16-50.
Blumenfeld, P.
1983: Le "tuilage des mégacristaux", un critère d'écoulement rotationnel pour les fluidalités des roches magmatiques; Application au granite de Barbey Bulletin de la Société géologique de France, v. 25, p. 309-318.
Blumenfeld, P. and Bouchez, J.L.
1988: Shear criteria in granite and migmatite deformed in the magmatic and solid states; Journal of Structural Geology, v. 10, p. 361-372.
Bossart, P., Dietrich, D., Greco, A., Ottiger, R., and Ramsay, J.G.
1988: The tectonic structure of the Hazara-Kashmir syntaxis, southern Himalayas, Pakistan; Tectonics, v. 7, p. 273-297.
Bouchez, J.L., Mainprice, D.H.,Trepied, L., and Doukhan, J.C.
1984: Secondary lineation in a high temperature quartzite (Galicia, Spain): an explanation for an abnormal fabric Journal of Structural Geology, v. 6, p. 159-165.
Brun, J.P. and Burg, J.P.
1982: Combined thrusting and wrenching in the Ibero-Armorican Arc: a corner effect during continental collision; Earth and Planetary Science Letters, v. 61, p. 319-332.
Brun, J.P. and Merle, O.
1988: Experiments on folding in spreading-gliding nappes; Earth and Planetary Science Letters, v. 145, p. 129-139.
Brunel, M.
1980: Quartz fabrics in shear-zone mylonite: evidence for a major imprint due to late strain increments; Tectonophysics, v. 64, p. T33-T44.
1986: Ductile thrusting in the Himalayas: shear sense criteria and stretching lineations; Tectonics, v. 5, p. 247-265.

Burg, J.P.

1986: Quartz shape fabric variations and c-axis fabrics in a ribbon mylonite: arguments for an oscillating foliation; Journal of Structural Geology, v. 8, p. 123-131.

Burg, J.P. and Laurent, Ph.

1978: Strain analysis of a shear zone in a granodiorite; Tectonophysics, v. 47, p. 14-42.

Burg, J.P., Bale, P., Brun, J.P., and Girardeau, J.

1987: Stretching lineation and transport direction in the Ibero-Armorican arc during siluro-devonian collision; Geodinamica Acta, v. 1, p. 71-87.

Casey, M., Dietrich, D., and Ramsay, J.G.

1983: Methods for determining deformation history for chocolate tablet boudinage with fibrous crystals; Tectonophysics, v. 92, p. 211-239.

Chinnery, M.A.

1969: Secondary Faulting, I. Theoretical aspects; Canadian Journal of Earth Sciences, v. 3, p. 163-174.

Choukroune, P.

1971: Contribution à l'étude des mécanismes de la déformation avec schistosité grace aux cristallisations syncinématiques dans les "zones abritées" ("pressure shadows"); Bulletin de la Societé géologique de France, v. 13, p. 257-271.

Choukroune, P. and Lagarde, J.L.

1977: Plans de schistosité et déformation rotationelle :l'exemple du gneiss de Champtoceaux (Massif Armoricain); Compte Rendue de l'Academie des Sciences de Paris, v. 284, p. 2331-2334.

Choukroune, P. and Seguret, M.

1968: Exemple de relations entre joints de cisaillement, fentes de tension, plis et schistosité (autochthone de la nappe de Gavarnie - Pyrenées Centrales; Revue de Géographie physique et de Géologie dynamique, v. 10, p. 239-247.

Choukroune, P., Ballevre, M., Cobbold, P.R., Gautier, Y., Merle, O., and Vuichard, J.P.

1986: Deformation and motion in the western Alpine Arc; Tectonics, v. 5, p. 215-226.

Choukroune, P., Gapais, D. and Merle, O.

1987: Shear criteria and structural symmetry; Journal of Structural Geology, v. 9, p. 525-530.

Cobbold, P.R.

1976: Mechanical effects of anisotropy during large finite deformation; Bulletin de la Société géologique de France, v. 17, p. 1497-1510.

1977: Description and origin of banded deformation structures. I: Regional strain, local perturbations and deformation bands; Canadian Journal of Earth Sciences, v. 14, p. 1721-1731.

Cobbold, P.R. and Quinquis, H.

1980: Development of sheath folds in shear regimes; Journal of Structural Geology, v. 2, p. 119-126.

Cobbold, P.R., Cosgrove, J.W., and Summers, J.M.

1971: Development of internal structures in deformed anisotropic rocks; Tectonophysics, v. 12, p. 23-53.

Cobbold, P.R., Means, W.D., and Bayly, M.B.

1984: Jumps in deformation gradients and particle velocities across propagating coherent boundaries; Tectonophysics, v. 108, p. 283-298.

Coward, M.P.

1976: Strain within ductile shear zones; Tectonophysics, v. 34, p. 181-197.

Coward, M.P. and Kim, J.H.

1981: Strain within thrust sheets. Geological Society of London, Special Publication no. 9, p. 275-292.

Coward, M.P. and Potts, G.J.

1983: Complex strain patterns developed at the frontal and lateral tips to shear zones and thrust zones; Journal of Structural Geology, v. 5, p. 383-399.

Cox, S.F.

1987: Antitaxial crack-seal vein microstructures and their relationship to displacement paths; Journal of Structural Geology, v. 9, p. 779-787.

Cox, S.F. and Etheridge, M.A.

1983: Crack-seal fibre growth mechanisms and their significance in the development of oriented layer silicate microstructures; Tectonophysics, v. 92, p. 147-170.

Davidson, A.

1984: Identification of ductile shear zones in the southwestern Grenville Province of the Canadian Shield; in Precambrian Tectonics Illustrated, (ed.) A. Kroner and R. Greiling, E. Schweizeart'sche Verlags buchhandlung, Stuttgart, p. 207-235.

Davis, G.H., Gardulski, A.F. and Lister, G.S.

1987: Shear zone origin of quartzite mylonite and mylonitic pegmatite in the Coyotte Mountains metamorphic core complex, Arizona; Journal of Structural Geology, v. 9, p. 289-297.

Dennis, A.J. and Secor, D.T.

1987: A model for the development of crenulations in shear zones with applications from the Southern Appalachian Piedmont; Journal of Structural Geology, v. 9, p. 809-817.

Dewey, J.F.

1965: Nature and origin of kink bands; Tectonophysics, v. 1, p. 459-494.

1969: The origin and development of kink bands in a foliated body; Geological Journal, v. 6, p. 193-216.

De Wit, M.J.

1976: Metamorphic textures and deformation: a new mechanism for the development of syntectonic porphyroblasts and its implications for interpreting timing relationships in metamorphic rocks; Geological Journal, v. 11, p. 71-100.

Dietrich, D. and Durney, D.W.

1986: Change of direction of overthrust shear in the Helvetic nappes of western Switzerland; Journal of Structural Geology, v. 8, p. 389-398.

Dixon, J.M.

1976: Apparent "double rotation" of porphyroblasts during a single progressive deformation; Tectonophysics, v. 34, p. 101-115.

Durney, D.W. and Ramsay, J.G.

1973: Incremental strains measured by syntectonic crystal growths; in Gravity and Tectonics; (ed.) K.A. De Jong and R. Scholten, Wiley, N.Y., 502 p.

Eisbacher, G.H.

1970: Deformation mechanics of mylonitic rocks and fractured granites in Cobequid Mountains, Nova Scotia, Canada; Geological Society of America Bulletin, v. 81, p. 2009-2020.

Elliot, D.

1972: Deformation paths in structural geology; Geological Society of America Bulletin, v. 83, p. 2621-2638.

Escher, A. and Watterson, J.

1974: Stretching fabrics, folds and crustal shortening; Tectonophysics, v. 22, p. 223-231.

Etchecopar, A. and Malavieille, J.

1987: Computer models of pressure shadows: a method for strain measurement and shear-sense determination; Journal of Structural Geology, v. 9, p. 667-677.

Fairburn, H.W.

1950: Pressure shadows and relative movements in a shear zone; Transactions of the American Geophysical Union, v. 31, p. 914-916.

Fernandez, A., Feybesse, J.L., and Mezure, J.F.

1983: Theoretical and experimental study of fabrics developed by different shaped markers in two-dimensional simple shear; Bulletin de la Société géologique de France, v. 25, p. 319-326.

Flinn, D.

1969: Grain contacts in crystalline rocks; Lithos, v. 3, p. 361-370.

Freund, R.

1974: Kinematics of transform and transcurrent faults; Tectonophysics, v. 21, p. 93-134.

Gamond, J.F.

1983: Displacement features associated with fault zones: a comparison between observed examples and experimental models; Journal of Structural Geology, v. 5, p. 33-46.

Gapais, D. and White, S.H.

1982: Ductile shear bands in a naturally deformed quartzite; Textures and Microstructures, v. 5, p. 1-17.

Ghosh, S.K.

1966: Experimental tests of buckling folds in relation to strain ellipsoid in simple shear deformations; Tectonophysics, v. 3, p. 169-185.

1975: Distortion of planar structures around rigid spherical bodies; Tectonophysics, v. 28, p. 185-208.

Ghosh, S.K. (cont'd.)

1977: Drag patterns of planar structures around rigid inclusions; in Energetics of Geological Processes, (ed.) S.K. Saxena and S. Bhattacharji, Springer-Verlag, p. 94-120.

1982: The problem of shearing along axial plane foliations; Journal of Structural Geology, v. 4, p. 63-68.

Ghosh, S.K. and Ramberg, H.

1976: Reorientation of inclusions by combination of pure shear and simple shear; Tectonophysics, v. 34, p. 1-70.

1978: Reversal of the spiral direction of inclusion-trails in paratectonic porphyroblasts; Tectonophysics, v. 51, p. 83-97.

Hanmer, S.

1981: Tectonic significance of the northeastern Gander Zone, Newfoundland: an Acadian ductile shear zone; Canadian Journal of Earth Sciences, v. 18, p. 120-135.

1982a: Microstructure and geochemistry of plagioclase and microcline in naturally deformed granite; Journal of Structural Geology, v. 4, p. 197-213.

1982b: Vein arrays as kinematic indicators in kinked anisotropic materials; Journal of Structural Geology, v. 4, p. 151-160.

1984a: The potential use of planar and elliptical structures as indicators of strain regime and kinematics of tectonic flow; Geological Survey of Canada, Paper 84-1B, p. 133-142.

1984b: Strain-insensitive foliations in polymineralic rocks; Canadian Journal of Earth Sciences, v. 21, p. 1410-1414.

1986a: Natural examples of the role of strain regime in the rotational behaviour or stiff inclusions; Abstracts of the Shear Criteria Meeting, Imperial College, London, p. 12.

1986b: Asymmetrical pull-aparts and foliation fish as kinematic indicators; Journal of Structural Geology, v. 8, p. 111-122.

1988a: Great Slave Lake Shear Zone, Canadian Shield: reconstructed vertical profile of a crustal-scale fault zone; Tectonophysics, v. 149, p. 245-264.

1988b: Ductile thrusting at mid-crustal level, southwestern Grenville Province; Canadian Journal of Earth Sciences, v. 25, p. 1049-1059.

1989: Initiation of cataclastic flow in a mylonite zone; Journal of Structural Geology, v. 11, p. 751-762.

1990: Natural rotated inclusions in n on-ideal shear; Tectonophysics, v. 176, p. 245-255.

Hanmer, S. and Ciesielski, A.

1984: A structural reconnaissance of the northwestern boundary of the Central Metasedimentary Belt, Grenville Province, Ontario and Québec; Geological Survey of Canada, Paper 84-1B, p. 121-131.

Hanmer, S. and Lucas, S.B.

1985: Anatomy of a ductile transcurrent shear: the Great Slave Lake Shear Zone, District of Mackenzie, N.W.T. (preliminary report); in Geological Survey of Canada, Paper 85-1B, p. 7-22.

Harland, W.B.

1971: Tectonic transpression in Caledonian Spitzbergen; Geological Magazine, v. 108, p. 27-42.

Harris, L.B.

1985: Direction changes in thrusting of the Schistes Lustrés in Alpine Corsica; Tectonophysics, v. 120, p. 37-56.

Harris, L.B. and Cobbold, P.R.

1985: Development of conjugate shear bands during bulk simple shearing; Journal of Structural Geology, v. 7, p. 37-44.

Hobbs, B.E., Means, W.D., and Williams, P.F.

1976: An outline of structural geology; Wiley and Sons, 571 p.

Hooper, R.J. and Hatcher, R.D.

1988: Mylonites from the Towaliga fault zone, central Georgia: products of heterogeneous non-coaxial deformation; Tectonophysics, v. 152, p. 1-17.

Hudleston, P.J.

1983: Progressive deformation and development of fabric across zones of shear in glacial ice; in Energetics of Geological Processes, (ed.) S.K. Saxena and S. Bhattacharji, p. 121-150.

Hutton, D.

1982: A tectonic model for the emplacement of the main Donegal granite, NW Ireland; Journal of the Geological Society of London, v. 139, p. 615-631.

Ingles, J.

1986: Terminations of ductile shear zones; Tectonophysics, v. 127, p. 87-95.

Jamieson, R.A. and Vernon, R.H.

1987: Timing of porphyroblast growth in the Fleur de Lys Supergroup, Newfoundland; Journal of metamorphic Geology, v. 5, p. 273-288.

Jessel, M.W.

1988: Simulation of fabric development in recrystallising aggregates - II. Example model runs; Journal of Structural Geology, v. 10, p. 779-793.

Jordan, P.G.

1987: The deformational behaviour of bimineralic limestone-halite aggregates; Tectonophysics, v. 135, p. 185-197.

Kerrich, R., Allison, I., Barnett, R.L., Moss, S. and Starkey, J.

1980: Microstructural and chemical transformations accompanying deformation of for stress corrosion cracking and superplastic flow; Contributions to Mineralogy and Petrology, v. 73, p. 221-242.

Knipe, R.J. and Law, R.D.

1987: The influence of crystallographic orientation and grain boundary migration on microstructural and textural evolution in an S-C mylonite; Tectonophysics, v. 135, p. 155-169.

Lacassin, R.

1987: Kinematics of ductile shearing from outcrop to crustal scale in the Monte Rosa nappe, Western Alps; Tectonics, v. 6, p. 67-88.

Lacassin, R. and Mattauer, M.

1985: Kilometre scale sheath fold at Mattmark and implications for transport direction in the Alps; Nature, v. 315, p. 739-742.

Lagarde, J.L. and Michard, A.

1986: Stretching normal to the regional thrust displacement in a thrust-wrench shear zone, Rehana Massif, Morocco; Journal of Structural Geology, v. 8, p. 483-492.

Lane, L., Ghent, E.D., Stout, M.Z., and Brown, R.L.

1989: PT history and kinematics of the Monashee Decollement near Revelstoke, British Columbia; Canadian Journal of Earth Sciences, v. 26, p. 231-243.

Law, R.D. and Potts, G.J.

1987: The Tarskvaig Nappe of Skye, northwest Scotland: a re-examination of the fabrics and their kinematic significance; Geological Magazine, v. 124, p. 231-248.

Law, R.D., Casey, M., and Knipe, R.J.

1986: Kinematic and tectonic significance of microstructures and crystallographic fabrics within quartz mylonites from the Assynt and Eriboll regions of the Moine thrust zone, NW Scotland; Philosophical Transactions of the Royal Society of Scotland, v. 77, p. 99-125.

Law, R.D., Knipe, R.J., and Dayan, H.

1984: Strain partitioning within thrust sheets: microstructural and petrofabric evidence from the Moine Thrust zone at Loch Eriboll, northwest Scotland; Journal of Structural Geology, v. 6, p. 477-497.

Lister, G.S. and Price, G.P.

1978: Fabric development in a quartz-feldspar mylonite; Tectonophysics, v. 49, p. 37-78.

Lister, G.S. and Snoke, A.W.

1984: S-C Mylonites; Journal of Structural Geology, v. 6, p. 617-638.

Lister, G.S. and Williams, P.F.

1979: Fabric development in shear zones: theoretical controls and observed phenomena; Journal of Structural Geology, v. 1, p. 283-297.

1983: The partitioning of deformation in flowing rock masses; Tectonophysics, v. 92, p. 1-33.

Lister, G.S., Boland, J.N., and Zwart, H.J.

1986: Step-wise growth of biotite porphyroblasts in pelitic schists of the western Lys-Caillouas massif (Pyrenees); Journal of Structural Geology, v. 8, p. 543-562.

Lloyd, G.E. and Ferguson, C.C.

1981: Boudinage structures: some new interpretations based on elastic-plastic finite element simulations; Journal of Structural Geology, v. 3, p. 117-128.

Malavieille, J.

1987: Kinematics of compressional and extensional ductile shearing deformation in a metamorphic core complex of the northeastern Basin and Range; Journal of Structural Geology, v. 9, p. 541-554.

Malavieille, J. and Cobb, F.

1986: Cinématique des déformations ductiles dans trois massifs métamorphiques de l'Ouest des Etats-Unis: Albion (Idaho), Raft River et Grouse Creek (Utah); Bulletin de la Société géologique de France, v. 2, p. 885-898.

Malavieille, J., Etchecopar, A., and Burg, J.P.

1982: Analyse de la géométrie des zones abritées: simulation et application à des exemples naturels; Comptes Rendus de l'Academie des Sciences, Paris, v. 294, p. 279-284.

Mandal, N. and Banerjee, S.

1987: Rotation rate versus growth of syntectonic porphyroblasts: the controlling parameter of the shape of the inclusion trail; Tectonophysics, v. 136, p. 165-169.

Mandl, G.

1987: Tectonic deformation by rotating parallel faults: the "bookshelf" mechanism; Tectonophysics, v. 141, p. 277-316.

Manz, R. and Wickham, J.

1978: Experimental analysis of folding in simple shear; Tectonophysics, v. 44, p. 79-90.

Marcoux, J., Brun, J.P.,, Burg, J.P., and Ricou, L.E.

1987: Shear structures in anhydrite at the base of thrust sheets (Antalya, Southern Turkey); Journal of Structural Geology, v. 9, p. 555-561.

Mattauer, M. and Collot, B.

1986: Continental subduction, thrusting and strike-slip faulting in the Canadian Cordillera; Bulletin de la Société géologique de France, v. 2, p. 899-909.

McCaig, A.M.

1987: Deformation and fluid-rock interaction in metasomatic dilatant shear bands; Tectonophysics, v. 135, p. 121-132.

Means, W.D.

1976: Stress and Strain: basic concepts in continuum mechanics for geologists; Springer Verlag, 339 p.

1981: The concept of steady-state foliation; Tectonophysics, v. 78, p. 179-199.

Means, W.D., Hobbs, B.E., Lister, G.S., and Williams, P.F.

1980: Vorticity and non-coaxialty in progressive deformations; Journal of Structural Geology, v. 2, p. 371-378.

Merle, O. and Brun, J.P.

1984: The curved translation path of the Parpaillion Nappe (French Alps); Journal of Structural Geology, v. 6, p. 711-719.

Michard, A., Bouchez, J.L., and Ouazzani-Touhami, M.

1984: Obduction-related planar and linear fabrics in Oman; Journal of Structural Geology, v. 6, p. 39-50.

Mugge, O.

1930: Bewegungen von Porphyroblasten in Phylliten und ihre Messung; Neues Jahrbuch fur Mineralogie, Geologie und Palaontologie, v. 61, p. 469-510.

Murphy, D.C.

1987: Suprastructure/infrastructure transition, east-central Cariboo Mountains, British Columbia: geometry, kinematics and tectonic implications; Journal of Structural Geology, v. 9, p. 13-29.

Nicolas, A. and Poirier, J.P.

1976: Crystalline plasticity and solid state flow in metamorphic rocks; Wiley, New York, 444 p.

Norrell, G.T., Teixell, A., and Harper, G.D.

1989: Microstructure of serpentinite mylonites from the Josephine ophiolite and serpentinitization in retrogressive shear zones, California; Geological Society of America Bulletin, v. 101, p. 673-682.

O'Brien, D.K., Wenk, H.-R., Ratschbacher, L., and You, Z.

1987: Preferred orientation of phyllosilicates in phyllonites and ultramylonites; Journal of Structural Geology, v. 9, p. 719-730.

Park, R.G.

1989: Foundations of Structural Geology; 2nd Ed., Blackie, U.S.A., 148 p.

Passchier, C.W.

1986: Flow in natural shear zones - the consequences of spinning flow regimes; Earth and Planetary Science Letters, v. 77, p. 70-80.

1987a: Efficient use of the velocity gradients tensor in flow modelling; Tectonophysics, v. 136, p. 159-163.

1987b: Stable positions of rigid objects in non-coaxial flow - a study in vorticity analysis; Journal of Structural Geology, v. 9, p. 679-690.

Passchier, C.W. (cont'd.)

1988: Analysis of deformation paths in shear zones; Geologische Rundschau, v. 77, p. 309-318.

1990a: A Mohr circle construction to plot the stretch history of material lines; Journal of Structural Geology, v. 12, p. 513-515.

1990b: Reconstruction of deformation and flow parameters from deformed vein sets; Tectonophysics, v. 180, p. 185-199.

Passchier, C.W. and Simpson, C.

1986: Porphyroclast systems as kinematic indicators; Journal of Structural Geology, v. 8, p. 831-844.

Passchier, C.W. and Urai, J.L.

1988: Vorticity and strain analysis using Mohr diagrams; Journal of Structural Geology, v. 10, p. 755-763.

Paterson, M.S. and Weiss, L.E.

1962: Experimental folding in rocks; Nature, v. 195, p. 1046-1048.

1965: Experimental deformation and folding in phyllite; Geological Society of America Bulletin, v. 77, p. 343-374.

Peltzer, G. and Tapponier, P.

1988: Formation and evolution of strike-slip faults, rifts and basins during the India-Asia collision: an experimental approach; Journal of Geophysical Research, v. 93, p. 15085-15117.

Philip, H. and Etchecopar, A.

1978: Exemple de variations de direction de cristallisation fibreuse dans un champ de contraintes unique; Bulletin de la Societé géologique de France, v. 20, p. 263-268.

Platt, J.P.

1984: Secondary cleavages in ductile shear zones; Journal of Structural Geology, v. 6, p. 439-442.

Platt, J.P. and Vissers, R.L.

1980: Extensional structures in anisotropic rocks; Journal of Structural Geology, v. 2, p. 397-410.

Poirier, J.P.

1985: Creep of Crystals: high-temperature deformation processes in metals, ceramics and minerals; Cambridge University Press, 260 p.

Poirier, J.P. and Guillopé ,M.

1979: Deformation induced recrystallisation of minerals; Bulletin de Minéralogie, v. 102, p. 67-74.

Powell, C. McA. and Vernon, R.H.

1979: Growth and rotation history of garnet porphyroblasts with inclusion spirals in a Karakoram schist; Tectonophysics, v. 54, p. 25-43.

Quinquis, H., Audren, C., Brun, J.P., and Cobbold, P.R.

1978: Intense progressive shear in Ile de Groix blueschists and compatibility with subduction or obduction; Nature, v. 273, p. 43-45.

Ramberg, H.

1955: Natural and experimental boudinage and pinch-and-swell structures; Journal of Geology, v. 63, p. 512-526.

1963: The evolution of drag folds; Geological Magazine, v. 100, p. 97-106.

1967: Folding and Fracturing of Rocks; McGraw Hill, New York, 568 p.

1975: Particle paths, displacement and progressive strain applicable to rocks; Tectonophysics, v. 28, p. 1-37.

Ramsay, J.G.

1980a: Shear zone geometry: a review; Journal of Structural Geology, v. 2, p. 83-99.

1980b: The crack-seal mechanism of rock deformation; Nature, v. 284, p. 135-139.

Ramsay, J.G. and Allison, I.

1979: Structural analysis of shear zones in an alpinised hercynian granite (Maggia Lappen, Pennine Zone, Central Alps); Schweizerische mineralogische und petrographische Mitteilurgen, v. 59, p. 251-279.

Ramsay, J.G. and Graham, R.H.

1970: Strain variation in shear belts; Canadian Journal of Earth Sciences, v. 7, p. 786-813.

Ramsay, J.G. and Huber, M.I.

1983: The techniques of modern structural geology, Volume 1: Strain analysis; Academic Press, London, 307 p.

1987: The techniques of modern structural geology, Volume 2: Folds and Fractures; Academic Press, London, 391 p.

Ramsay, J.G., Casey, M., and Kligfield, R.

1983: Role of shear in development of the Helvetic fold-thrust belt of Switzerland; Geology, v. 11, p. 439-442.

Reches, Z. and Johnson, A.M.

1976: A theory of concentric kink and sinusoidal folding and of monoclinal flexuring of compressible elastic multilayers; Tectonophysics, v. 35, p. 295-334.

Ridley, J.

1986: Parallel stretching lineations and fold axes oblique to a shear displacement direction - a model and observations; Journal of Structural Geology, v. 8, p. 647-653.

Robin, P.Y.

1979: Theory of metamorphic segregation and related processes; Geochimica Cosmochimica Acta, v. 43, p. 1587-1600.

Rosenfeld, J.L.

1968: Garnet rotations due to major Paleozoic deformations in Southeast Vermont; in Studies of Appalachian Geology, (ed.) E.A. Zen, Wiley, N.Y., p. 185-202.

1970: Rotated garnets in metamorphic rocks; Geological Society of America Special Paper 129, 105 p.

Rutter, E.H.

1976: The kinetics of rock deformation by pressure solution; Philosophical Transactions of the Royal Society of London, v. A283, p. 203-219.

1983: Pressure solution in nature, theory and experiment; Journal of the Geological Society of London, v. 140, p. 725-740.

Saltzer, S.D. and Hodges, K.V.

1988: The Middle Mountain shear zone, southern Idaho: Kinematic analysis of an early Tertiary high-temperature detachment; Geological Society of America Bulletin, v. 100, p. 96-103.

Sanderson, D.J. and Marchini, R.D.

1984: Transpression; Journal of Structural Geology, v. 6, p. 449-549.

Schmid, S.M., Zingg, A. and Handy, M.

1987: The kinematics of movements along the Insubric Line and the emplacement of the Ivrea Zone; Tectonophysics, v. 135, p. 47-66.

Schoneveld, C.

1977: A study of some typical inclusion patterns in strongly paracrystalline - rotated garnets; Tectonophysics, v. 39, p. 453-471.

1978: A study of some typical inclusion patterns in strongly paracrystalline rotated garnets; Tectonophysics, v. 47, p. 179-183.

Schwerdtner, W.M.

1973a: Schistosity and penetrative mineral lineation as indicators of paleostrain directions; Canadian Journal of Earth Sciences, v. 10, p. 1233-1243.

1973b: A scale problem in paleo-strain analysis; Tectonophysics, v. 16, p. 47-54.

Selkman, S.

1978: Stress and displacement analysis of boudinage by the finite element method; Tectonophysics, v. 44, p. 115-139.

Sibson, R.H.

1986: Earthquakes and lineament infrastructure; Philosophical Transactions of the Royal Society of London, v. A317, p. 63-79.

Simpson, C.

1985: Deformation of granitic rocks across the brittle-ductile transition; Journal of Structural Geology, v. 7, p. 503-511.

1986: Determination of movement sense in mylonites. Journal of Geological Education, 34, 246-261.

Simpson, C. and Schmid, S.M.

1983: An evaluation of criteria to deduce the sense of movement in sheared rocks; Geological Society of America Bulletin, v. 94, p. 1281-1288.

Simpson, C. and Wintsch, R.P.

1989: Evidence for deformation-induced K-feldspar replacement by myrmekite; Journal of metamorphic Geology, v. 7, p. 261-275.

Sirieys, P.

1984: Déformation homogénéisée des roches par glissements hétérogènes continus et discontinus; Bulletin de la Société géologique de France, v. 26, p. 185-192.

Spry, A.

1969: Metamorphic Textures; Pergamon Press, Oxford, 350 p.

Stephanson, O. and Berner, H.

1971: The finite element method in tectonic processes; Physics of the Earth and Planetary Interiors, v. 4, p. 301-321.

Stromgard, K.E.

1973: Stress distribution during deformation of boudinage and pressure shadows; Tectonophysics, v. 16, p. 215-248.

Takagi, H.

1986: Implications of mylonitic microstructures for the geotectonic evolution of the Median Tectonic Line, central Japan; Journal of Structural Geology, v. 8, p. 3-14.

Takagi, H. and Ito, M.

1988: The use of asymmetric pressure shadows in mylonites to determine the sense of shear; Journal of Structural Geology, v. 10, p. 347-360.

Talbot, C.J.

1970: The minimum strain ellipsoid using deformed quartz veins; Tectonophysics, v. 9, p. 47-76.

1979: Fold trains in a glacier of salt in southern Iran; Journal of Structural Geology, v. 1, p. 5-18.

1982: Obliquely foliated dykes as deformed incompetent single layers; Geological Society of America Bulletin, v. 93, p. 450-460.

Tapponier, P., Peltzer, G., Le Dain, A.Y., Armijo, R., and Cobbold, P.R.

1982: Propagating extrusion tectonics in Asia: New insights from simple experiments with plasticine; Geology, v. 10, p. 611-616.

Treagus, S.H.

1981: A theory of stress and strain variations in viscous layers, and its geological implications; Tectonophysics, v. 70, p. 75-103.

1983: A theory of finite strain variation through contrasting layers and its bearing on cleavage refraction; Journal of Structural Geology, v. 5, p. 351-368.

1988: Strain refraction in layered systems; Journal of Structural Geology, v. 10, p. 517-527.

Treagus, J.E. and Treagus, S.H.

1981: Folds and the strain ellipsoid: a general model; Journal of Structural Geology, v. 3, p. 1-18.

Tullis, J.

1983: Deformation of feldspars; in Feldspar Mineralogy (ed. P.H. Ribbe). Mineralogy Society of America Reviews in Mineralogy, v. 2, p. 297-323.

Tullis, J. and Yund, R.A.

1977: Experimental deformation of dry Westerly Granite; Journal of Geophysical Research, v. 82, p. 5705-5718.

1979: The brittle-ductile transition for dry Westerly Granite as a function of temperature and pressure; in Proceedings of Conference II, Experimental studies of rock friction with application to earthquake prediction, National Earthquake Hazards Reduction Program, United States Geological Survey, p. 511-542.

1985: Dynamic recrystallisation of feldspar: a mechanism for ductile shear zone formation; Geology, v. 13, p. 238-241.

Urai, J., Means, W.D. and Lister, G.S.

1986: Dynamic recrystallization of minerals; American Geophysical Union Monograph, v. 36, p. 161-200.

Van den Driessche, J.

1986a: Cinématique de la déformation ductile dans la Cordillère canadienne: relations chevauchements-décrochements; Bulletin de la Société géologique de France, v. 2, p. 911-920.

1986b: Structures d'enroulement et sens de cisaillement. Exemples et modèles; Compte Rendu de l'Academie des Sciences, Paris, v. 303, p. 413-418.

Van den Driessche, J. and Brun, J.P.

1987: Rolling structures at large shear strain; Journal of Structural Geology, v. 9, p. 691-704.

Van der Molen, I.

1985: Interlayer material transport during layer-normal shortening. Part I. The model; Tectonophysics, v. 115, p. 275-295.

Van der Pluijm, B.A.

1984: An unusual 'crack-seal' vein geometry; Journal of Structural Geology, v. 6, p. 593-597.

Vernon, R.H.

1968: Microstructures of high-grade metamorphic rocks at Broken Hill, Australia; Journal of Petrology, v. 9, p. 1-22.

1981: Optical microstructure of partly recrystallized calcite in some naturally deformed marbles; Tectonophysics, v. 8, p. 601-612.

1987: A microstructural indicator of shear sense in volcanic rocks and its relationship to porphyroclast rotation in metamorphic rocks; Journal of Geology, v. 95, p. 127-133.

Vernon, R.H. (cont'd.)

1988: Microstructural evidence of rotation and non-rotation of mica porphyroblasts; Journal of Metamorphic Geology, v. 6, p. 595-601.

Vernon, R.H., Williams, V.A., and D'Arcy, W.F.

1983: Grain-size reduction and foliation development in a deformed granitoid batholith; Tectonophysics, v. 92, p. 123-145.

Vialon, P.

1979: Les déformations continues-discontinues des roches anisotropes; Eclogae Geologicae Helveticae, v. 72, p. 531-549.

Vissers, R.L.M.

1987: The effect of foliation orientation on the inferred rotation axes and rotation angles of rotated porphyroblasts; Tectonophysics, v. 139, p. 275-283.

Von Brun, V. and Talbot, C.J.

1986: Formation of subglacial intrusive clastic sheets in the Dwyka formation of northern Natal, South Africa; Journal of Sedimentary Petrology, v. 56, p. 35-44.

Weijermars, R. and Rondeel, H.E.

1984: Shear band foliation as indicator of sense of shear: Field observations in central Spain; Geology, v. 12, p. 603-606.

Wheeler, J.

1987: The determination of true shear senses from the deflection of passive markers in shear zones; Journal of the Geological Society of London, v. 144, p. 73-77.

White, S.H.

1976: The effects of strain on microstructures, fabrics and deformation mechanisms in quartzites; Philosophical Transactions of the Royal Society of London, v. A283, p. 69-86.

White, S.H. and Knipe, R.J.

1978: Microstructure and cleavage development in selected slates; Contributions to Mineralogy and Petrology, v. 66, p. 165-174.

White, S.H. and Wilson, C.J.L.

1978: Microstructure of some quartz pressure fringes; Neues Jahrbuch fur Mineralogie, Abhandlungen, v. 134, p. 33-51.

White, S.H., Bretan, P.G., and Rutter, E.H.

1986: Fault-zone reactivation: kinematics and mechanisms; Philosophical Transactions of the Royal Society of London, v. A317, p. 81-97.

White, S.H., Burrows, S.E., Carreras, J., Shaw, N.D., and Humphreys, F.J.

1980: On mylonites in ductile shear zones; Journal of Structural Geology, v. 2, p. 175-187.

Wickham, J.S.

1973: An estimate of strain increments in a naturally deformed carbonate rock; American Journal of Science, v. 273, p. 23-47.

Wilcox, R.E., Harding, T.P., and Seely, D.R.

1973: Basic Wrench Tectonics; American Association of Petroleum Geologists Bulletin, v. 57, p. 74-96.

Williams, P.F.

1972: 'Pressure shadow' structures in foliated rocks from Bermagui, New South Wales; Journal of the Geological Society of Australia, v. 18, p. 371-377.

1976: Relationships between axial-plane foliations and strain; Tectonophysics, v. 30, p. 181-196.

1977: Foliation: a review and discussion; Tectonophysics, v. 39, p. 305-328.

Williams, P.F. and Schoneveld, C.

1981: Garnet rotation and the development of axial plane crenulation cleavage; Tectonophysics, v. 78, p. 307-334.

Williams, P.F. and Urai, J.L.

1989: Curved vein fibres-an alternative explanation; Tectonophysics, v. 158, p. 311-333.

Wilson, R.W.

1971: On syntectonic porphyroblast growth; Tectonophysics, v. 11, p. 239-260.

Wintsch, R.P.

1986: The possible effects of deformation on chemical processes in metamorphic fault zones; in Metamorphic Reactions, kinetics textures and deformation , (ed.) Thompson A.B. and Rubie, D.C., Springer-Verlag, p. 251-268.

Yardley, B.W.D.

1981: Effect of cooling on the water content and mechanical behaviour of metamorphosed rocks; Geology, v. 9, p. 405-408.

Zwart, H.J. and Oele, J.A.

1966: Rotated magnetite crystals from the Rocroi Massif (Ardennes); Geologie en Mijnbouw, v. 45, p. 70-74.